Algorithm Theoretical Basis Document

MODIS Phycoerythrin Pigment Concentration

(April 1999)

Frank E. Hoge
Building N-159, Room E200
National Aeronautics and Space Administration
Goddard Space Flight Center
Wallops Flight Facility
Wallops Island, VA 23337

TELEPHONE: (757)-824-1567
E-MAIL: hoge@osb1.wff.nasa.gov
FAX: (757) 804-1036

April 1, 1999

TABLE OF CONTENTS

ABSTRACT

This algorithm theoretical basis document (ATBD) describes the development of a still newer methodology for the retrieval of the phycourobilin (PUB) absorption coefficient, phycourobilin-rich phycoerythrins [PEB(+)] and the phycourobilin-deficient phycoerythrins [PEB(-)] . This algorithm is firmly based on ocean color physics and directly inverts oceanic water-leaving radiance (or reflectance) models in the visible MODIS bands. Post-launch, the algorithm will be validated by airborne laser-induced phycoerythrin, PEB(+) and PEB(-), fluorescence acquired during overflights of research ships gathering concurrent surface pigment data, optical/shipboard laser fluorometer data in support of MODIS overpasses. On-going phycoerythrin algorithm research, validation, and other issues are also discussed. This revised version has been updated to address comments received as a result of periodic MODIS ATBD Reviews.

The principal change within this revision is the PEB(+) and PEB(-) in addition to PUB. Direct airborne laser validation of the modeled-unmodeled PE absorption by linear matrix inversion at 488nm, $a_{PE}(488)$, using 4 MODIS bands is also provided.

1.0 Introduction

This Introduction includes the identification, overview, scope, and list of applicable documents pertaining to phycoerythrin absorption coefficient retrieval via linear matrix inversion of an oceanic radaince/reflectance model.

1.1. Identification of the Algorithm.

This algorithm theoretical basis document (ATBD) describes the retrieval of phycoerythrin pigment absorption coefficent. (Specific absorption coefficents are not availble at this time to convert to concentration). More specifically the complete algorithm provides for the retrieval of the absorption coefficients of phycourobilin (PUB), phycourobilin-rich phycoerythrins, PEB(+) and the phycourobilin-deficient phycoerythrins, PEB(-). This algorithm is specifically identified as Ocean Group, MODIS Level 2 Data Product parameter #3320 and Modis Product #33.

1.2. Overview of the algorithm.

There are 3 major algal pigment groups [Bidigare et al 1990; Vernet et al 1990] found in marine phytoplankton and bacteria: the chlorophylls, carotenoids, and phycobilins. The phycobilins are phycoerythrin and phycocyanin. The phycoerythrins are further subdivided into phycourobilin-rich phycoerythrins, PEB(+), and the phycourobilin-deficient phycoerythrins, PEB(-). This algorithm addresses the retrieval of the PUB, PEB(+), and PEB(-) phycoerythrin absorption coefficients. Algorithm details are given in Appendix A.

1.3. Scope.

This document primarily addresses the retrieval of the PUB and the PEB(+) and PEB(-) phycoerythrins. However, the matrix inversion of the oceanic radiance model simultaneously provides the absorption coefficients of phytoplankton and CDOM together with the total constituent backscatter (TCB). From the latter quantity the total backscatter can be easily obtained.

1.4 List of Applicable Documents.

Since 1979 the phycoerythrin pigment has been measured by airborne laser-induced fluorescence methods [Hoge and Swift 1981; Hoge and Swift 1986a, Hoge and Swift 1986b; Hoge and Swift 1990]. Its airborne detection using upwelled radiances was first noted in 1986 [Hoge and Swift 1986a; Hoge and Swift 1986b] and detailed in 1990 [Hoge and Swift 1990]. Some documents/reprints relative to the phycoerythrin algorithm are specifically:

1. (Appendix A, herein). Hoge, Frank E., C. Wayne Wright, Paul E. Lyon, Robert N. Swift, James K. Yungel, "Satellite Retrieval of the Absorption Coefficient of Phytoplankton Phycoerythrin Pigment: Theory and Feasibility Status", submitted 1999.

2. (Appendix B, herein). Hoge, Frank E., C. Wayne Wright, Paul E. Lyon, Robert N. Swift, James K. Yungel, Satellite retrieval of inherent optical properties by inversion of an oceanic radiance model: A preliminary algorithm, Applied Optics **38**, 495-504 (1999).

3. (Appendix C, herein) Hoge,Frank E., Wright, C. Wayne, Kana, Todd M., Swift, Robert N., and Yungel, James K., Spatial variability of oceanic phycoerythrin spectral types derived from

airborne laser-induced fluorescence measurements, Applied Optics 37, 4744-4749, 1998.

4. (Appendix D, herein) Hoge, Frank E. and Paul E. Lyon, "Satellite Retrieval of Inherent Optical Properties by Linear Matrix Inversion of Oceanic Radiance Models: An Analysis of Model and Radiance Measurement Errors", Jour. Geophys. Res. 101, 16,631- 16,648, (1996).

5. Hoge, F. E. and R. N. Swift, Phytosynthetic Accessory Pigments: Evidence for the Influence of Phycoerythrin on the Submarine Light Field, Remote Sensing of Environment 34, 19-25, 1990.

6. Hoge, F. E., and R. N. Swift, Chlorophyll Pigment Concentration Using Spectral Curvature Algorithms: An Evaluation of Present and Proposed Satellite Ocean Color Sensor Bands, Applied Optics, 25, 3677-3682 (1986b).

7. Hoge, F. E., and R. N. Swift, Active-Passive Correlation Spectroscopy: A New Technique for Identifying Ocean Color Algorithm Spectral Regions, Applied Optics, 25, 2571-2583 (1986a).

8. Culver, Mary E., and Mary Jane Perry, Detection of phycoerythrin fluorescence in upwelling irradiance spectra, Eos Trans. AGU 75, 233 (1994).

The success of using oceanic radiance model inversion for the satellite retrievals is demonstrated by the recent recovery of the CDOM absorption coefficient using CZCS data [Hoge et al. 1995c] and retrieval of phytoplankton absorption coefficent, CDOM absorption coefficient, and total constituent backscatter from airborne water-leaving radiances [Hoge et al., 1999; Appendix

B herein]. Appendix A describes the successful retrieval of the unmodeled/modeled retrieval of phycoerythrin absorption coefficent at 488nm, $a_{PE}(488)$.

2.0 Overview and Background Information

Oceanic phytoplankton chlorophyll is known to produce a very significant influence on the optical properties of the ocean. The chlorophyll-driven optical properties are in fact so strong as to allow global satellite mapping of the pigment concentration in the upper ocean using upwelled water-leaving radiances.

Extensive experimental evidence has been presented to strongly suggest that upwelled water-leaving spectral radiances also include physical backscattering and absorption effects of photosynthetic accessory pigments such as phycoerythrin [Hoge and Swift 1986a; Hoge and Swift 1986b; Hoge and Swift 1990]. In the water column, the presence of phycoerythrin has been measured over wide regions of the ocean using well established airborne laser-induced spectral fluorescence techniques [Hoge and Swift 1981, Hoge and Swift 1983; Hoge and Swift 1985; Hoge and Swift 1990]. The laser-induced fluorescence validates the physical process of absorption that is the basis of the algorithm described herein. In particular, active-passive correlation spectroscopy methods [Hoge and Swift 1986a,b,c,d, Hoge et al., 1987; Hoge and Swift 1987] have revealed that concurrently measured water-leaving spectral radiances in the ~600 nm spectral region were highly correlated with the laser-induced phycoerythrin pigment fluorescence. The curvature algorithm [Campbell and Esaias 1983; Campbell and Esaias 1985] was used, together with the airborne laser data, to produce the active-passive correlation spectra [Hoge and Swift 1986a] that allowed the detection of phycoerythrin. The analysis was performed on data sets in which the phycoerythrin and

chlorophyll fluorescence were not coherent in order to permit the unambiguous evaluation of results. To demonstrate to the reader that phycoerythrin affects the water-leaving radiances, the retrieval of phycoerythrin [Hoge and Swift 1986a] using a curvature algorithm (applied to bands not available on MODIS) has been given [Hoge and Swift 1990]. Recently, modeled-unmodeled phycoerythrin retrieval at 488nm has been demonstrated using airborne water-leaving radiances [Appendix A].

As added proof, phycoerythrin fluorescence has recently been seen by other investigators in upwelling radiance spectra. The fluorescence was detected as an increase in the 560-600nm region of surface upwelling irradiance spectra in Lake Washington [Culver and Perry 1994]. The absorption of solar in-water irradiance by the phycoerythrin pigment and the resulting emission of fluorescence at ~560-600nm is physically analogous to the absorption of chlorophyll and its emission at ~683nm. The observation of phycoerythrin fluorescence by Culver and Perry [1994] (in addition to the airborne work discussed previously) demonstrates that phycoerythrin absorption is occurring and detectable with an absorption-based inversion algorithm as discussed herein.

2.1. **Experimental Objective**.

The intended use of the phycoerythrin data product is to allow scientific investigators to study the global distribution(s) of the phycoerythrin pigment and in so doing allow definition of the diversity of phycoerythrin-bearing species such as cyanobacteria. When used in conjunction with chlorophyll distribution, phycoerythrin allows global phytoplankton species variability studies. This is shown in Figure 1 wherein the airborne laser-induced phycoerythrin and chlorophyll fluorescence scatter plot clearly shows the species variability across a Gulf Stream warm core ring [Hoge and

Swift 1983; Hoge and Swift 1985].

2.2. Historical Perspective.

Previously, phycoerythrin has been measured passively by using the 3-band curvature algorithm. The previous uses of the empirical curvature algorithm have been detailed [Hoge and Swift 1986a; Hoge and Swift 1986b; Hoge and Swift 1990]. The curvature algorithm has been shown to retrieve the phycoerythrin pigment in the presence of chlorophyllous (chlorophyll plus phaeophytin) pigment and in the presence of strong chromophoric dissolved organic matter concentrations [Hoge et al 1986a; Hoge and Swift 1986b; Hoge and Swift 1986c, Hoge and Swift 1986d, Hoge and Swift 1993, Hoge et al 1993a; Hoge et al 1993b]. The phycoerythrin pigment has never been detectable using empirical 2-band radiance ratios similar to those used for the satellite Coastal Zone Color Scanner (CZCS) [Hoge et al 1987; Hoge and Swift 1990].

Herein, the phycoerythrin pigment will be retrieved by using oceanic radiance model inversion by matrix methods. Phycoerythrin retrieval using matrix model inversion is undergoing testing using Airborne Oceanographic Lidar (AOL) active-passive ocean color [Hoge et al 1986a; Hoge et al 1986b; Hoge and Swift 1986b; Appendix A herein] data (previously used to successfully retrieve the pigment with the curvature algorithm). It can be reported that model inversion is expected to be successful since previously undetectable chromophoric dissolved organic matter (CDOM) has now been successfully retrieved [Hoge et al. 1995c; Hoge et al., 1999 or Appendix B herein]. The same model inversion methods are being applied to the phycoerythrin retrieval as described in subsequent sections.

2.3. Instrument Characteristics.

Specific spectral bands are required for the model-inversion algorithm. It requires satellite bands to accommodate the PEB(-), PEB(+), and PUB absorption occurring at or near 580, 560, and 495nm respectively [Hoge et al., 1998]. Figure 1 found in Appendix A show the MODIS bands in relation to the PEB(+), PEB(-), and PUB absorption spectra. Figure B1 found in Appendix A shows the details of the gaussian models fitted to the spectra. The model-inversion algorithm is thus ideally, but not optimally, suited for the MODIS instrument.

3.0 Algorithm Description.

The algorithm description is accomplished in 2 segments: the Theoretical Description of Section 3.1 and the Practical Considerations of Section 3.2.

3.1 Theoretical Description

This Theoretical Description is accomplished in 4 sections that address the physics of the algorithm, the mathematical description, the uncertainty estimates, and phycoerythrin and other issues.

3.1.1 Physics of the Algorithm.

Oceanic water-leaving radiances are generated from the incident solar irradiance by the total backscatter and the total absorption of sea water and its constituents. The total backscatter is the rigorous sum of the backscatter of sea water and all the constituents. The total absorption is the rigorous sum of the absorption of sea water and all the constituents. (This assumes that small trans-

spectral contributions due to solar-induced fluorescence and Raman scattering can be ignored). For the purpose of describing the algorithm, assume that the following absorbing constituents are present within the satellite scene: phytoplankton chlorophyllous pigment, PEB(+), PEB(-), PUB, and CDOM. In combination with sea water, these absorbing constituents are assumed to give rise to constituent backscatter, b_{bt}. Thus, at least 6 independent bands are required to retrieve the constituent backscatter and the absorption from the five specific absorbers. The phytoplankton and CDOM absorption coefficients together with the total constituent must be retrieved simultaneously, otherwise their absorption/scattering contributions will be erroneously propagated into the PEB(+), PEB(-), and PUB absorption coefficients.

3.1.1.1 Band Selection for Phycoerythrin Retrieval

As discussed in a previous section Figure 1 and Figure 1B of Appendix A show the MODIS bands in relation to the absorption spectra of phycoerythrin, phytoplankton, CDOM, and constituent backscatter respectively. The reader should consult Appendix A for the details.

3.1.2 Mathematical Description of the Phycoerythrin Algorithm

The phycoerythrin retrieval requires a water-leaving radiance model. A suitable model is described in Appendix A.

3.1.2.1 PUB, PEB(+), PEB(-) Phycoerythrin Algorithm

Phycoerythrin Pigment Absorption Coefficient by Linear Matrix Inversion of a Radiance Model.

The reader is referred to Appendix A for the details (and Appendix B and Appendix C for additional supporting information). The inversion methods described in Appendices A, B, and C are fully applicable to reflectance models [Carder and Stewart 1985; Carder et al., 1986; Carder et al., 1989; Carder et al., 1991; Morel 1988; Sathyendranath et al., 1989; Roesler and Perry 1995; Gordon et al., 1988] with relatively minor modifications. Also, geometrical shape factors may be included in the model, otherwise backscatter coefficient retrievals may contain errors of $\leq$40% depending on the solar angle and hydrosol constituents [Weideman et al., 1995].)

3.1.2.2 Phycoerythrin Algorithm: Other Considerations

The reader is reminded to consult Appendices B and C for supporting details.

3.1.3 Variance or Uncertainty Estimates.

3.1.3.1 Model Simulations

The matrix inversion procedure has undergone simulations with synthetic data (and tests with real data; see Appendix A.) Oceanic radiance model simulations have been completed to evaluate the effects of (a) radiance and (b) model errors on the absorption of phytoplankton, CDOM and TCB [Hoge and Lyon 1996]. Airborne field experiments have also been conducted to address the performance the algorithm/matrix inversion methodology [Hoge et al., 1999; and Appendix A]. To perform the simulations a wide range of constituent backscatter , b_{bt} , phytoplankton chlorophyllous pigment absorption a_{ph} , and CDOM/detritus absorption a_d are assumed to be present. A set of "satellite radiances" are then calculated and stored as an image. Then, to investigate the effects of computer round-off errors the inversion is first executed with no radiance or model errors present.

Preliminary results suggest that the inversion is stable and rapid. The algorithm and machine precision is more than adequate. Airborne field experiments have shown the model to be stable and perform well even in the presence of instrument induced noise [Hoge et al., 1998; and Appendix A herein].

3.1.3.2 Retrieval Error Studies Using Airborne Upwelled Radiances

To date (April 1999) only the unmodelled absorption at 488nm that exceeds the phytoplankton and CDOM absorption has been successfully retrieved, concurrntly with the absorption coefficients of phytoplankton and CDOM as well as total constituent backscatter.

3.1.4. Phycoerythrin Research and Other Issues

Efforts continue in the search for improvements to the phycoerythrin retrieval algorithm. The recent construction of the Shipboard Laser Fluorometer (SLF) has allowed the observation of the high spectral resolution observation of the long-wavelength (~585) PEB(-) fluorescence shift to the short wavelength emission of PEB(+) characteristic of the presence of additional PUB chromophores within the phycoerythrin pigment structure. This instrumentation will allow further validation of the wide area spectral shift observations by the Airborne Oceanographic Lidar [Hoge et al., 1998]. The solar-induced phycoerythrin fluorescence has been observed in the 560-600nm region [Culver and Perry 1994].

3.2 Practical Considerations

3.2.1 Programming and Procedural Considerations

To this point, the reader is aware that error propagation studies are only partially complete

for the IOP retrievals [Hoge and Lyon 1996]. Accordingly, it is expected that some adjustments in the proposed algorithmic procedure will be needed. At this time it is anticipated that the major changes in the algorithm will occur in the model constants. For example, to convert to concentration, the specific absorption coefficients for phycoerythrin for defined oceanic provinces should be used but are simply not available at this time. Our knowledge of appropriate specific absorption coefficients is expected to continually improve, even after launch. Thus, reprocessing of the data should be expected. It is believed that data users will find the results to consistently improve as the MODIS sensor data matures and as model constants improve.

3.2.2 Calibration and Validation

The calibration and validation of the phycoerythrin algorithm and its resultant product will be conducted by additional ship and airborne measurements.

The most critical model parameter(s) that affect the phycoerythrin retrieval are expected to be the chlorophyllous (and the phycoerythrin) pigment spectral specific absorption coefficient variability. This is especially true since the phycoerythrin absorption is only ~1/3 that of chlorophyll at the same wavelength. Thus, a small error in the chlorophyll absorption retrieval and model determination at 488 and 551nm can significantly affect the phycoerythrin retrieval. The CDOM spectral slope and the backscatter wavelength ratio exponent model extrapolation exponent ($n \sim 1.5$) have not displayed inordinate error sensitivity during error analysis simulations. Of highest concern is the lack of widely tested backscatter models.

3.2.2.1 Shipboard Calibration/Validation

Required ship optical measurements should include down-welled irradiance, water-leaving radiances and the inherent optical property, a_{CDOM}. Necessary ship pigment measurements include phytoplankton chlorophyllous pigment, and phycoerythrin pigment (especially with the SLF).

3.2.2.2 Airborne Calibration/Validation

The phycoerythrin algorithm will be further validated by airborne laser-induced and water Raman normalized fluorescence similar to that shown in Appendix A. Immediate post-launch validation efforts of the model-inversion algorithm will be very intensive and will seek to identify possible errors well before the algorithm is used for satellite retrievals. The concurrent upwelled radiances from the NASA Airborne Oceanographic Lidar's ADAS will be inverted and compared to the fluorescence (as has been done in previous algorithm development; Appendix A). The CDOM absorption coefficient as retrieved by the matrix inversion methodology will be validated by airborne retrieval of the CDOM absorption coefficient [Hoge et al 1995a,b,c].

Intermediate IOP products such as the (1) CDOM absorption coefficient, a_{CDOM}, (2) phytoplankton absorption, a_{ph}, and (3) total constituent backscatter, b_{bt}, must also be validated in order to insure that their values are not causing errors in the subsequent phycoerythrin retrieval in which they are used. The a_{CDOM} absorption coefficient is retrieved directly from the airborne 355nm laser-induced and water-Raman-normalized CDOM fluorescence [Hoge et al 1995c; Hoge et al 1993b]. The absorption, a_{ph}, is concurrently obtained by airborne 532nm laser-induced fluorescence within the same spectrum as the phycoerythrin fluorescence (see Appendix A). The agreement of airborne laser-derived chlorophyllous pigment fluorescence with ship-derived pigment [Hoge and Swift 1993] and satellite-derived pigment [Smith et al 1987] has been previously demonstrated. The

use of on-wavelength depth-resolved laser backscatter [Hoge et al 1988] of the water-column and all constituents ($b_{bw} + b_{bt}$) will be explored to provide truth for the constituent backscatter, b_{bt} .

Finally, there are on-going cooperative field programs (ship/aircraft) that are addressing the measurement of both CDOM (by absorption/fluorescence) and phycoerythrin (by extractions). These cooperative efforts will be continued and/or complemented by new ones particularly during the intensive immediate post-launch phase.

A Shipboard Laser Fluorometer (SLF) has recently been constructed and tested on 3 cruises. Having 512 channels it provides remarkable spectral resolution and easily demonstrated the PEB(+) and PEB(-) spectral separation. Since the PEB pigment fluoresces (and PUB does not) the NASA Airborne Oceanographic Lidar (AOL) has two bands to detect the PEB(+) and PEB(-). The successful demonstration of the PEB(+) and PEB(-) spectral shifts in coastal/open-ocean transition regions has been demonstrated [Hoge et al., 1998].

3.2.2.3 Self-Calibration

Self-calibration techniques have been under development and show promise for providing MODIS scene pixels for which the phytoplankton chlorophyllous pigment is determined without the use of surface measurements [Hoge 1994]. The technique exploits the invariance of the empirical curvature algorithm to non-absorbing backscatter (NAB) and CDOM absorption to find pixels having pigment values of 0.35 mg/m^3. The application to MODIS chlorophyllous pigment retrieval (and therefore the improvement of the phycoerythrin retrieval) has been fully described [Hoge 1994].

3.2.3 Quality Control

The initial quality control will consist of a straightforward comparison of the output of the

DAAC with that obtained in our computing laboratory for randomly selected images. Other QC procedures must be developed but do not presently occupy a high priority in comparison to the more pressing near-term algorithm development and validation needs. The self-calibration described in Section 3.2.2.3 is also a quality control procedure that will be used to monitor the algorithm computation sequence.

3.2.4 Exception Handling

There should be no need for handling unusual conditions. The reason for this is that the input to the algorithm are water-leaving radiances that are already quality controlled. Pre-launch testing of the algorithm using simulated and airborne data should give complete identification of the possible exceptions, if any.

3.2.5 Data Dependencies

The phycoerythrin algorithm requires water-leaving radiances. As discussed in a previous section, starting values, if needed, such as chlorophyllous pigment absorption, needed for the phycoerythrin inversion, may be obtained from other MODIS products.

3.2.6 Output Products

The phycourobilin (PUB) and the phycoerythrobilin (PEB), both PEB(+) and PEB(-) absorption coefficient output products, should each have an image format that is identical to the chlorophyllous pigment product. Of course the products being displayed are the PUB and PEB absorption coefficent and not chlorophyllous pigment.

(Scientists are expected to use the PUB and PEB products in conjunction with the chlorophyllous pigment product to create PUB/chlorophyll, PEB(+)/chlorophyll, and PEB(-)/chlorophyll ratio images that are indicative of mesoscale species variability [Hoge and Swift 1983; Hoge and Swift 1985]).

4.0 Constraints, Limitations, and Assumptions

4.1 Assumptions:

1. The chlorophyllous pigment specific absorption coefficient spectral model is assumed to be applicable to the oceanic province where the satellite image was acquired. Initially, only one model (Appendix A) will be used. As more experience is gained, models must be produced for use in several General Oceanic Provinces (GOP) such as the Pacific Basin, North Atlantic etc. The GOP's will eventually be further subdivided into still smaller oceanic provinces having their chlorophyllous pigment model parameters. Likewise, the phycoerythrin specific absorption coefficient models must be continually configured for each province when possible.

2. The CDOM specific absorption coefficient spectral model, at launch, is assumed to be universally applicable with a spectral slope of 0.014 [1/m]. It is well known that the CDOM spectral slope has a small degree of spatial variability [Hoge et al 1993b] however, error analyses indicate that other absorption models (such as the chlorophyllous pigment described above) will most heavily influence the phycoerythrin retrieval errors. As more experience is gained, different CDOM spectral slope values will be defined for the General Oceanic Provinces (GOP) such as the Pacific Basin, North Atlantic etc. Again the GOP's will eventually be further subdivided into still smaller oceanic provinces having their own specific CDOM spectral slope model parameter.

3. Initially, the constituent backscatter spectral model, $b_{\underline{bt}}(\lambda)$, will be assumed to be the same throughout the world's oceans. This spectral model is probably the least well understood. As with the specific absorption coefficient spectral models, with more experience, several models can be produced for use in several General Oceanic Provinces (GOP). Then, different total backscatter spectral models will eventually be assigned to still smaller oceanic provinces.

4. It is assumed that trans-spectral effects such as solar-induced CDOM fluorescence and water Raman scatter are small and can be ignored.

4.2 Constraints and Limitations:

1. Needless to say, the algorithm can only be applied to water-leaving radiances.

5.0 References:

Bidigare, Robert R., Michael E. Ondrusek, John H.Morrow, Dale A. Kiefer, In vivo absorption properties of algal pigments, SPIE Vol. 1302 Ocean Optics X, 290-302.

Campbell, Janet W., and Wayne E. Esaias, Basis for spectral curvature algorithms in remote sensing of chlorophyll, Appl. Opt., 22, 1084-1093, 1983.

Campbell, Janet W., and Esaias, Wayne E., Spatial patterns in temperature and chlorophyll on Nantucket Shoals from airborne remote sensing data, May 7-9, 1981, Jour. of Mar. Res., 43, 139-161, 1985.

Carder, K. L., and R.G. Steward, A remote-sensing reflectance model of a red-tide dinoflagellate off west Florida, Limnol. Oceanogr., 30(2), 286-298, 1985.

Carder, K. L., R.G. Steward, J.H. Paul, and G.A. Vargo, Relationships between chlorophyll and ocean color constituents as they affect remote-sensing reflectance models, Limnol. Oceanogr., 31(2), 403-413 (1986).

Carder, K. L. , R. G. Steward, G. R. Harvey, and P. B. Ortner, Marine humic and fulvic acids: Their effects on remote sensing of ocean chlorophyll, Limno. Oceanogr. 34, 68-81 (1989).

Carder, K.L., S.K. Hawes, K.A. Baker, R.C. Smith, R.G. Steward, and B. G. Mitchell, Reflectance model for quantifying chlorophyll a in the presence of productivity degradation products, Jour. Geophys. Res. 96, No. C11, 20,599-20,611 (1991).

Culver, Mary E., and Mary Jane Perry, Detection of phycoerythrin fluorescence in upwelling irradiance spectra, Eos Trans. AGU 75, 233 (1994).

Culver, Mary E., and Mary Jane Perry, Detection of phycoerythrin fluorescence in upwelling irradiance spectra, Eos Trans. AGU 75, 233 (1994).

Gordon, Howard R., Brown, Otis B., Evans, Robert H., Brown, James W., Smith, Raymond C., Baker, Karen S., and Clark, Dennis K., A semianalytic radiance model of ocean color, Jour. of Geophys. Res., 93, 10,909-10,924 (1988).

Hoepffner, Nicolas, and Shubha Sathyendranath, Determination of the major groups of phytoplankton pigments from the absorption spectra of total particulate matter, Jour,. Geophys. Res. 98, 22,789- 22,803 (1993).

Hoge, F. E., and R. N. Swift, Airborne simultaneous spectroscopic detection of laser-induced water Raman backscatter and fluorescence from chlorophyll a and other naturally occurring pigments, Applied Optics, 20, No. l8, 3l97 (l98l).

Hoge, F. E., and R. N. Swift, Airborne dual-laser excitation and mapping of phytoplankton photopigments in a Gulf Stream warm core ring, Applied Optics, 22, 2272-228l (l983).

Hoge, F. E., and R. N. Swift, Airborne mapping of laser-induced fluorescence of chlorophyll a and phycoerythrin in a Gulf Stream warm core ring, Paper No. 18 in Mapping Strategies in Chemical Oceanography (A. Zirino, ed.), Advances in Chemistry Series No. 209, American Chemical Society, Washington, DC, 335-372 (l985).

Hoge, F. E., and R. N. Swift, Active-passive correlation spectroscopy: A new technique for identifying ocean color algorithm spectral regions, Applied Optics, 25, 2571-2583 (1986a).

Hoge, F. E., and R. N. Swift, Chlorophyll pigment concentration using spectral curvature algorithms: An evaluation of present and proposed satellite ocean color sensor bands, Applied Optics, 25, 3677-3682 (1986b).

Hoge, F. E., R. E. Berry, and R. N. Swift, Active-passive airborne ocean color measurement: l. Instrumentation, Applied Optics, 25, 39-47 (1986a).

Hoge, F. E., R. N. Swift, and J. K. Yungel, Active-passive airborne ocean color measurement: 2. Applications, Applied Optics, 25, 48-57 (1986b).

Hoge, F. E., C. W. Wright, and R. N. Swift, Radiance-ratio algorithm wavelengths for remote

oceanic chlorophyll determination, Applied Optics,26, 2082-2094 (1987).

Hoge, F. E., and R. N. Swift, Ocean color spectral variability studies using solar-induced chlorophyll fluorescence, Applied Optics, 26, 18-21, (1987).

Hoge, F. E., C. Wayne Wright, William B. Krabill, Rodney R. Buntzen, Gary D. Gilbert, Robert N. Swift, James K. Yungel,and Richard E. Berry, Airborne lidar detection of subsurface oceanic scattering layers, Applied Optics 27, 3969-3977 (1988).

Hoge, F. E. and R. N. Swift, Phytosynthetic accessory pigments: Evidence for the influence of phycoerythrin on the submarine light field, Remote Sensing of Environment 34, 19-25 (1990).

Hoge, Frank E. , Robert N. Swift, James Y. Yungel, Anthony Vodacek, Fluorescence of dissolved organic matter: A comparison of North Pacific and North Atlantic Oceans during April 1991, Jour. Geophys. Res. 98, No. C12, 22,779-22,787 (1993a).

Hoge, Frank E. , Anthony Vodacek, Neil V. Blough, Inherent optical properties of the ocean: Retrieval of the absorption coefficient of chromophoric dissolved organic matter from fluorescence measurements, Limno. and Oceanogr., 38(7) 1394-1402 (1993b).

Hoge, F.E., and R.N. Swift, The influence of chlorophyll pigment upon upwelling spectral radiances from the North Atlantic Ocean: An active-passive correlation spectroscopy study, Deep Sea Res.

40, 265-277 (1993).

Hoge, Frank E., Asymmetrical spectral curvature algorithms: oceanic constituents sensitivities, Applied Optics 33, 7764-7769 (1994).

Hoge, F.E., M.E. Williams, R.N. Swift, J.K. Yungel, and A. Vodacek, Satellite retrieval of the absorption coefficient of chromphoric dissolved organic matter in continental margins, Jour. Geophys. Res. 100, 24847-24854, (1995c).

Hoge, Frank E., Robert N. Swift, and James K. Yungel, Oceanic radiance model development and validation: Application of airborne active-passive ocean color spectral measurements, Applied Optics, 34, 3468-3476, (1995b).

Hoge, Frank E., Anthony Vodacek, Robert N. Swift, James Y. Yungel, Neil V. Blough, Inherent optical properties of the ocean: Retrieval of the absorption coefficient of chromophoric dissolved organic matter from airborne laser spectral fluorescence measurements, Applied Optics, 34, 7032-7038, (1995a).

Hoge, Frank E., C. Wayne Wright, Paul E. Lyon, Robert N. Swift, James K. Yungel, "Satellite Retrieval of the Absorption Coefficient of Phytoplankton Phycoerythrin Pigment: Theory and Feasibility Status", submitted 1999, (Appendix A, herein).

Hoge, Frank E., C. Wayne Wright, Paul E. Lyon, Robert N. Swift, James K. Yungel, Satellite retrieval of inherent optical properties by inversion of an oceanic radiance model: A preliminary algorithm, Applied Optics **38**, 495-504 (1999); (Appendix B, herein).

Hoge,Frank E., Wright, C. Wayne, Kana, Todd M., Swift, Robert N., and Yungel, James K., Spatial variability of oceanic phycoerythrin spectral types derived from airborne laser-induced fluorescence measurements, Applied Optics 37, 4744-4749, 1998; (Appendix C, herein).

Hoge, Frank E. and Paul E. Lyon, "Satellite Retrieval of Inherent Optical Properties by Linear Matrix Inversion of Oceanic Radiance Models: An Analysis of Model and Radiance Measurement Errors", Jour. Geophys. Res. 101, 16,631- 16,648, (1996); (Appendix D, herein).

Morel, Andre, Optical modeling of the upper ocean in relation to its biogenous matter content (Case I waters), Jour. Geophys. Res., 93, 10,749-10,768 (1988).

Roesler, Collin S., and Mary Jane Perry, In situ phytoplankton absorption, fluorescence emission, and particulate backscattering spectra determined from reflectance, Jour. Geophys. Res. **100**, 13,279 - 13,294 (1995).

Sathyendranath, S., Luigi Lazzara and Louis Prieur, Variations in the spectral values of specific absorption of phytoplankton, Limnol. and Oceanogr. 32, 403-415 (1987).

Sathyendranath, S., L. Prieur, and A. Morel, A three-component model of ocean colour and its

application to remote sensing of phytoplankton pigment in coastal waters, Int. J. Remote Sensing, **10**, 1373-1394, 1989.

Sathyendranath, S., Frank E. Hoge, Trevor Platt, and Robert N. Swift, Detection of phytoplankton pigments from ocean color: improved algorithms, Appl. Opt. 33, 1081-1089 (1994).

Smith, R. C., O. B. Brown, F. E. Hoge, K. S. Baker, R. H. Evans, R. N. Swift, and W. E. Esaias, Multiplatform sampling (ship, aircraft, and satellite) of a Gulf Stream warm core ring. Appl. Opt. 26: 2068-2081 (1987).

Vernet, M., B. G. Mitchell, O. Holm-Hansen, Adaptation of synechococcus in situ determined by variability in intracellular phycoerythrin-543 at a coastal station off the Southern California coast, USA, Marine Ecology 63, 9-16 (1990).

Weideman, Alan D., Robert H. Stavn, J.R.V. Zanefeld, and M.R. Wilcox, Error in predicting hydrosol backscattering form remotely sensed reflectance, Jour. Geophys. Res. **100**, 13,163 - 13,177 (1995).

Figures

Figure 1. Species variability as indicated by phycoerythrin vs chlorophyll fluorescence.

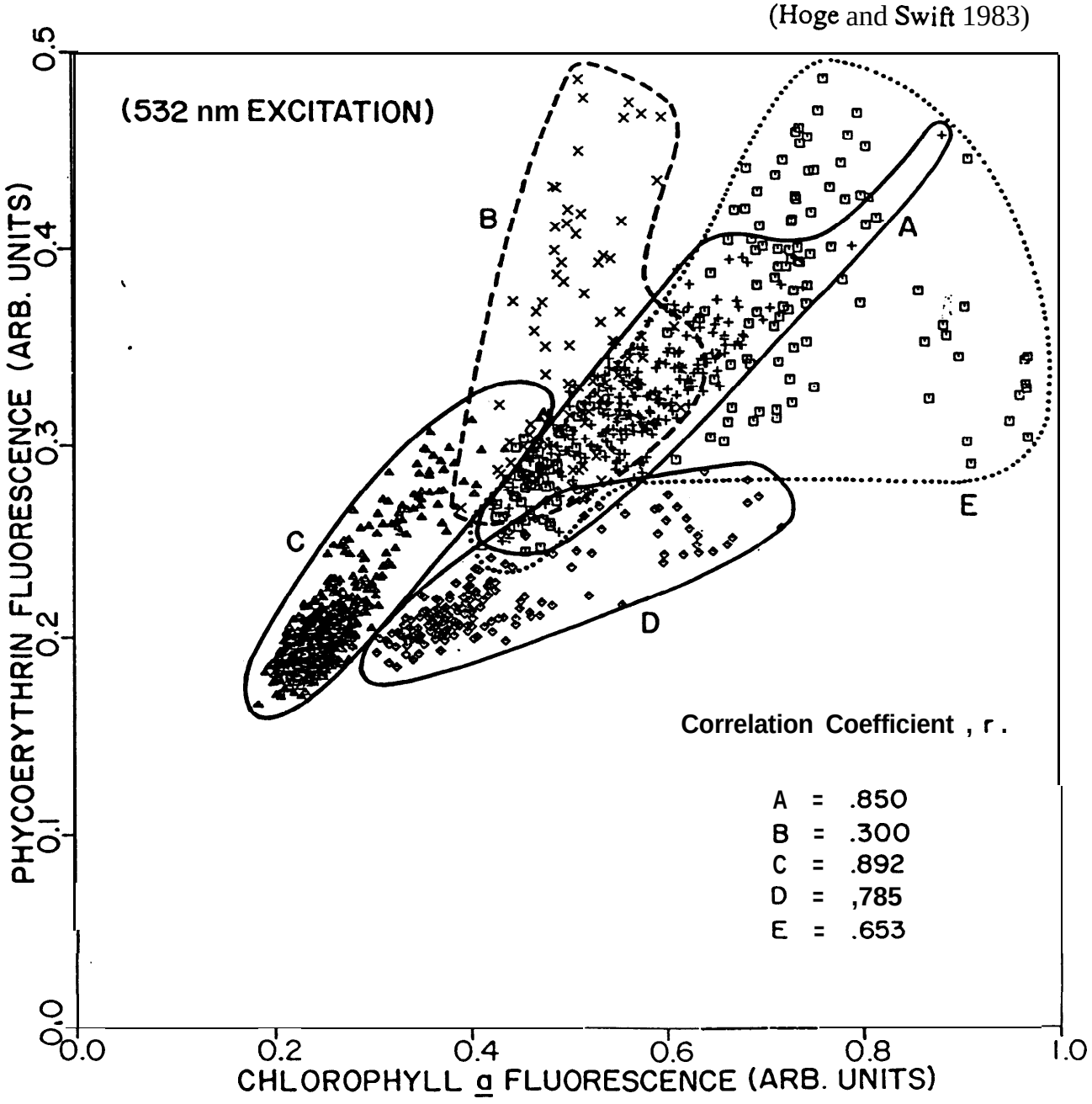
(Hoge and Swift 1983)
(532 nm EXCITATION)
PHYCOERYTHRIN FLUORESCENCE (ARB. UNITS)
CHLOROPHYLL a FLUORESCENCE (ARB. UNITS)
0.0
0.1
0.2
0.3
0.4
0.5
0.6
0.8
1.0
A
B
C
D
E
Correlation Coefficient , r .
A = .850
B = .300
C = .892
D = ,785
E = .653

Figure 1

APPENDIX A

Satellite Retrieval of the Absorption Coefficient of Phytoplankton Phycoerythrin Pigment: Theory and Feasibility Status

Frank E. Hoge and C. Wayne Wright

National Aeronautics and Space Administration

Goddard Space Flight Center

Wallops Flight Facility

Wallops Island, Virginia 23337

Paul E. Lyon, Robert N. Swift, James IS. Yungel

E. G. & G. Inc.

Wallops Flight Facility

Wallops Island, Virginia 23337

ABSTRACT

Oceanic radiance model inversion methods are used to develop a comprehensive algorithm for retrieval of phycoerythrobilin pigment absorption coefficient deficient in phycourobilin pigment, PEB(-), phycoerythrobilin pigment absorption coefficient rich in phycourobilin pigment, PEB(+), and phycourobilin pigment, PUB, (together with the usual "big-three" inherent optical properties: total backscattering coefficient and the absorption coefficients of CDOM/detritus and phytoplankton). This fully-modeled inversion algorithm is then simplified to yield a hybrid modeled-unmodeled inversion algorithm in which the phycoerythrin, PE, absorption coefficient is retrieved as unmodeled 488nm absorption (that exceeds the modeled phytoplankton and CDOM/detritus absorption coefficients). Each algorithm was applied to water-leaving radiances, but only hybrid modeled-unmodeled inversions yielded viable retrievals of the phycoerythrin absorption coefficient. Validation of the phycoerythrin absorption coefficient retrieval was achieved by relative comparison with airborne laser-induced phycoerythrobilin fluorescence. The modeled-unmodeled retrieval of four inherent optical properties by direct matrix inversion is very rapid and well-conditioned but the accuracy is strongly limited by the accuracy of the three principal IOP models across all four spectral bands. Several research areas are identified to enhance the radiance-model-based retrievals: (a) improved phycoerythrobilin and phycourobilin absorption coefficient models, (b) phycoerythrin spectral shifts induced by phycourobilin chromophore substitution at chromophore binding sites, (c) specific-absorption-sensitive phytoplankton absorption modeling, (d) total constituent backscattering model, (e) unmodeled carotinoid and phycocyanin absorption that are not now accounted-for in the chlorophyll dominated phytoplankton absorption coefficient model and (f) iterative inversion techniques to

solve for six constiuents with only five radiances. While considerable progress has been made toward the satellite recovery of phycoerythrin absorption, the maturity of the retrieval is presently insufficient for routine global application. Instead it must currently be used on a regional basis where localized ship and aircraft validation can be made available.

OCIS Codes: 010.4450, 280.0280, 300.6550, 030.5620

Introduction

There are 3 major algal pigment groups' found in marine phytoplankton and bacteria: the chlorophylls, carotenoids, and phycobilins. The phycobilins are phycoerythrin (PE) and phycocyanin. PE is a class of pigment-protein macromolecules with chromophores that absorb light in the ~480-580 spectral region. In cyanobacteria, for example, the functional light harvesting unit is a hexameric protein aggregate (sometimes associated with an additional pigment-protein monomer) that contains from 34-38 covalently bound chromophores[2,3,4,5,6,7,8] These chromophores are of two types: phycoerythrobilin (PEB) having its absorption peak at -565 nm and phycourobilin (PUB) having its absorption peak in the -495 nm region. PEB is necessary for energy transfer between units of the photosynthetic light harvesting antenna and is therefore found in all PE-containing marine cyanobacteria. Truth data in the form of airborne laser-induced PEB fluorescence is frequently available[9] to validate passive remote retrievals. The PUB pigment is not fluorescent so airborne validation is not directly available for this pigment.

Some strains of cyanobacteria have PUB substituted at selected chromophore binding sites on the PE molecule conferring greater light absorption in the blue-green region of the spectrum, while maintaining relatively efficient energy transfer between units. A high degree of PUB substitution is notable in specific strains of the ecologically important marine cyanobacterium genus, *Synechococcus*[4]. The PE spectral absorption band peaks near 565 nm when only PEB chromophores are present (Figure 1 a) [10]. However, the presence of PUB chromophores (with their absorption band peak at 495nm) cause a 10-15 nm blue-shift in the peak wavelength of the PEB absorption spectrum. Specifically, for PUB-containing PE the PEB absorption band occurs near

550 nm regardless of the relative amounts of PUB and PEB (Figure 1). Because of this PUB-induced spectral blue-shift of PEB absorption, the retrieval algorithm to be discussed later must allow for PE spectral absorption with a peak at ~550nm (in addition to the inherent 565nm PEB absorption peak). Thus, naturally occuring PE-containing phytoplankton can possess varying levels of absorption: at ~565nm due to PEB (under PUB pigment deficient conditions), at ~550nm due to PEB (when any amount of PUB substitution occurs at some selected PE chromophore sites), and PUB absorption at -495nm. To facilitate and simplify subsequent discussion of the above pigment absorption bands define: PEB(PUB deficient) = PEB(-) peaking at ~565nm. Similarily, define PEB(PUB present) = PEB(+) peaking at ~550nm. (The grey vertical bars in Figure 1 label the position and approximate width of some available MODIS bands.

Extensive experimental evidence demonstrates that upwelled water-leaving spectral radiances include backscattering and absorption effects of photosynthetic accessory pigments such as phycoerythrin. For example, phycoerythrin pigment has been measured over wide areas of the ocean by active (laser) airborne fluorescence methods since 1979[11] while its passive (solar) detection using upwelled radiances was first noted in 1986[12] and detailed in 1990[9]. The effects of phycoerythrin on the submarine light field have also been seen by other investigators. For example, fluorescence of phycoerythrin was detected as an increase in the 560-600nm region of surface upwelling irradiance spectra in Lake Washington[13]. The airborne active-passive experiments and the in-water observation of solar induced fluorescence[13] fully validate the physical process of *in vivo* absorption by phycoerythrin. It is the purpose of this paper to present

(1) the radiance model inversion theory for PE absorption coefficient retrieval and (2) the current status of the feasibility of its retrieval. Since the absorption of the phycoerythrobilins is only -10% of the chlorophyll and carotenoid absorption in the 495nm and 545nm regions', then IOP models for total backscattering, phytoplankton absorption, and CDOM/detritus must concurrently possess low variability and high accuracy.

Previous oceanic radiance model inversion theory described retrieval of only three inherent optical properties (IOP's): total backscattering, absorption coefficient of chromophoric dissolved organic matter (CDOM)/detritus and the absorption coefficient of phytoplankton[14]. (The retrieval of these three IOPs has also been demonstrated using airborne water-leaving radiances? We strongly recommend that the reader become familar with the content of the latter papers since some of the material is not repeated within this paper.)

Herein, the radiance model inversion theory is extended to accomodate PEB(-) absorption peaking at ~565nm, PEB(+) peaking at ~550nm, and PUB absorption peaking at -495nm. This general theory is then (a) adapted or simplified to provide unmodeled retrieval of the phycoerythrin absorption coefficient and (b) then applied to airborne water-leaving radiances to demonstrate the feasibility of its retrieval. The resulting PE absorption coefficient retrieval is then compared with airborne laser-induced PEB fluorescence.

Phycoerythrin retrieval (and attendant total backscattering coefficient, phytoplankton absorption coefficient, and CDOM/detritus absorption coefficient) allows scientific investigation of the

global distribution(s) of the phycoerythrin pigment and in so doing permits definition of the diversity of phycoerythrin-bearing species especially cyanobacteria. When used in conjunction with chlorophyll distribution, phycoerythrin distribution studies allow global phytoplankton variability studies. The global retrieval of the PE absorption coefficient may also improve understanding of the global nitrogen cycle. This is possible since, for example, the PE-containing ***trichodesmium*** simultaneously fixes nitrogen gas and conducts oxygen-evolving photosynthesis'!

Linear Matrix Inversion of an Oceanic Radiance Model: Retrieval of Modeled IOP's

The oceanic radiance model" used for our retrievals has been validated for precision[18], used for inversion studies[14] describing the retrieval of three inherent optical properties (total backscattering, absorption coefficient of CDOM/detritus and the absorption coefficient of phytoplankton), and applied to airborne water-leaving radiances to demonstrate a preliminary satellite algorithm for retrieval of these three IOPs[15]. In Appendix A the 3-band radiance model inversion theory is extended to accomodate phycoerythrin absorption due to PEB(+), PEB(-), and PUB absorption. The phycoerythrin models for PEB(+), PEB(-), and PUB absorption are described in Appendix B together with the IOP models for phytoplankton, CDOM/detritus, and total constituent backscattering. (Appendices are used to improve the continuity and comprehension of the main body of this paper.)

Linear Matrix Inversion of an Oceanic Radiance Model: Retrieval of Unmodeled Absorption

If IOP models do not accurately describe the actual in-water constituents for all wavelengths used in the linear inversion, then the retrieval success may be compromised[14]. To fully describe the PE absorption, the three phycoerythrin IOP models described in Appendix B should be utilized. To accomodate the retrieval of PE 3 bands are required: one each for PEB(+), PEB(-), and PUB. Including the three bands for phytoplankton, CDOM/detritus, and backscattering, a total of 6 bands are thus required when PE is fully modeled. All the IOP models must accurately describe the IOP's spectral shapes through 6 wavelengths which span at least ~150nm (from 412nm to 565nm). This is especially difficult, for example, when one considers that present backscattering models are used to describe the composite scattering from *all* constituents. Also, the natural spectral variability of phytoplankton absorption alone cannot yet be modeled and further contributes errors to the IOP retrievals.

In this section we describe how the fully-modeled retrieval procedure (described in Appendix A) can be simplified to recover absorption that is not modeled. As discussed previously, additional absorption is contributed by the PE pigment throughout the ~480-565nm region. To demonstrate the retrieval of unmodeled absorption, let us recover the additional absorption (phycoerythrin) at 488nm that exceeds the absorption described by the phytoplankton and CDOM/detritus models. First suppose that the phytoplankton, CDOM/detritus, and backscattering can be (a) modeled by Gaussian, exponential, and wavelength ratio models[14,15] respectively and

(b) satisfactorily retrieved by a 3-band inversion using the 412, 531, and 551nm MODIS bands. Suppose further that we desire the absorption at 488nm that is not modeled by the above phytoplankton, CDOM/detritus, and backscattering models. Then, for additional absorption at 488nm, data in this MODIS band would then be used. Using the results from Appendix B, and the Gaussian notation defined therein, the retrieval matrix would then have the following form for λ_1 = 412, λ_2 = 488, λ_3 = 531, and λ_4 = 551nm:

$$\begin{array}{llll} 0 & G_{N,\lambda_r}(\lambda_1, \lambda_{g,ph}, g_{ph}) & \exp[-S(\lambda_1-\lambda_d)] & (\lambda_b/\lambda_1)^n\, v(\lambda_i) \\ 1 & G_{N,\lambda_r}(\lambda_2, \lambda_{g,ph}, g_{ph}) & \exp[-S(\lambda_2-\lambda_d)] & (\lambda_b/\lambda_2)^n\, v(\lambda_i) \\ 0 & G_{N,\lambda_r}(\lambda_3, \lambda_{g,ph}, g_{ph}) & \exp[-S(\lambda_3-\lambda_d)] & (\lambda_b/\lambda_3)^n\, v(\lambda_i) \\ 0 & G_{N,\lambda_r}(\lambda_4, \lambda_{g,ph}, g_{ph}) & \exp[-S(\lambda_4-\lambda_d)] & (\lambda_b/\lambda_4)^n\, v(\lambda_i) \end{array}$$

$$\begin{array}{lll} a_{PE}(488) & & -a_w(\lambda_1) - b_{bw}(\lambda_1)\, v(\lambda_1) \\ \bullet\ a_{ph}(\lambda_{r,ph}) & = & -a_w(\lambda_2) - b_{bw}(\lambda_2)\, v(\lambda_2) \\ a_d(\lambda_d) & & -a_w(\lambda_3) - b_{bw}(\lambda_3)\, v(\lambda_3) \\ b_{bt}(\lambda_b)] & & -a_w(\lambda_4) - b_{bw}(\lambda_4)\, v(\lambda_4) \end{array} \qquad (4)$$

Notice that the unmodeled PE absorption is being retrieved at the 488nm spectral location as evidenced by the 1 in the PE column within the D matrix and $a_{PE}(488)$ in the IOP vector, p. This arrangement provides for the retrieval of the unmodeled absorption at 488nm that is not fully accounted for by the phytoplankton and CDOM models.

Airborne Field Experiments in the Middle Atlantic Bight

Airborne experiments have been conducted in the Middle Atlantic Bight to test the retrieval of multiple IOP's from water-leaving radiances. We chose a flight track for April 3, 1995 that extended from near the mouth of Delaware Bay southeast to the Sargasso Sea as shown in Figure 2[15]. The complete outbound transect allows a stringent test of the algorithm since 5 different watermasses are traversed: coastal, shelf, slope, Gulf Stream, and Sargasso Sea. (The inbound flight line results were not available since other experiments were conducted thereon.) The airborne active (laser) and passive (solar) instrumentation and its calibration has been previously described". The retrieval of the water-leaving radiances from the at-aircraft radiances by removal of the reflected sky radiance and the reflected path radiance has also been recently described elsewhere'?

Retrieval Results

Figure 3 shows the results of the 4X4 matrix inversion described by equation 4 to retrieve the "excess" absorption coefficient at 488nm together with the CDOM/detritus absorption coefficient, phytoplankton absorption coefficient, and total constituent backscattering at 412nm. In Figure 3a the retrieved absorption coefficient at 488nm is compared to the laser-induced phycoerythrin fluorescence emission. Therein, the laser-induced phycoerythrin PEB fluorescence emission has been regressed to the passively retrieved 488nm absorption coefficient. (The regression was necessary since work is still in progress to develop an algorithm to directly convert the laser-

induced and water-Raman normalized phycoerythrobilin fluorescence to absorption coefficient or to PE pigment concentration.)

The illustrated $a_{PE}(488)$ absorption is attributed to both PUB and PEB pigment absorption. However, it is more likely that the majority of the PE absorption derived in the 488nm band is caused by the presence of the PUB pigment since 488nm is near the PUB absorption peak (review Figure 1). Additionally, from field observations, it is more likely that PUB-containing species will be found in mid-shelf and offshore waters[10,19] where much of the flight data were taken. Furthermore, if the absorption were only PEB, and the absorption were extrapolated from 488nm to the peak absorption of either PEB(+) or PEB(-), the level of absorption at these respective peaks would be inordinately high: 3 to 5 times higher than the absorption found at 412nm for both phytoplankton and CDOM. Since there is such a high correlation between $a_{PE}(488)$ and the laser induced fluorescence of PEB, it follows that the PUB pigment levels are highly correlated to the PEB pigment levels (and this is actually observed in field data'?. As stated previously, PUB does not fluoresce so there is no truth data for PUB to compare with the $a_{PE}(488)$ retrieved absorption.

Figure 3b compares the standard airborne laser-derived CDOM absorption coefficient*' with the passively retrieved CDOM absorption coefficient at 412nm, $a_{CDOM}(412)$. Figure 3c compares the airborne laser-derived phytoplankton absorption coefficient with the passively retrieved phytoplankton absorption coefficient at 412nm, $a_{ph}(412)$. Finally Figure 3d illustrates the passively retrieved total constituent backscattering (TCB) coefficient at 412nm. No airborne laser

instrumentation is yet available to provide truth for the retrieved backscattering product.

The Accessory Pigment Validation Dilemma

To date, satellite algorithms have addressed primarily the retrieval of chlorophyllous pigment. The retrieval of accessory pigments of chlorophyll (e.g. phycoerythrin) provides an immediate validation problem when fluorescence methods are used: inherently high correlation between chlorophyll and the accessory pigment (both of which require concurrent validation). If chlorophyll and PE fluorescence are highly correlated, then a passive retrieval of PE may be erronously attributed to chlorophyll since no independent evidence exists to the contrary. This undesirable (from a validation standpoint) correlation occurs naturally. For example, within a mono-specific bloom of cyanobacteria the chlorophyll:phycoerythrin pigment ratio within each cell is highly likely to be relatively constant over the bloom (leading to linearly correlated fluorescence emissions from both pigments). Fortunately, within large experimental regions, small validation areas can be frequently found for which there is low correlation between chlorophyll and phycoerythrin fluorescence emissions'. Within these regions of low correlation one has increased confidence in the fluorescence-validated pigment absorption coefficients. We will now specifically highlight such important low-correlation areas for chlorophyll and PE and discuss the performance of the PE retrieval algorithm within these specific regions.

Figure 4a, Segment A, shows laser-induced and water Raman normalized chlorophyll and PEB fluorescence having negative correlation: the PEB fluorescence is increasing in the early portion of the Segment while the chlorophyll fluorescence is declining. This is an important region to

evaluate the simultaneous retrieval of both PE and phytoplankton absorption coefficients. In Figure 4b the corresponding oceanic region, Segment A', shows the retrieved $a_{PE}(488)$ is correlated to the laser-induced PEB fluorescence throughout the segment (but obviously not correlated to the phytoplankton chlorophyll fluorescence as demonstrated in Segment A). Likewise, Figure 4c, Segment A", shows that the inversion is simultaneously retrieving the phytoplankton absorption coefficient but not the PE absorption coefficient. Thus, within Segments A, A', and A" the data suggests that the algorithm is successfully retrieving the PE and phytoplankton absorption coefficients concurrently. Similarily, Segments B, B', and B" also suggest (but not as strongly) that the algorithm is concurrently retrieving the PE and phytoplankton absorption coefficients. In other regions it is not easy to determine the success of the concurrent retrievals because of the high correlation that naturally exists between the PE and chlorophyll.

The PE inversion (equation 4) was then applied at other MODIS wavelengths longer than 488nm (and thus more consistent with PEB absorption at 550nm and ~570nm). These retrievals had much lower PE correlation than shown in Figure 4b and were, unfortunately, deemed unsuccessful.

Discussion

Linear matrix inversion methods have been applied to an oceanic radiance model to develop an algorithm for retrieval of the phycoerythrin pigment absorption coefficient. Simultaneously, the algorithm retrieves the usual "big-three" inherent optical properties: total constituent

backscattering coefficient and the absorption coefficients of CDOM/detritus and phytoplankton. The oceanic radiance model inversion is made possible through the use of IOP models for phycoerythxin, phytoplankton, CDOM/detritus, and total backscattering.

When applied to water-leaving radiances at 412, 443,488, 531, and 551nm and one other non-MODIS band, 460nm, the fully-modeled matrix inversion algorithm did not produce a satisfactory retrieval using presently available PE models. The present PE models are based on laboratory absorption spectra of cultures having varying amounts of PUB substituted at chromophore binding sites. The light and nutrient history of the cultures probably do not correspond well to the naturally occuring species being remotely sensed. In addition to the PE model, the retrieval difficulties are probably due to the total constituent backscattering coefficient model. The total constituent backscattering model is used to represent the backscattering of all constituents and accordingly must account for their combined variability; an intimidating and highly challenging requirement. Additional research effort is recommended to identify the specific weaknesses within the PE and TCB models.

The fully-modeled inversion algorithm was then simplified to yield a hybrid modeled-unmodeled inversion algorithm in which the phycoerythrin absorption coefficient was instead retrieved as unmodeled 488nm absorption (that exceeded the modeled phytoplankton and CDOM/detritus absorption coefficients). The algorithm was then applied to the same water-leaving radiances at 412, 488, 53 1, and 55 lnm. The hybrid modeled-unmodeled inversions yielded viable retrievals of the phycoerythrin absorption coefficient. Validation of the

phycoerythrin absorption coefficient retrieval was achieved by comparison with airborne laser-induced phycoerythrobilin fluorescence. To date the most troubling finding is the inadequacy of the longer wavelength (>488nm) modeled-unmodeled retrievals.

The modeled-unmodeled retrieval of four inherent optical properties by direct matrix inversion is very rapid and well-conditioned but the accuracy is strongly limited by the accuracy of the phytoplankton, CDOM-detritus, and TCB IOP models across all four spectral bands. Additionally, there are several issues with the modeled-unmodeled inversion algorithm that should be addressed in future studies. Some of the major questions are briefly described below.

The spectral shift of the PEB absorption spectrum caused by the presence of the PUB pigment is not considered in the modeled-unmodeled inversion technique. As shown in Figure 1, the PEB absorption at 488nm is elevated by the spectral shift of the absorption peak in the presence of PUB. The retrieved absorption attributed to PEB (and the concentration derived from the absorption) will be higher than the true value when the PEB absorption peak is blue shifted. This could cause errors in the derived factors used to convert absorption of PEB to concentrations of PEB pigment.

The modeled-unmodeled inversion technique does not account for the full spectral shape of the PEB absorption. PEB absorption occurs in MODIS bands 488, 531 and 551nm [at different relative levels depending on whether it is PEB(+) or PEB(-)], yet for this modeled-unmodeled technique it is only accounted for in the 488nm band. PE absorption at 531 and

551nm is erroneously embedded in the phytoplankton and CDOM absorption coefficient retrievals. The current 4 band inversion technique was developed from a 3 band inversion arranged to retrieve the "big-three" IOPs. Therefore, it is possible that the phytoplankton model employed for retrieval of 3 constituents has elevated absorption values within the 531 and 551nm bands that account for unmodeled PEB absorption. Since the PEB absorption and phytoplankton absorption are highly correlated as determined by the fluorescence data, this unmodeled absorption may not cause gross errors in the other IOP retrievals. Of course, more accurate retrievals can be accomplished by fully modeling the PEB spectral shapes in all sensor bands.

The above problems could be resolved with a fully modeled inversion that calculates all six IOPs: phytoplankton, CDOM/detritus, TCB, PEB(-), PEB(+), and PUB. This will require more accurate spectral models for the "big-three" IOPs. Also, since there are at most 5 MODIS ocean color bands available in the region from 412nm to 560nm, iterative inversion techniques combined with some additional spectral information will be needed to solve for all 6 IOP values with only 5 bands. Use of the 667nm band is not recommended since it would greatly complicate the phytoplankton spectral model (by requiring a chlorophyll absorption peak at 665nm). Additional bands, especially in the blue-green region of the spectrum, are recommended on future satellites to accommodate more complex inversion techniques.

In addition to the weakness of the TCB model and the PE models, more effort should be expended on the effect of the PUB chromophore substitution on the remotely sensed radiances themselves. While the absorption spectral shifts are seen in laboratory spectra, we need to

determine the extent of the shift ***in situ*** and thus how precisely the effect must be modeled. Furthermore, we have used a single Gaussian phytoplankton spectral model to account for the combined absorption of chlorophyll, carotinoids, and phycocyanin. The inclusion of chlorophyll-dependent parameters within this Gaussian model (to account for specific absorption and/or cell packaging variations) also requires additional research efforts to determine the required precision of such parameterizations.

Appendix A. Linear Matrix Inversion of an Oceanic Radiance Model: Retrieval of Modeled IOP's

It has been shown[14,15] that $a + b_b v = 0$ where v ($\equiv 1\text{-}1/X$) contains the water-leaving radiances and downwelling irradiance and thus is proportional to the remote sensing reflectance. b_b is the total backscattering coeffkient, and is the scalar sum of the backscattering of sea water b_{bw} and all constituents, b_{bt}. I.e., $b_b = b_{bw} + b_{bt}$. Herein, b_{bt} is called the total constituent backscattering (TCB) coefficient and is the rigorous sum of the backscattering of all the individual constituents. Thus, the backscattering from all constituents is combined into this single modelable entity, the total constituent backscattering, b_{bt} b_{bw} is a fundamental constant and can be obtained from published data.

The total absorption coefficient, a, is the scalar sum of the absorption of sea water a_w and all constituents, a_t. I.e., $a = a_w + a_t$. Herein, a, is called the total constituent absorption (TCA). Any number of absorbing (and backscattering) constituents can be accommodated by invoking the linear summability principle for IOP's. a_{w} is a fundamental constant and can also be obtained from published data*'.

Initially assume that there are only six principal oceanic constituent absorbers: phycourobilin $a_{pub}(\lambda_i)$, phycoerythrobilin having phycourobilin chromophore substitution, $a_{pcb(+)}(\lambda_i)$, phycoerythrobilin deficient in phycourobilin chromophore substitution, $a_{pcb(-)}(\lambda_i)$, phytoplankton, a_{ph}, chromophoric dissolved organic matter, $a_{CDOM}(\lambda_i)$, and detritus, $a_{detr}(\lambda_i)$. (Lower case pub,

peb-, and peb+ are used in place of the PUB, PEB(-), and PEB(+) for brevity and readability especially in subscripted notation.) The IOP models are more fully described in Appendix B. The total constituent absorption is a, = $a_{pub}(\lambda_i) + a_{peb-}(\lambda_i) + a_{peb+}(\lambda_i) + a_{ph}(\lambda_i) + a_{CDOM}(\lambda_i) + a_{detr}(\lambda_i)$. To reduce the complexity without severely compromising the retrievals, recall that the detritus absorption has the same spectral form as the CDOM: it declines exponentially with increasing wavelength? The spectral slope of the detritus is, however, considerably more variable. Ranging from 0.004 to 0.020 [1/nm] it encompasses the CDOM slope of 0.014 [1/nm] found by Bricaud[24] and the 0.017 determined by Hoge et al.“. The mean spectral slope of detritus is -0.011 ± 0.002 [1/nm][23]. Thus the complexity of the analysis is reduced if we assume that the spectral average over all detritus spectral absorption a_{detr} yields a slope that is equal to the CDOM spectral slope, S. Then, under this assumption the CDOM spectral absorption, a_{CDOM}, and the detritus absorption, a_{detr}, are indistinguishable and modeled as a single entity, $a_d = a_{CDOM} + a_{detr}$. With these assumptions the total absorption now becomes $a = a_w(\lambda_i) + a_{pub}(\lambda_i) + a_{peb-}(\lambda_i) + a_{peb+}(\lambda_i) + a_{ph}(\lambda_i) + a_d(\lambda_i)$.

At any wavelength λ_i, the model inversion equation, $a + b_b v = 0$, describing the IOP's then becomes,

$$a_{pub}(\lambda_i) + a_{peb-}(\lambda_i) + a_{peb+}(\lambda_i) + a_{ph}(\lambda_i) + a_d(\lambda_i) + b_{bt}(\lambda_i)\, v(\lambda_i) = h(\lambda_i) \qquad \text{(A1)}$$

where, $h(\lambda_i)$ is known as the hydrospheric vector, $h(\lambda_i) \equiv -a_w(\lambda_i) - b_{bw}(\lambda_i)\, v(\lambda_i)$ since it contains all the hydrospheric constants, sea water absorption and backscattering. Of course it also

contains oceanic water-leaving radiances via the v's[14,15].

Equation (Al) contains 6 unknowns for each spectral radiance measurement and no unique solution is possible. Additional equations are provided by IOP spectral models for $a_{pub}(\lambda_i)$, $a_{peb-}(\lambda_i)$, $a_{peb+}(\lambda_i)$, $a_{ph}(\lambda_i)$, $a_d(\lambda_i)$, and $b_{bt}(\lambda_i)$. These IOP models and Gaussian notations are fully described in detail in Appendix B. Substitution of the models into equation Al gives,

$$a_{pub}(\lambda_{r,pub})\, G_{N,\lambda r}(\lambda_i, \lambda_{g,pub}, g_{pub}) + a_{peb-}(\lambda_{r,peb-})\, G_{N,\lambda r}(\lambda_i, \lambda_{g,peb-}, g_{peb-}) + a_{peb+}(\lambda_{r,peb+})\, G_{N,\lambda r}(\lambda_i, \lambda_{g,peb+}, g_{peb+}) + a_{ph}(\lambda_r)\, G_{N,\lambda r}(\lambda_i, \lambda_{g,ph}, g_{ph}) + a_d(\lambda_d) \exp[-S(\lambda_i - \lambda_d)] + b_{bt}(\lambda_b)(\lambda_b / \lambda_i)^n v(\lambda_i) = -a_w(\lambda_i) - b_{bw}(\lambda_i) v(\lambda_i). \quad (A2)$$

Notice that the desired IOP's at their reference wavelengths $a_{pub}(\lambda_{r,pub})$, $a_{peb-}(\lambda_{r,peb-})$, $a_{peb+}(\lambda_{r,peb+})$, $a_{ph}(\lambda_r)$, $a_d(\lambda_d)$, and $b_{bt}(\lambda_b)$ are linearly related to the vector of hydrospheric constants, sea water absorption and backscattering, and radiances (via the v's) on the right side of equation A2. This is very similar to the equation previously used to analyze the effects of radiance and model errors[14] and retrieve the three primary IOP's from airborne water-leaving radiances? The explicit inversion matrices can be immediately written down. For example, six observational sensor wavelengths at $\lambda_1, \lambda_2, \lambda_3, \lambda_4, \lambda_5, \lambda_6$ are used to enumerate or label the rows of the matrices. The six constituent absorbers/scatterers at their reference wavelengths $a_{pub}(\lambda_{r,pub})$, $a_{peb-}(\lambda_{r,peb-})$, $a_{peb+}(\lambda_{r,peb+})$, $a_{ph}(\lambda_{r,ph})$, $a_d(\lambda_d)$, and $b_{bt}(\lambda_b)$ respectively label the columns of the explicit matrix arrangement of equation (A2). Using the mathematical description of the IOP models

given in Appendix B, we find that,

$$G_{N,\lambda r}(\lambda_1,\lambda_{g,pub},g_{pub})\,G_{N,\lambda r}(\lambda_1,\lambda_{g,peb-},g_{peb-})\,G_{N,\lambda r}(\lambda_1,\lambda_{g,peb+},g_{peb+})\,G_{N,\lambda r}(\lambda_1,\lambda_{g,ph},g_{ph})\exp[-S(\lambda_1-\lambda_d)](\lambda_b/\lambda_1)^n\,v(\lambda_1)$$

$$G_{N,\lambda r}(\lambda_2,\lambda_{g,pub},g_{pub})\,G_{N,\lambda r}(\lambda_2,\lambda_{g,peb-},g_{peb-})\,G_{N,\lambda r}(\lambda_2,\lambda_{g,peb+},g_{peb+})\,G_{N,\lambda r}(\lambda_2,\lambda_{g,ph},g_{ph})\exp[-S(\lambda_2-\lambda_d)](\lambda_b/\lambda_2)^n\,v(\lambda_2)$$

$$G_{N,\lambda r}(\lambda_3,\lambda_{g,pub},g_{pub})\,G_{N,\lambda r}(\lambda_3,\lambda_{g,peb-},g_{peb-})\,G_{N,\lambda r}(\lambda_3,\lambda_{g,peb+},g_{peb+})\,G_{N,\lambda r}(\lambda_3,\lambda_{g,ph},g_{ph})\exp[-S(\lambda_3-\lambda_d)](\lambda_b/\lambda_3)^n\,v(\lambda_3)$$

$$G_{N,\lambda r}(\lambda_4,\lambda_{g,pub},g_{pub})\,G_{N,\lambda r}(\lambda_4,\lambda_{g,peb-},g_{peb-})\,G_{N,\lambda r}(\lambda_4,\lambda_{g,peb+},g_{peb+})\,G_{N,\lambda r}(\lambda_4,\lambda_{g,ph},g_{ph})\exp[-S(\lambda_4-\lambda_d)](\lambda_b/\lambda_4)^n\,v(\lambda_4)$$

$$G_{N,\lambda r}(\lambda_5,\lambda_{g,pub},g_{pub})\,G_{N,\lambda r}(\lambda_5,\lambda_{g,peb-},g_{peb-})\,G_{N,\lambda r}(\lambda_5,\lambda_{g,peb+},g_{peb+})\,G_{N,\lambda r}(\lambda_5,\lambda_{g,ph},g_{ph})\exp[-S(\lambda_5-\lambda_d)](\lambda_b/\lambda_5)^n\,v(\lambda_5)$$

$$G_{N,\lambda r}(\lambda_6,\lambda_{g,pub},g_{pub})\,G_{N,\lambda r}(\lambda_6,\lambda_{g,peb-},g_{peb-})\,G_{N,\lambda r}(\lambda_6,\lambda_{g,peb+},g_{peb+})\,G_{N,\lambda r}(\lambda_6,\lambda_{g,ph},g_{ph})\exp[-S(\lambda_6-\lambda_d)](\lambda_b/\lambda_6)^n\,v(\lambda_6)$$

$$\begin{array}{lll}
a_{pub}(\lambda_{r,pub}) & -a_w(\lambda_1) - b_{bw}(\lambda_1)\,v(\lambda_1) \\
a_{peb-}(\lambda_{r,peb-}) & -a_w(\lambda_2) - b_{bw}(\lambda_2)\,v(\lambda_2) \\
a_{peb+}(\lambda_{r,peb+}) & -a_w(\lambda_3) - b_{bw}(\lambda_3)\,v(\lambda_3) \\
a_{ph}(\lambda_{r,ph}) = & -a_w(\lambda_4) - b_{bw}(\lambda_4)\,v(\lambda_4) \\
a_d(\lambda_d) & -a_w(\lambda_5) - b_{bw}(\lambda_5)\,v(\lambda_5) \\
b_{bt}(\lambda_b)] & -a_w(\lambda_6) - b_{bw}(\lambda_6)\,v(\lambda_6)
\end{array} \qquad \text{(A3)}$$

Or,

$$\mathbf{Dp = h} \qquad \text{(A3a)}$$

The column matrix, or vector, of hydrospheric constants (sea water absorption and sea water backscattering), radiances is defined as,

$$\mathbf{h} = \begin{matrix} -a_w(\lambda_1) - b_{bw}(\lambda_1)\, v(\lambda_1) \\ -a_w(\lambda_2) - b_{bw}(\lambda_2)\, v(\lambda_2) \\ -a_w(\lambda_3) - b_{bw}(\lambda_3)\, v(\lambda_3) \\ -a_w(\lambda_4) - b_{bw}(\lambda_4)\, v(\lambda_4) \\ -a_w(\lambda_5) - b_{bw}(\lambda_5)\, v(\lambda_5) \end{matrix} \qquad \text{(A4)}$$

p denotes the state vector of unknown IOP's

$$\mathbf{p} = [a_{pub}(\lambda_{r,pub}),\ a_{peb-}(\lambda_{r,peb-}),\ a_{peb+}(\lambda_{r,peb+}),\ a_{ph}(\lambda_{r,ph}),\ a_d(\lambda_d),\ b_{bt}(\lambda_b)]^T \qquad \text{(A5)}$$

where T is the transpose. (If specific absorption and backscattering coefficients are available, then constituent concentrations can be obtained' from these IOP's[14].

The solution of equation A3a for the unknown IOP's is

$$\mathbf{p} = \mathbf{D}^{-1}\ \mathrm{h}$$

where $\mathbf{D}^{-1}$ is the inverse of D.

The D matrix must be computed and inverted for every pixel or oceanic radiance spectrum since it contains data in addition to model parameters. (To reduce the number of matrix elements that need computation and thus improve the speed of the inversions, the matrix elements in D in equation A3 can be further simplified by prudent choice of reference wavelengths[14].

Appendix B. IOP Spectral Models

Phycourobilin and Phycoerythrobilin IOP Models

Descriptive information about phycoerythrobilin and phycourobilin has already been given in the Introduction. Absorption spectra of PEB and PUB pigments[1,10,26] found in phycoerythrin-containing phytoplankton are shown in Figure B1. It is important to point out here, as we did in the main body of this paper, that the PEB spectral peak is found at ~565nm for PUB deficient species but shifts to ~550nm for "PUB-rich" and "PUB-intermediate" strains". Single Gaussians will be used to analytically represent the PEB(PUB-rich), PEB(+), the PEB(PUB-deficient), PEB(-), and the PUB spectral absorption coefficients. To simplify the notation, the following symbols are defined:

$$G(\lambda_i , \lambda_{g,k} , g_k) = \exp[-(\lambda_i - \lambda_{g,k})^2 / 2g_k^2], \qquad (B1)$$

$$G_{N,\lambda_r}(\lambda_i , \lambda_{g,k} , g_k) = \exp[-(\lambda_i - \lambda_{g,k})^2 / 2g_k^2] / \exp[-(\lambda_r - \lambda_{g,k})^2 / 2g_k^2], \qquad (B2)$$

where G is a single Gaussian and G_{N,λ_r} is a single Gaussian normalized at the reference wavelength, λ_r. The parameter g_k defines the spectral width of the Gaussian about the peak wavelength $\lambda_{g,k}$. The subscript k, represents an IOP modeled by a Gaussian.

When there is no substitution, the phycoerythrobilin pigment absorption coefficient is then,

$$a_{peb\text{-}}(\lambda_i) = a_{peb\text{-}}(\lambda_{r,peb\text{-}})\ G_{N,\lambda r}(\lambda_i\ ,\ \lambda_{g,peb\text{-}}\ ,\ g_{peb\text{-}}), \qquad \text{(B3)}$$

where lower case peb- is used in place of PEB(-) to save space and improve readibility in subscripted notation.

When there is PUB substitution, the phycoerythrobilin pigment absorption coefficient is,

$$a_{peb+}(\lambda_i) = a_{peb+}(\lambda_{r,peb+})\ G_{N,\lambda r}(\lambda_i\ ,\ \lambda_{g,peb+}\ ,\ g_{peb+}). \qquad \text{(B4)}$$

These PEB Gaussians are plotted within Figure Blb and Blc respectively. The Gaussian widths are $g_{peb\text{-}} = 40.5\text{nm}$ (with peak wavelength $\lambda_{g,peb\text{-}} = 575\text{nm}$) and $g_{peb+} = 33.4\text{nm}$ (with peak wavelength $\lambda_{g,peb+} = 555\text{nm}$ respectively.

Similarily, for the PUB absorption coefficient the Gaussian formulation is,

$$a_{pub}(\lambda_i) = a_{pub}(\lambda_{r,pub})\ G_{N,\lambda r}(\lambda_i\ ,\ \lambda_{g,pub}\ ,g_{pub}) \qquad \text{(B5)}$$

This PUB Gaussian is plotted within Figure Bld for $g_{pub} = 12.0\text{nm}$ and $\lambda_{g,pub} = 492\text{nm}$.

During actual inversion applications, the Gaussian peaks $\lambda_{g,pcb-}$, $\lambda_{g,pcb+}$ and $\lambda_{g,pub}$ need not be located precisely coincident with the respective PEB and PUB absorption peaks as long as the spectral width parameters, g_{pcb-}, g_{pcb+} and g_{pub} permit accurate representation of the relative specific absorption coefficient in the sensor observational bands being used in the retrieval.

Phytoplankton Model. A single Gaussian is used to represent the phytoplankton pigment absorption coefficient[14,15] due to chlorophyll, carotinoids, and phycocyanin (with the phycoerythrin separately modeled as previously discussed above). The phytoplankton absorption coefficient is dominated by chlorophyll and the model should probably peak in the 420-460nm blue-green absorption region,

$$a_{ph}(\lambda_i) = a_{ph}(\lambda_{r,ph})\, G_{N,\lambda r}(\lambda_i, \lambda_{g,ph}, g_{ph}) \qquad \text{(B6)}$$

Again, the Gaussian peak need not be located precisely coincident with the chlorophyll absorption peak (~440nm) as long as the spectral width parameter, g_{ph}, permits accurate representation of the relative specific absorption coefficient in the sensor observational bands (Figure B2a).

CDOM/detritus Model. A good representation of the spectral absorption coefficient of chromophoric dissolved organic matter[24,25] and the detrital absorption[22,23] at any wavelength, λ_i

relative to the CDOM and detritus absorption coefficient at a reference wavelength λ_d is (Figure B2b),

$$a_d(\lambda_i) = a_d(\lambda_d) \exp [-S(\lambda_i - \lambda_d)], \quad \text{(B7)}$$

(where S is the spectral slope). (Again, to reduce the complexity of the analysis herein, we have assumed that the spectral average over all detritus absorption yields a slope that is equal to the CDOM spectral slope[14]. The reference wavelength, λ_d, need not coincide with the sensor observational bands. However, reference wavelengths in the red are avoided since the CDOM and detrital absorption are lower in these regions. For those wishing to separately include the detritus along with the CDOM absorption, it is evident how one can extend the matrix inversion to include it. Because of the dominant character of CDOM, and for brevity, the CDOM/detritus absorption, a_d, may from time to time be referred to as CDOM absorption.)

Backscattering Model. The following model is used to describe the total constituent backscattering coefficient at any wavelength λ_i relative to the total constituent backscattering at a reference wavelength[14,15] λ_b,

$$b_{bt}(\lambda_i) = b_{bt}(\lambda_b) (\lambda_b / \lambda_i)^n , \quad \text{(B8)}$$

where n is parameterized by an empirical radiance ratio described below. This TCB model

(Figure B2c) was chosen by analogy with the work of others. For example, Morel[27] provided a backscattering model for chlorophyll that varied inversely with wavelength. Similarly, for non-absorbing backscatterers such as coccoliths, Gordon et al.[17] used a $(550/\lambda)^n$ where n >1. Sathyendranath et al.[28] suggested a $(1/\lambda)^n$ model for detrital particles. Lee et al.[29] used a similar model and showed that the exponent can vary from 0 - 2.4. Maffione et al.[30,31] field measurements showed that the spectral backscattering exponent can vary from 2.0 to 4.1. Finally, by inverting (a) a diffuse attenuation coefficient model and (b) the radiance model, we have recently shown that the TCB model in equation B8 is valid from ~410-580nm[14]. Accordingly, the reference wavelength, λ_b, and computations of $b_{bt}(\lambda_i)$ are confined to this range. The reference wavelength, λ_b, need not coincide with the sensor observational bands[14].

Error analyses have shown that the accuracy of the CDOM absorption retrieved by linear inversion is strongly dependent on the accuracy of the exponent ***n*** in the TCB spectral model[14]. Accordingly, the spatially variable ***n*** exponent[30,31,32] should not be held constant. Instead, the ***n*** exponent needs to be varied to accommodate the different types of scattering constituents in the water masses under observation. This is accomplished by varying ***n*** based on a "radiance-ratio", L_{412}/L_{551}. Using extensive airborne active-passive airborne data, this "radiance-ratio" was found to be linearly related to the exponent ***n*** such that[15]

$$n = a_1 L_{412}/L_{551} + a_2. \qquad (B9)$$

The scale and offset, a, and a_2, used to convert the radiance-ratio to the exponent n depend to some extent on the concentration of the constituent scatterers that make up the TCB coefficient.

The use of a constant scale and offset to convert the radiance ratio to an exponent n will cause errors in the CDOM retrieval. More data and analyses are needed to derive a set of "typical" parameters one can expect for different types of reflectance spectra. The parameters a, and a_2, were derived by minimizing the error in the retrieved CDOM coefficient as compared to the airborne data available for the data set. Hopefully, a table of values can be eventually produced to allow a user to choose the a, and a_2 parameters based on spectral shapes and/or geographic regions. The need to vary the n exponent would be eliminated if improved backscattering spectral models were available to better represent the diverse types of scatterers. Choosing an uncomplicated backscattering spectral model to represent many different constituents requires empirical methods to fit the various combinations of scattering constituents found in the global oceans. Further development of the wavelength ratio TCB model is recommended.

Notation

a	total absorption coefficient, $a_w + a_{,,}$ (m^{-1})
a_{CDOM}	absorption coefficient of chromophoric dissolved organic matter (m^{-1})
a_d	absorption coefficient of CDOM and detritus (m^{-1})
a_{detr}	absorption coefficient of detritus (m^{-1})
a_{ph}	absorption coefficient of phytoplankton (m^{-1})
a_{pub}	absorption coefficient of phycourobilin (m^{-1})
a_{peb}	absorption coefficient of phycoerythrobilin (m^{-1})
a_{peb+}	abs. coeff. for PEB having PUB chromophore substitution
a_{peb-}	abs. coeff. for PEB deficient in PUB chromophore substitution
a_t	total constituent absorption (TCA) (m^{-1})
a_w	absorption coefficient of water, (m^{-1})
b_b	total backscattering coefficient, $b_{bt} + b_{,,}$ (m^{-1})
b_{bt}	total constituent backscattering (TCB), (m^{-1})
b_{bw}	backscattering of seawater (m^{-1})
CDOM	chromophoric dissolved organic matter
D	data and model matrix
g	phytoplankton Gaussian model spectral width parameter
G	Gaussian model
$G_{N,\lambda r}$	Gaussian model normalized at λ_r
h	vector of hydrospheric constants
IOP	inherent optical property

k	subscript labeling an IOP being modelled by a Gaussian
n	total constituent backscattering wavelength-ratio spectral model exponent
p	oceanic state vector of retrieved IOP's
PE	phycoerythrin pigment
PEB	phycoerythrobilin pigment
PEB(+)	PEB with PUB substitution at chromophore binding sites
PEB(-)	PEB with negligible PUB substitution
PUB	phycourobilin pigment
S	spectral slope for a_d model
TCA	total constituent absorption, a,
TCB	total constituent backscattering, b_{bt}
v	(1 - l/X) (dimensionless)
X	$b_b/(b_b + a)$ (dimensionless)
λ_b	reference wavelength for total constituent backscattering (TCB), (nm)
λ_d	reference wavelength for CDOM/detritus absorption, (nm)
λ_g	peak wavelength for Gaussian absorption model (nm)
λ_i	wavelength of observational bands, i = 1, 2, 3 . . .
λ_r	common reference wavelength for all IOP's
λ	wavelength (nm)

Acknowledgements

The continued support and encouragement of the MODIS Project and of NASA Headquarters Ocean Biology/Biogeochemmistry Program managers is gratefully acknowledged.

References

1. Robert R. Bidigare, Michael E. Ondrusek, John H.Morrow, Dale A. Kiefer, "In vivo absorption properties of algal pigments," SPIE 1302, Ocean Optics X, 290-302 (1990).

2. T. M. Kana, N. L. Feiwel, and L. C. Flynn, "Nitrogen starvation in marine Synechococcus strains: clonal differences in phycobiliprotien breakdown and energy coupling," Marine Ecology Progress Series 88, 75-82 (1992).

3. T. M. Kana and P.M. Glibert. "Effect of irradiances up to 2000 $\mu E\ m^{-2}\ s^{-1}$ on marine *Synechococcus* WH7803: I. Growth, pigmentation, and cell composition," Deep-Sea Res. 34, 479-495 (1987).

4. L. J. Ong and A.N. Glazer, "Phycoerythrins of marine unicellular cyanobacteria. I. Bilin types and locations and energy transfer pathways in *Synechococcus* spp. phycoerythrins," J. Biol. Chem. 266, 9515-9527 (1991).

5. R. V. Swanson, L.J. Ong, S.M. Wilbanks, and A. Glazer, "Phycoerythrins of Marine Unicellular Cyanobacteria, II. Characterization of phycobiliprotiens with unusually high phycourobilin," Jour. Biol. Chem. 266, 9528-9534 (1991).

6. S. M. Wilbanks, R. de Lorimier, and A. Glazer, "Phycoerythrins of Marine Unicellular Cyanobacteria, III. Sequence of a class 11 phycoerythrin," Jour. Biol. Chem. 266, 9535-9539

(1991).

7. L. J. Ong and A. Glazer, “Structural studies of phycobiliprotiens in unicellular marine cyanobacteria", in Light-Energy Transduction in Photosynthesis: Higher Plant and Bacterial Models, S.E. Stevens, Jr. and D.A. Bryant, Eds., published by The American Society of Plant Physiology (1988).

8. S. M. Wilbanks and A. Glazer, “Rod structure of a phycoerythrin II-containing phycobilisome. I. Organization and sequence of the gene cluster encoding the major phycobiliprotein rod components in the genome of marine *Synechococcus* SP WH8020.," Jour. Biol. Chem. 268, 1226-1235 (1993).

9. F. E. Hoge and R. N. Swift, "Phytoplankton Accessory Pigments: Evidence for the Influence of Phycoerythrin on the Submarine Light Field”, Remote Sensing of Environ. 34, 19-25 (1990).

10. Frank E. Hoge, C. Wayne Wright, Todd M. Kana, Robert N. Swift, and James K. Yungel, “Spatial variability of oceanic phycoerythrin spectral types derived from airborne laser-induced fluorescence measurements,” Appl. Opt. 37, 4744-4749 (1998).

11. F. E. Hoge and R. N. Swift, “Airborne simultaneous spectroscopic detection of laser-induced water-Raman backscatter and fluorescence from chlorophyll a and other naturally occurring pigments”, Appl. Opt. 20, 3197-3205 (1981).

12. F. E. Hoge and R. N. Swift, “Active-passive correlation spectroscopy: A new technique for identifying ocean color algorithm spectral regions”, Appl. Opt. 25, 2571-2583 (1986).

13. Mary E. Culver and Mary Jane Perry, “Detection of phycoerythrin fluorescence in upwelling inadiance spectra,” Eos Trans. AGU 75, 233 (1994).

14. Frank E. Hoge and Paul E. Lyon, “Satellite Retrieval of Inherent Optical Properties by Linear Matrix Inversion of Oceanic Radiance Models: An Analysis of Model and Radiance Measurement Errors,” Jour. Geophys. Res. **101, 16,631-** 16,648 (1996).

15. Frank E. Hoge, C. Wayne Wright, Paul E. Lyon, Robert N. Swift and James **K.** Yungel, “Satellite retrieval of inherent optical properties by inversion of an oceanic radiance model: A preliminary algorithm,” Appl. Opt. 38, **495-504** (1999).

16. D. G. **Capone,** J.P. Zehr, H.W. Paerl, B. Bergman, and E.J. Carpenter, "***Trichodesmium,*** a globally significant marine cyanobacterium,” Science 276, 1221-1229 (199’7).

17. Howard Gordon, O.B. Brown, R.H. Evans, J.W. Brown, R.C. Smith, **K.S.** Baker, and D.K. Clark, “A semianalytic radiance model of ocean color,” J. Geophys. Res. 93, **10,909-10,924** (1988).

18. F. E. Hoge, R.N. Swift, and J.K. Yungel, “Oceanic radiance model development and

validation: application of airborne active-passive ocean color spectral measurements," Appl. Opt. 34, 3468-3476 (1995).

19. R. J. Olson, S.W. Chisholm, E.R. Zettler, and E.V. Armbrust, "Pigments, size, and distribution of ***Synechococcus*** in the North Atlantic and Pacific Oceans," Limnol. Oceanogr. 35, 45-58 (1990).

20. Frank E. Hoge, Anthony Vodacek, Robert N. Swift, James Y. Yungel, Neil V. Blough, "Inherent optical properties of the ocean: Retrieval of the absorption coefficient of chromophoric dissolved organic matter from airborne laser spectral fluorescence measurements," Appl. Opt. 34, 7032-7038 (1995).

21. Robin M. Pope and Edward S. Fry, "Absorption spectrum (380-700nm) of pure water: II. Integrating cavity measurements," Appl. Opt. 36, 8710-8723 (1997).

22. N. Hoepffner and S. Sathyendranath, "Determination of the major groups of phytoplankton pigments from the absorption spectra of total particulate matter," J. Geophys. Res., 98, 22,789-22,803 (1993).

23. Collin S. Roesler, Mary Jane Perry, and Kendall L. Carder, "Modeling in situ phytoplankton from total absorption spectra in productive inland marine waters," Limnol. and Oceanogr. 34,

15 10-1523 (1989).

24. A. Bricaud, A. Morel, and L. Prieur, “Absorption by dissolved organic matter of the sea (yellow substance) in the UV and visible domains,” Limnol. Oceanogr. 26, 43-53 (1981).

25. F. E. Hoge, A. Vodacek, N.V. Blough, “Inherent optical properties of the ocean: Retrieval of the absorption coefficient of chromophoric dissolved organic matter from fluorescence measurements,” Limno. and Oceanogr. 38, 1394-1402 (1993).

26. M. Vemet, B. G. Mitchell, 0. Holm-Hansen, “Adaptation of synechococcus in situ determined by variability in intracellular phycoerythrin-543 at a coastal station off the Southern California coast, USA,” Marine Ecology 63, 9-16 (1990).

27. Andre’ Morel, “Optical modeling of the upper ocean in relation to its biogenous matter content (case I waters),” J. Geophys. Res. 93, 10,749-10,768 (1988).

28. S. Sathyendranath, L. Prieur, and A. Morel, “A three-component model of ocean colour and its application to remote sensing of phytoplankton pigment in coastal waters,” Int. J. Remote Sens. 10, 1373-1394 (1989).

29. Z. P. Lee, K.L. Carder, S.K. Hawes, R.G. Steward, T.G. Peacock, and C.O. Davis, “Model for the interpretation of hyperspectral remote-sensing reflectance,” Appl. Opt. 33, 5721-5732

(1994).

30. R. A. Maffione, D.R. Dana, J.M. Voss, “Spectral dependance of optical backscattering in the ocean,” Proceedings of the Optical Society of America annual meeting, Portland, Oregon, September 10-15, 1995, paper MDD4, p. 57 (1995).

31. Robert A. Maffione and D.R. Dana, Instruments and methods for measuring the backward-scattering coefficient of ocean waters, Appl. Opt. 36, 6057-6067 (1997).

32. Maffione, R.A. and D.R. Dana, “In-situ characterization of optical backscattering and attenuation for lidar applications,” Selected Papers on Lidar Remote Sensing of Natural Waters: from Theory to Practice, V. Feigels and Y. Kopelevich, SPIE 2964 152-163 (1996a).

Author Address List

Frank E. Hoge and C. Wayne Wright

Building N-159

National Aeronautics and Space Administration

Goddard Space Flight Center

Wallops Flight Facility

Wallops Island, Virginia 23337

hoge@osbl.wff.nasa.gov

Paul E. Lyon, Robert N. Swift and James K. Yungel

E. G. & G. Services Inc.

Wallops Flight Facility

Wallops Island, Virginia 23337

Figure Captions

Figure 1. PEB excitation (absorption) spectra of three cultures of phytoplankton having phycoerythrin: PUB-rich (WH 8102), PUB-intermediate (WH 7803), and PUB-deficient (WH 8018)[10]. The peak of the PEB excitation (absorption) spectrum shifts ~15nm toward the blue when PUB chromophores are substituted within the hexameric protein aggregate. The vertical bars illustrate the location of the 412, 488, 531, and 551nm MODIS bands.

Figure 2. The outbound flight track of the NASA P3-B aircraft with Airborne Oceanographic Lidar (AOL) and passive radiometeric subsystems on April 3, 1995. (The inbound flight track data was not available for analyses because of other experiments.)

Figure 3. (a) Comparison of the airborne laser-induced phycoerythrobilin pigment fluorescence with the passively retrieved unmodeled absorption coefficient at 488nm, $a_{PE}(488)$. The laser-induced fluorescence has been scaled and offset to provide improved agreement with the passively retrieved absorption coefficient. (b) Comparison of the standard airborne laser-derived CDOM absorption coefficient" with the passively retrieved CDOM/detritus absorption coefficient at 412nm, $a_d(412)$. (c) Comparison of the airborne laser-derived phytoplankton absorption coefficient with the passively retrieved phytoplankton absorption coefficient at 412nm, $a_{ph}(412)$. (d) The passively retrieved total constituent backscattering (TCB) coefficient at 412nm, $b_{bt}(412)$. The total backscattering may be obtained by adding the backscattering of water at 412 nm, $b_{bw}(412)$. No airborne laser instrumentation is yet available to provide truth for the retrieved backscatteri ng product.

Figure 4. (a) Two segments, A and B, displaying negative correlation between laser-induced phycoerythrobilin fluorescence and chlorophyll fluorescence. These negative correlation regions are important for illustrating phycoerythrin absorption coefficient retrieval in the presence of normally-correlated phytoplankton chlorophyll. (b) Two segments, A' and B', displaying correlation of the retrieved unmodeled phycoerythrin absorption coefficient, $a_{PE}(488)$, and the phycoerythrobilin fluorescence. (c) Two segments, A" and B", displaying correlation of the retrieved phytoplankton absorption coefficient, $a_{ph}(412)$, and the chlorophyll fluorescence. Comparing segments A, A', and A" the data strongly suggests that the multiband model inversion is simultaneously retrieving both the phycoerythrin absorption coefficient and the phytoplankton absorption coefficient. Similarily, comparing segments B, B', and B" the data suggests, but less convincingly, that the multiband model inversion is concurrently retrieving both the phycoerythrin and the phytoplankton absorption coefficients.

Figure B1. (a) Excitation (absorption) spectra of phycoerythrin PEB having various degrees of PUB substitution at chromophore binding sites. The presence of PUB causes a 10-15nm blue-shift in the PEB absorption. This figure panel is identical to Figure 1 and is provided here for improved understanding of the analytical models. (b) Gaussian model fit to the absorption spectrum of PEB that is deficient in PUB substitution. The optimum fit is chosen to occur at the MODIS band positions not the peak wavelength. (c) Same as (b) except for PEB that is rich in PUB substitution. (d) Gaussian model fit to the absorption spectrum of PUB. The optimum fit is chosen to occur at the 488nm MODIS band position.

Figure B2. (a) The phytoplankton model analytically represented by a single Gaussian, (b) the CDOM/detritus exponential model, (c) the total constituent backscattering (TCB) wavelength ratio model.

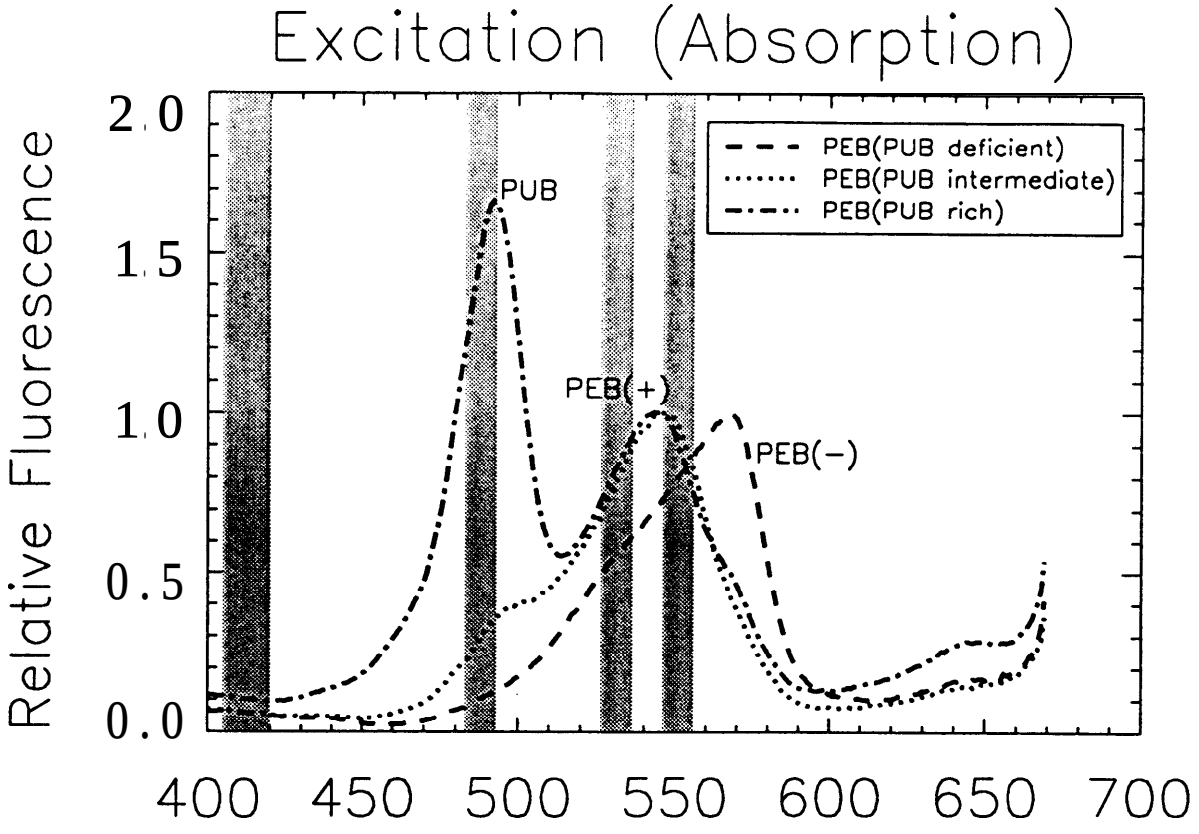
Excitation (Absorption)
Relative Fluorescence
2.0
1.5
1.0
0.5
0.0
400
450
500
550
600
650
700
PUB
PEB(+)
PEB(−)
PEB(PUB deficient)
PEB(PUB intermediate)
PEB(PUB rich)

Figure 1

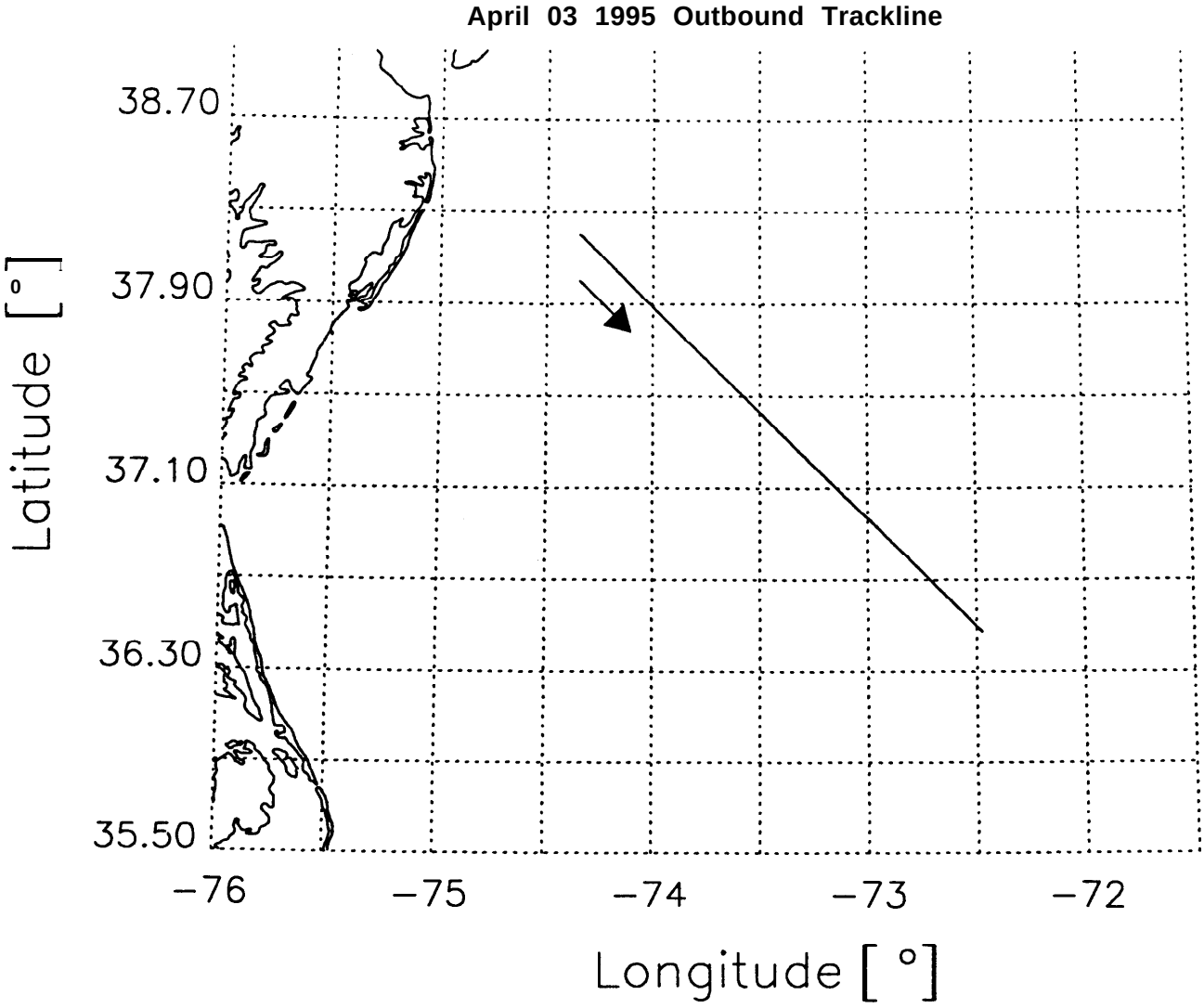
April 03 1995 Outbound Trackline
38.70
37.90
37.10
36.30
35.50
Latitude [°]
−76
−75
−74
−73
−72
Longitude [°]

Figure 2

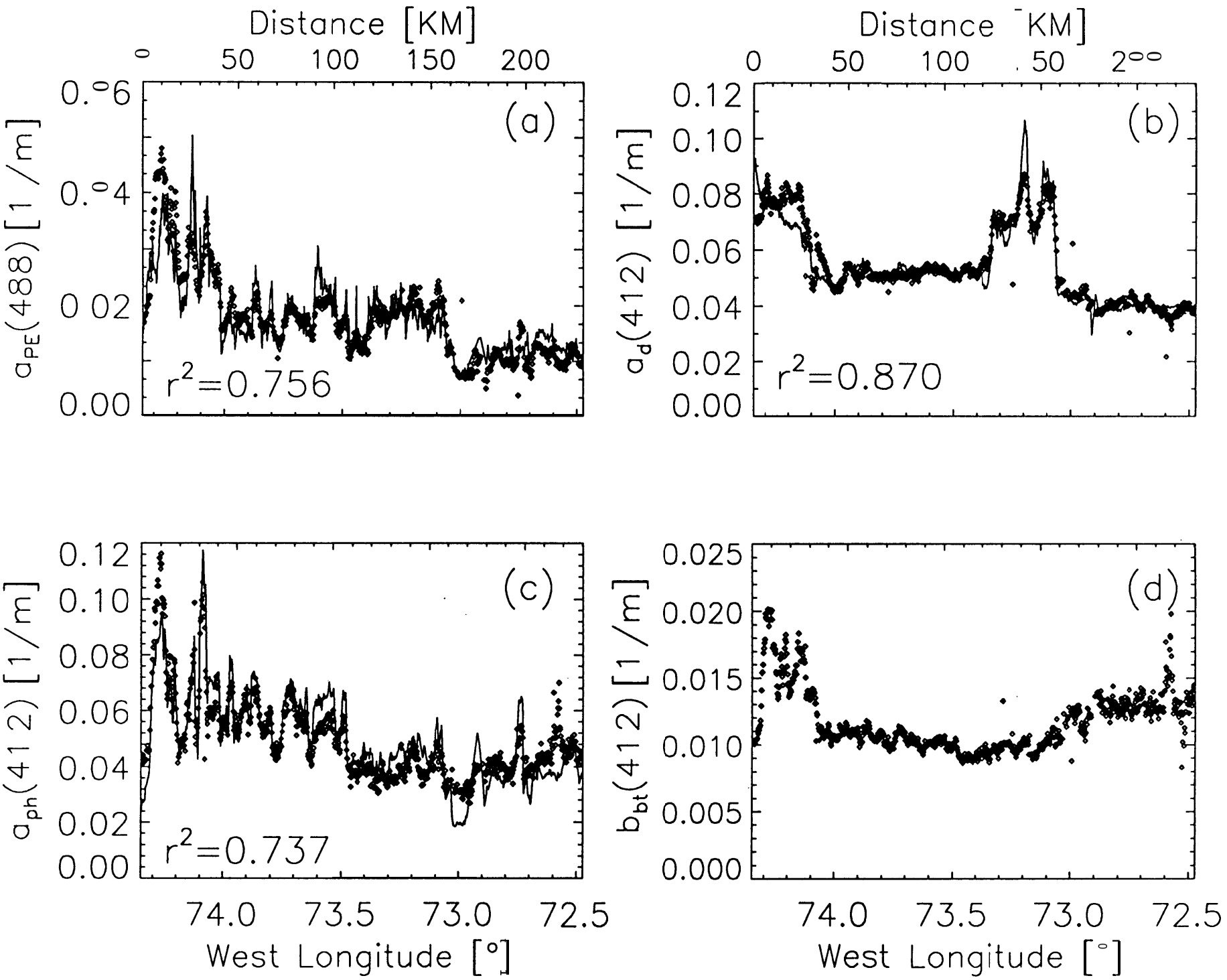
Distance [KM]
0
50
100
150
200
0.06
0.04
0 02
0.00
$a_{PE}(488)$ [1/m]
(a)
r^2=0.756
Distance [KM]
0
50
100
150
200
0.12
0.10
0.08
0.06
0.04
0.02
0.00
$a_d(412)$ [1/m]
(b)
r^2=0.870
0.12
0.10
0.08
0.06
0.04
0.02
0.00
$a_{ph}(412)$ [1/m]
(c)
r^2=0.737
0.025
0.020
0.015
0.010
0.005
0.000
$b_{bt}(412)$ [1/m]
(d)
74.0
73.5
73.0
72.5
West Longitude [°]
74.0
73.5
73.0
72.5
West Longitude [°]

Figure 3

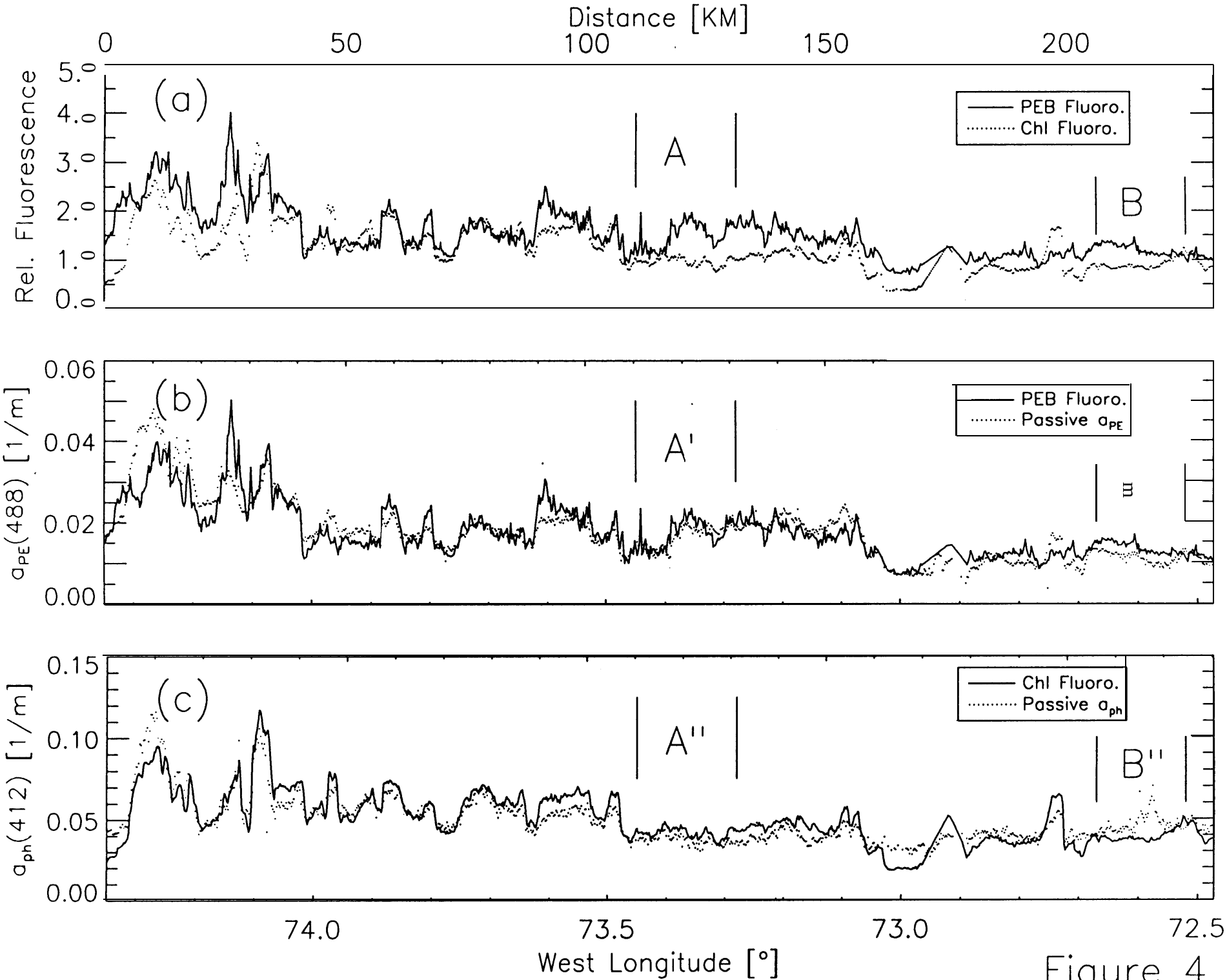
Distance [KM]
0
50
100
150
200
(a)
Rel. Fluorescence
PEB Fluoro.
Chl Fluoro.
A
B
(b)
$a_{PE}(488)$ [1/m]
PEB Fluoro.
Passive a_{PE}
A'
B'
(c)
$a_{ph}(412)$ [1/m]
Chl Fluoro.
Passive a_{ph}
A''
B''
74.0
73.5
73.0
72.5
West Longitude [°]

Figure 4

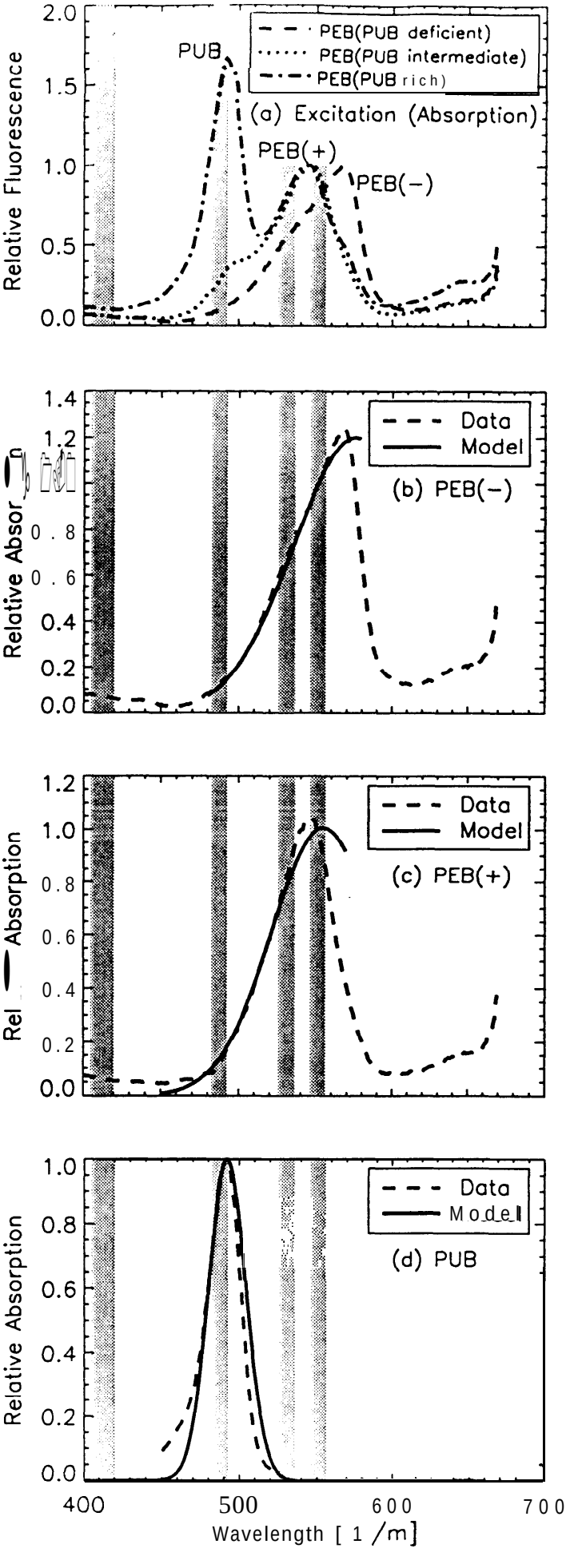
PEB(PUB deficient)
PEB(PUB intermediate)
PEB(PUB rich)
PUB
(a) Excitation (Absorption)
PEB(+)
PEB(−)
Relative Fluorescence
2.0
1.5
1.0
0.5
0.0
Data
Model
(b) PEB(−)
1.4
1.2
0.8
0.6
0.4
0.2
0.0
Data
Model
(c) PEB(+)
1.2
1.0
0.8
0.6
0.4
0.2
0.0
Data
Model
(d) PUB
Relative Absorption
1.0
0.8
0.6
0.4
0.2
0.0
400
500
600
700
Wavelength [1 /m]

Figure B1

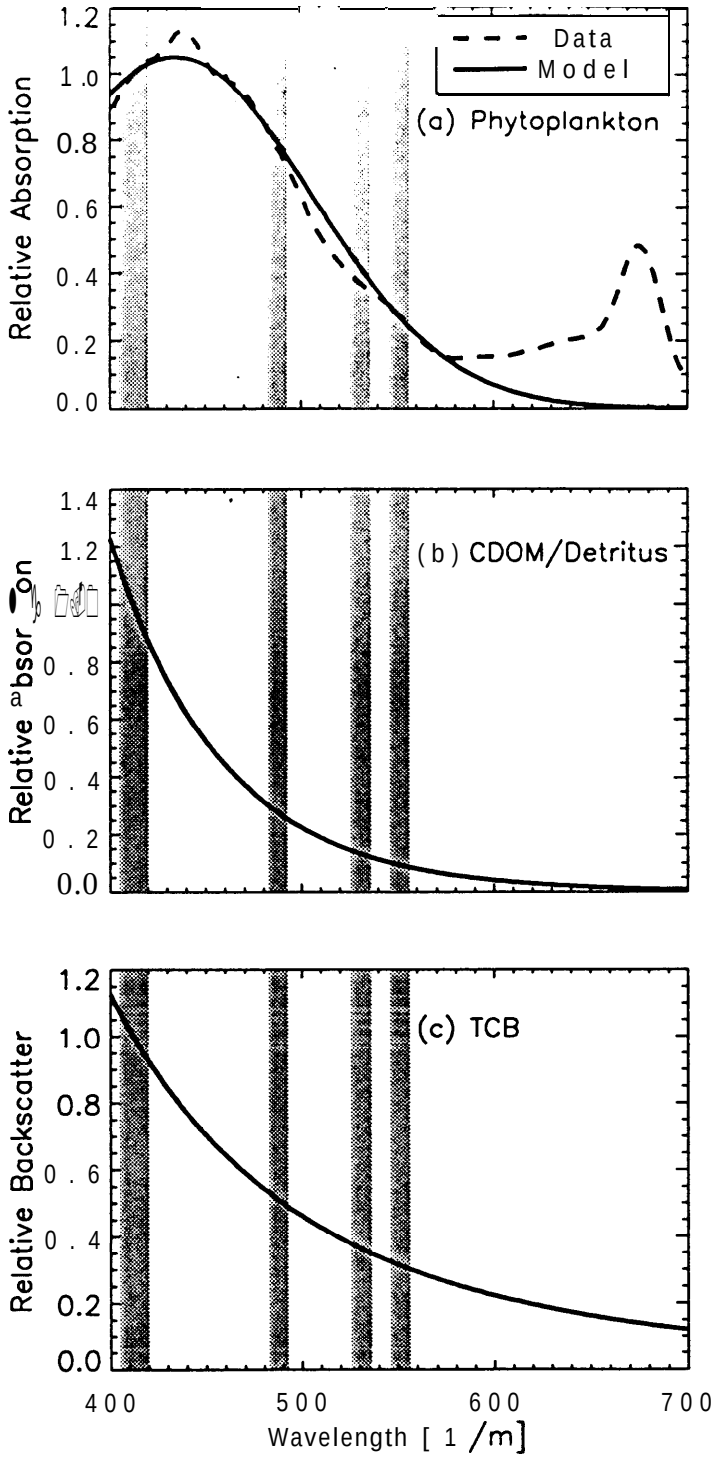
Data
Model
(a) Phytoplankton
Relative Absorption
1.2
1.0
0.8
0.6
0.4
0.2
0.0
(b) CDOM/Detritus
1.4
1.2
0.8
0.6
0.4
0.2
0.0
(c) TCB
Relative Backscatter
1.2
1.0
0.8
0.6
0.4
0.2
0.0
400
500
600
700
Wavelength [1 /m]

Figure B2

APPENDIX B

Satellite retrieval of inherent optical properties by inversion of an oceanic radiance model: a preliminary algorithm

Frank E. Hoge, C. Wayne Wright, Paul E. Lyon, Robert N. Swift, and James K. Yungel

Satellite retrieval of inherent optical properties by inversion of an oceanic radiance model: a preliminary algorithm

Frank E. Hoge, C. Wayne Wright, Paul E. Lyon, Robert N. Swift, and James K. Yungel

A previously published radiance model inversion theory has been field tested by using airborne water-leaving radiances to retrieve the chromophoric dissolved organic matter (CDOM) and detritus absorption coefficient, the phytoplankton absorption coefficient, and the total backscattering coefficient. The radiance model inversion theory was tested for potential satellite use by comparing two of the retrieved inherent optical properties with concurrent airborne laser-derived truth data. It was found that (1) matrix inversion of water-leaving radiances is well conditioned even in the presence of instrument-induced noise, (2) retrieved CDOM and detritus and phytoplankton absorption coefficients are both in reasonable agreement with absorption coefficients derived from airborne laser-induced fluorescence spectral emissions, (3) the total backscattering retrieval magnitude and variability are consistent with expected values for the Middle Atlantic Bight, and (4) the algorithm performs reasonably well in Sargasso Sea, Gulf Stream, slope, and shelf waters but is less consistent in coastal waters.

OCZS *codes:* 010.3640, 010.4450, 280.3640, 300.6280.

1. Introduction

Present empirical radiance ratio algorithms1 applied to satellite ocean color data provide an estimate of only the chlorophyll pigment and cannot properly account for the absorption and backscattering from other constituents including chromophoric dissolved organic matter (CDOM). Our object in this paper is to describe the results from field tests of a theory2 for simultaneously retrieving three dominant inherent optical properties (IOP's) of water-leaving ocean radiance: the CDOM and detritus absorption, phytoplankton absorption, and total backscattering coefficients from satellite ocean color data by linear matrix inversion of a water-leaving radiance model. (Note that the ***variable,*** total constituent backscattering (TCB), is actually retrieved and the total backscattering is simply obtained by adding the ***constant*** backscattering coefficient of seawater.)

Radiance model inversion is tested using airborne ocean color radiance spectra acquired during two missions flown under clear sky conditions. The performance of the algorithm is primarily evaluated using concurrent airborne laser-induced fluorescence data with a limited amount of supporting measurements made from samples acquired during a cruise of the University of Delaware Research Vessel (R/V) Cape Henlopen. Airborne laser-induced fluorescence data were chosen as the primary test set because of ready availability of large numbers of essentially paired active (laser-induced fluorescence) and passive ocean color radiance spectra and the previously demonstrated agreement between ship-derived chlorophyll and CDOM measurements. More than 7000 pairs of such active and passive spectra are acquired along ~450-km flight track in a single hour covering several different types of water masses. By comparison, ship data to support a similar radiance algorithm evaluation would require more than 24 h to traverse and would thus have considerable smearing because of advection and natural changes in the phytoplankton population. Moreover, the number of supporting ship samples would be far lower and statistically less robust.

At this stage of development, the algorithm is designated preliminary because (1) airborne laser-induced chlorophyll fluorescence data were used for

F. E. Hoge and C. W. Wright are with NASA, Wallops Flight Facility, Building N159, Wallops Island. Virginia 23337. P. E. Lyon. R. N. Swift, and J. K. Yungel are with EG&G, Incorporated, Wallops Flight Facility, Wallops Island, Virginia 2X1.37.

Received 26 May 1998; revised manuscript received 22 September 1998.

phytoplankton absorption coefficient validation with only partial supporting ship observations of CDOM and chlorophyll; (2) the coastal zone retrievals are not as consistent as the shelf, slope, Gulf Stream, and Sargasso Sea retrievals; (3) the CDOM and detritus absorption coefficient is treated as a single IOP to reduce the required number of spectral bands; and (4) one of the three IOP's (backscattering coefficient) has not been validated.

The detailed theoretical development for linear matrix inversion of an oceanic radiance model has been given elsewhere.2 The reader is urged to become familiar with the paper in Ref. 2 because much of the salient material is not repeated here.

2. Linear Matrix Inversion Methodology

There are many constituents within the ocean that contribute to upwelled spectral radiance, and any number of absorbers and backscattering components can in principle be retrieved. But for the preliminary algorithm presented in this paper, the principal constituents are assumed to be phytoplankton absorption, $a_{ph}(\lambda_i)$; CDOM and detritus absorption, $a_d(\lambda_i)$; and TCB, $b_{bt}(\lambda_i)$. It has been shown2 that these three IOP's can be retrieved from the following matrix equation:

$$a_{ph}(\lambda_g)\exp[-(\lambda_i - \lambda_g)^2/2g^2] + a_d(\lambda_d)\exp[-S(\lambda_i - \lambda_d)] + b_{bt}(\lambda_b)(\lambda_b/\lambda_i)^n v(\lambda_i) = h(\lambda_i), \quad (1)$$

where $h(\lambda_i) = -[a_w(\lambda_i) + b_w(\lambda_i)v(\lambda_i)]$ is the column matrix, or vector, of hydrospheric constants (seawater absorption and backscattering) and the oceanic water-leaving radiances. See Appendix A for the definitions of symbols. The $a_w(\lambda_i)$ and $b_w(\lambda_i)$ are seawater constants. Each of the IOP models for the chlorophyll absorption coefficient, the CDOM and detritus absorption coefficient, and the TCB have already been described.2 The IOP model reference wavelengths λ_g, A,, and A, need not coincide with the sensor observational bands.2 The matrix formulation of the radiance model inversion exemplified by Eq. (1) is a powerful framework for IOP retrievals as well as analysis of errors in the retrievals.2 These error analyses2 have shown that the accuracy of the CDOM and detritus absorption retrieved by linear inversion is strongly dependent on the accuracy of the exponent n in the TCB spectral model $b_{bt}(\lambda) = b_{bt}(\lambda_b)(\lambda_b/\lambda)^n$. Although we obtained reasonable inversions with a constant n value, better results are presently obtained if n is not held constant but allowed to vary with the constituent-driven radiances. Accordingly, the spatially variable n exponent[3–6] should be varied to accommodate the different types of scattering constituents in the water masses under observation. We accomplished this by varying n bused on a radiance ratio, L_1/L_3, using two of the three bands being inverted. Numerous airborne active-passive[7–9] data sets have shown that this radiance ratio is linearly related to the exponent n such that

$$n = a_1 L_1/L_3 + a_2. \quad (2)$$

At the present stage of our algorithm approach we empirically derive n for each individual data set by experimentally minimizing the error in the retrieved CDOM and detritus coefficient compared with CDOM absorption derived from the laser-induced fluorescence measured with the NASA Airborne Oceanographic Lidar (AOL). For example, the best retrievals were found when the n factor algorithm for the 3 April 1995 inversions used a scale a, of 0.282 and an offset a_2 of 3.82 whereas the 20 April 1995 transects used an a, of 0.245 and an offset a_2 of 4.41. These values of a_1 and a_2 are not global, and other unpublished data sets have given optimal IOP retrievals with slightly different a $_1$ and a_2 values. The need to vary the n exponent would be eliminated if improved backscattering spectral models were available to better represent the diverse types of scatterers. Finding a single backscattering spectral model to represent a multitude of constituents requires empirical methods to fit the various combinations of these scatterers found in the global oceans.

Equation (1) is linear in the three IOP's at their reference wavelengths $a_{ph}(\lambda_g)$, $a_d(\lambda_d)$, and b_b(A,). Three sensor wavelengths are required to provide an even-determined, consistent solution. The oceanic state vector of unknown IOP's at their reference wavelengths, $p = [a_{ph}(\lambda_g), a_d(\lambda_d), b_b(\lambda_b)]^T$, where T denotes the transpose, is the solution of a matrix equation of the form $\mathbf{Dp} = h$, where D is the data model matrix and h is the vector of seawater absorption and backscattering hydrospheric constants and radiance data.2 It is important to emphasize that the D matrix must be inverted for each radiance spectrum because it contains radiance data in addition to model parameters. It is potentially possible to extend the matrix inversion to a larger number of constituents as long as accurate IOP models can be found to satisfactorily represent the spectral absorption and backscattering of each (and sufficient sensor bands are available in the observational data to yield a solution). (The column vectors in the D matrix can be reformulated so that the constants that represent the spectral models can be referenced to the first chosen sensor band wavelength A,. This simplifies the matrix inversion and retrieves constituent IOP's as they exist at measured radiance wavelengths. Accordingly, an alternate form of the D matrix has been given[2] together with suggestions for the derivation of constituent concentrations from the IOP state vector $\mathbf{p}$. Our preliminary algorithm in this paper focuses on even-determined solutions in which the number of IOP's (unknowns) is equal to the number of sensor bands (equations). In this case, the solutions, if obtainable, are unique. Future algorithm studies will address overdetermined least squares, weighted least squares, and other solutions.

3. Algorithm Validation with Airborne Laser Spectrofluorometry

A. Phytoplankton Absorption Coefficient Validation

In our analysis we utilized AOL laser-induced fluorescence measurements to validate retrieved IOP's. During the past ~13 years this technique proved valuable for testing algorithms for the retrieval of CDOM, chlorophyll, and potentially phycoerythrin from water-leaving radiance spectra. We corrected the laser-induced fluorescence measurements for variation in the surface layer attenuation properties by normalizing these backscattered signals with the concurrent laser-induced water Raman signal.[10] Numerous comparisons have shown good agreement between airborne water Raman-normalized laser-induced chlorophyll fluorescence (F/R) measurements acquired with the AOL and ship-derived chlorophyll extraction measurements.[7–9,11–15] Regressions between the extracted chlorophyll measurements and the AOL F/R values yielded a consistent F/R:μg/l conversion factor over various sections of the north Atlantic Ocean in spite of the known fluorescence and unit chlorophyll variability that was due to nutrient and phytoplankton physiology. The effects of light history are minimized by flying under clear skies near the middle of the day.

Because of (a) the high variability of the fluorescence per unit chlorophyll biomass and (b) the circuitous nature of biomass-to-absorption conversions, we use a more direct fluorescence-to-absorption conversion to provide a test data set to evaluate the retrieved phytoplankton absorption coefficient. There is strong evidence that the fluorescence per unit of phytoplankton absorption coefficient is constant across wide areas of the ocean surface layer. Specifically, for a 170-km distance a constant fluorescence-to-phytoplankton absorption coefficient provided remarkable agreement between observed water-leaving radiances and forward-modeled radiances whereas the chlorophyll biomass varied8 from 0.7 to 27 mg/m^3. Thus we assume that the fluorescence per unit of phytoplankton absorption coefficient is constant across the entire experiment track lines. The laser-induced chlorophyll F/R ratios are converted to absorption values through equations of the form $F/R = k_0[a_{ph}(412)]^{k1}$ or $\exp\{\ln[(F/R)/k_0]/k_1\} = a_{ph}(412)$ where k_0 and k_1 are constants. Fluorescence per unit of phytoplankton absorption coefficient conversion factors is sometimes adjusted for different locations and dates to account for possible nutrient, light history, or species physiology. Accordingly, the parameters k_0 and k_1 were derived for each mission location and date to secure the best agreement with the passively retrieved phytoplanktonhbsorption coefficient.

B. Chromophoric Dissolved Organic Matter and Detritus Absorption Coefficient Validation

Recently it was firmly established through ship and laboratory experiments that the absorption coefficient of CDOM is linearly related to the CDOM fluorescence.[16–19] Subsequently it was shown that the CDOM absorption coefficient IOP can be retrieved from airborne laser-induced and water Raman-normalized CDOM fluorescence in a variety of oceanographic locations? Because the detritus contributes little fluorescence to the airborne laser-induced fluorescence signal,[16,19] the retrieved CDOM and detritus absorption coefficient will be only slightly larger than the airborne laser-derived CDOM absorption coefficient truth.

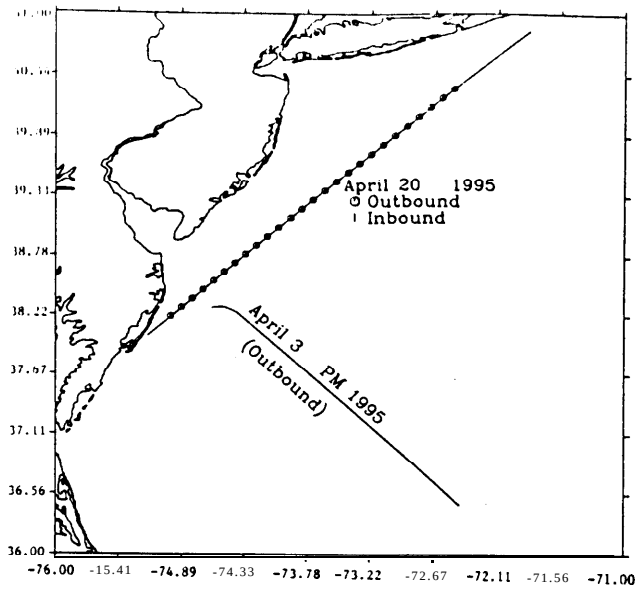

Fig. 1. Flight location of the AOL system and spectroradiometers aboard the NASA P-3B aircraft during the afternoon of 3 April 1995 is shown by the outbound southeast ground track line. This flight traversed five water masses: coastal, shelf, slope, Gulf Stream, and Sargasso Sea. Flight of the AOL system and spectroradiometers aboard the NASA P-3B aircraft on 20 April 1995 is shown by the outbound (toward the northeast) and inbound (toward the southwest) ground track lines. These latter track lines traversed only shelf and coastal water types.

C. Total Backscattering Validation

No airborne laser system is presently available for the retrieval of the total backscattering coefficient. Thus no truth data are available for the TCB IOP. Furthermore, little backscattering data are available from ship cruises, perhaps because multiband instrumentation has only recently become available.3 The passively retrieved backscattering coefficient is consistent with noncontemporaneous determinations for the Middle Atlantic Bight.

4. Airborne Field Experiments in the Middle Atlantic Bight

Two airborne experiments conducted in the Middle Atlantic Bight (MAB) were selected for the purpose of testing the retrieval of IOP's from water-leaving radiances by radiance model inversion. Figure 1 shows a sampling line occupied during a flight on the afternoon of 3 April 1995 and by the University of Delaware R/V Cape Henlopen on 2 April 1995. The

complete outbound transect allows a stringent test of the algorithm because five different water masses were traversed: Sargasso Sea, Gulf Stream, continental slope, shelf, and coastal. (The inbound transect was not analyzed because other experiments were conducted during that portion of the flight.) To further test the algorithm in continental shelf and coastal waters, we selected an active-passive data set acquired during a flight conducted between Wallops Island, Virginia, and Block Island, Rhode Island, on 20 April 1995 as shown in Fig. 1. This latter flight was not supported by observations from a research vessel.

A. Passive (Solar) Data

A 256-channel ocean-viewing spectroradiometer was used to gather upwelled spectral radiance during the flights conducted from the NASA Goddard Space Flight Center P-3B aircraft. This spectroradiometer was set to provide spectral coverage between ~400 and 730 nm and was calibrated by viewing a Labsphere reflectance plaque illuminated by a National Institute of Standards and Technology (NIST) traceable irradiance standard lamp. The radiometer calibration was also checked for consistency by viewing an internally illuminated 0.75m-diameter calibration sphere placed beneath the aircraft. This calibration sphere is similar to the one described by others.20 The output radiance of the calibration sphere is also traceable to NIST sources. The sphere was a part of a sea-viewing wide field-of-view sensor intercalibration round-robin experiment (SIRREX)[21] calibration activity. An AOL team member participated in a subsequent SIRREX forum to further enhance our knowledge of the characterization of the plaque and the sphere. The spectral calibration of the spectroradiometer is validated by viewing a Hg-Cd source. The spectroradiometer was found by repeated laboratory experiments to be at least as stable as the NIST traceable sources. When further tested against nonfilament radiance sources such as light-emitting diodes, the stability was likewise found to equal such sources. The field of view (~2 mrad) and integration time (~350 ms) yield a pixel size of ~0.3 m × 45 m for a flight speed of ~125 m/s of the P-3B aircraft. The radiometer pixels are located ~30° off nadir (port or starboard) to avoid Sun glint. (The 10-pulse/s laser footprints are each ~0.3 m in diameter but are located directly under the aircraft at 5° off nadir toward the nose of the aircraft. Thus the active and passive pixels are not coincident but are never more than 90 m apart.)

Although the $E_d(0^-)$ was obtained from an irradiance model, an uncalibrated zenith-viewing 256-channel spectroradiometer was used to monitor the hemispherical sky for variability caused by clouds. Because the airborne data were largely acquired under blue sky conditions, no retrieval improvement was found by using actual downwelling irradiance data. An infrared radiometer (Heimann KT-19 Radiation Thermometer) was used to concurrently measure sea surface temperature thus allowing identification and interpretation of important oceanographic features such as the Gulf Stream western boundary.

B. Active (Laser) Data

The laser-induced fluorescence data were acquired with the AOL. The laser-induced fluorescence measurement methods were analogous to those already described.[7,8,22] Briefly, 355-nm laser pulses are transmitted into the ocean to induce the broad spectrum CDOM fluorescence (~360-650 nm) and water Raman emission (~402 nm) from the surrounding water molecules.[22] The resulting F/R ratio $F_{CDOM}(450)/R(402)$, is linearly related to the CDOM absorption coefficient [16,19] and provides the truth data for comparison with the CDOM and detritus absorption coefficient retrieved from the upwelled radiances.9

Also, 532-nm laser pulses are transmitted vertically downward into the ocean to induce chlorophyll (and phycoerythrin fluorescence emission[23,24]) from waterborne phytoplankton and water Raman emission from the surrounding seawater molecules. The concurrent chlorophyll (~670 −690-nm) and phycoerythrin (~540–595-nm) fluorescence and water Raman spectral emissions (~645 nm) are collected by the same telespectroradiometer.

A spectral and radiometric calibration is also performed on the laser receiver radiometer before and after each flight mission by viewing the 0.75-m-diameter calibration sphere placed beneath the aircraft laser-viewing port. Because the laser receiver radiometer contains photomultiplier tubes (PMT's), additional steps are taken to maintain the calibration during flight. Immediately following the 0.75-m sphere calibration, a lo-cm-diameter calibration sphere within the AOL system is viewed by mechanically introducing (at the focal plane of the telescope) the radiation through fiber optics. The 10-cm sphere calibration is followed by viewing 40-ns pulsed radiation from a bank of red light-emitting diodes located behind the diffraction grating and in front of the fiber-optic face plate. The small calibration sphere allows immediate transfer of the 0.75-m sphere calibration into the aircraft domain at any time. The pulsed light-emitting diodes then provide transfer of the ground (and onboard) dc tungsten lamp calibrations to the wide bandwidth-pulsed portion of the AOL detection/amplification/digitization system. Calibration is maintained in flight by periodically viewing the 10-cm calibration sphere.

The original AOL system[25–30] was recently modified to provide more complete rejection of the 532-nm laser excitation wavelength from the instrument spectrometer and substantial reduction of scattered light. Specifically, a narrow-band (notch) transmission filter was placed into the collimated segment of the light path and rejects considerable amounts of backscattered 532-nm radiation from the spectrometer. (The 532-nm pulse reflected from the notch filter is viewed by a PMT and is used to define the ocean surface target temporally and initiate digitization of

the fluorescence spectra.) Additional modifications include the removal of rigid light guides and all turning mirrors comprising the original optical axis. A fiber-optic face plate now occupies the focal plane of the new in-line optical path and transports the spectral radiation to mechanically reconfigured banks of original PMTs. The resolution of each of the 84 channels of the fiber-optic face plate system is ~4 nm. However, the number of PMT's currently available within the redesigned spectrometer is only 28, therefore groups of three fiber optical channels were optically combined at each PMT to achieve ~12 nm per output band for this experiment. The signal path from the PMT's through and including digitization remains essentially the same as reported previously.[25–29] Compared with the original light guides, the fiber-optic channels have superior scattered-light rejection that is attributed to a considerably smaller viewing or acceptance angle.

5. Retrieval of Water-Leaving Radiances from At-Aircraft Oceanic Radiances

Although the flight altitude was only 150 m, reflected sky radiance and reflected path radiance must each be removed from the at-aircraft radiances. The reflected sky radiance correction is performed by selecting a measured sky radiance spectrum representing that portion of the sky being reflected into the down-looking spectroradiometer. Then 0.021 of this sky radiance[31] is subtracted from all at-aircraft radiance spectra. The path radiance correction was developed from ocean radiance spectra acquired during passes conducted at altitudes of 150, 235, 300, and 320 m over a portion of the same water mass on the morning of 3 April 1995. The nominal amount of path radiance per meter of flight altitude determined from this earlier data set was applied to the data acquired over the entire flight line during the afternoon mission. To validate the atmospheric correction methodology, IOP retrievals were performed with radiance data acquired at several different altitudes during the morning mission. The results (not shown) demonstrated that these reflected sky and path radiance correction procedures were quite satisfactory.

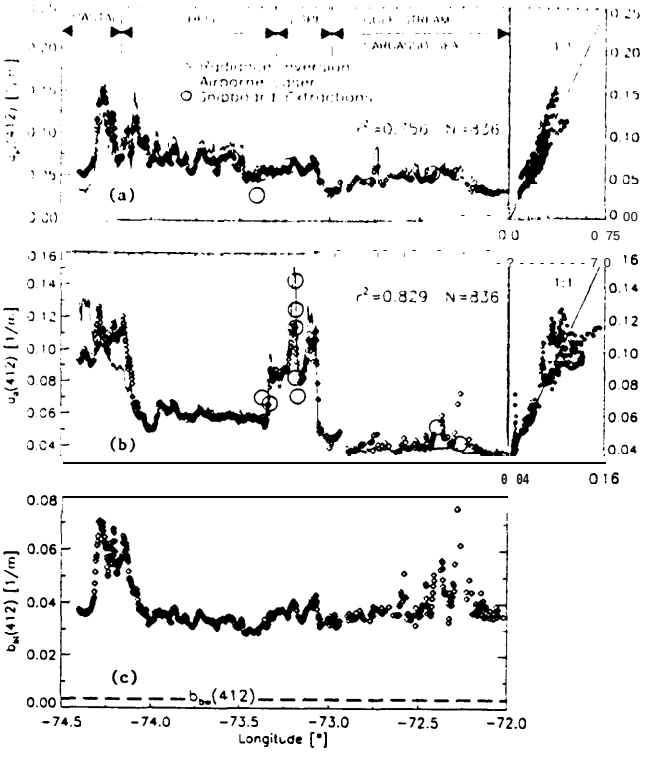

Fig. 2. (a) Along-track profile of phytoplankton absorption coefficient at 412 nm, $a_{ph}(412)$, retrieved from airborne water-leaving radiances plotted with chlorophyll absorption derived from concurrent airborne laser-induced F/R measurements obtained on the outbound portion of a flight to the Sargasso Sea during the afternoon of 3 April 1995. These parameters are also graphed as a scatter-plot immediately to the right of the profile presentation. Limited absorption values derived from the supporting ship chlorophyll measurements are shown plotted as open circles. (b) Along-track profile of the CDOM and deritus absorption coefficient at 412 nm, $a_d(412)$, retrieved from the airborne water-leaving radiances plotted along with CDOM absorption measurements derived from airborne laser-induced CDOM F/R. These parameters are also graphed in the form of a scatterplot immediately to the right of the profile presentation. A limited number of supporting ship-derived CDOM absorption measurements are shown as open circles. (c) Along-track profile of the TCB coefficient, $b_{bt}(412)$, retrieved from the airborne water-leaving radiances. No truth data were available to validate the retrieved TCB.

6. Inherent Optical Property Retrieval Results

The inversion of the data model or D matrix[2] can be performed in several ways but we frequently use lower- upper triangular decomposition. If needed, singular value decomposition methods can also provide a quantitative evaluation of any suspected near singularities.[""]

We used sensor bands that are near those of present and planned satellite sensors. The methodology is adapted easily to other band sets. The chosen bands (412, 490, 565-nm) allow one to (a) avoid the high variability of the phytoplankton absorption at 443 nm (because, in agreement with the research of others,[33] unpublished analyses of our airborne active-passive data suggest that the 443-nm band does not provide the best retrieval results), and (b) employ the 565-nm band to avoid the phycoerythrobilin absorption near 545 nm (and provide further reduced CDOM and phytoplankton absorption relative to bands at ~550 nm). Use of the 490-nm band can carry a penalty of possible contamination from unmodeled phycourobilin absorption at 495 nm. Likewise, use of the 555-nm band radiances can potentially suffer from unmodeled phycoerythrobilin absorption. These latter two error sources are not considered serious but are undergoing evaluation.

The outbound southeast flight track of 3 April 1995 [Figs. 2(a)-2(c)] shows the inversion of the airborne water-leaving spectral radiance values plotted as open diamonds. The retrieved phytoptankton absorption coefficient [Fig. 2(a)] is compared with the absorption coefficients derived from the airborne

laser-induced chlorophyll F/R values shown as a solid curve. Also shown within Fig. 2(a) as open circles are chlorophyll absorption values derived from chlorophyll extraction measurements made from samples obtained by the R/V Cape Henlopen on 2 April, the day prior to the AOL flight. The open circles were used because of the rather busy appearance of the laser-derived and the model-retrieved phytoplankton absorption coefficient already present. The actual phytoplankton absorption value and its geographic position are located at the center of each circle. A specific absorption coefficient of 0.038 m^{-1} mg m^{-3} was used to convert the chlorophyll concentration measurements supplied by Rich Geider (University of Delaware) into units of absorption for direct comparison with the airborne remote-sensing data. A specific absorption coefficient of 0.038 m^{-1} mg m^{-3} is within published measurements of *in vivo* absorption by phytoplankton.[34] The retrieved phytoplankton absorption coefficient diverges from the 532-nm laser-determined absorption values as the track line approaches the coastal region at approximately 74.25 °W longitude. Although the algorithm performs satisfactorily in Sargasso Sea, Gulf Stream, slope, and shelf waters, it is not yet satisfactory for use in coastal waters where unmodeled scatterers and absorbers may compromise the inversion accuracy. (No laser fluorescence data were obtained for a small section of the track line, around -72.8 °W longitude.)

Similarly, the retrieved CDOM and detritus absorption coefficient [Fig. 2(b)] is compared with the airborne laser-derived CDOM absorption coefficients.[19] Laboratory CDOM absorption measurements on samples acquired from the Cape Henlopen on the day prior to the remote-sensing flight are shown as open circles. These surface truthing CDOM measurements were supplied by Anthony Vodacek (University of Maryland). Familiar CDOM absorption signatures can be identified readily in Fig. 2(b). For example, the offshore decline of CDOM absorption is a central characteristic of the MAB.[9,16,19,22] The radiance-retrieved midshelf values of $a_d(412)$ are consistent with other noncontemporaneous ship, aircraft, and satellite determinations of the CDOM absorption coefficient in the MAB.[9,16,19] Another central characteristic of the CDOM absorption coefficient in the MAB is the abrupt decline at the Gulf Stream western boundary.[9,16,19] During these experiments, the Gulf Stream western boundary was located at -73.1 °W longitude (as determined by the sea surface temperature measurements, not shown) near where the CDOM abruptly declines. The error in the CDOM and detritus retrieval around 74.25 °W longitude is thought to be caused by errors in the estimated n exponent of the TCB spectral model. The empirical formula used to derive n does not work well for the combination of reflectances found within that particular segment.

In Fig. 2(c) no backscattering truth data were available to compare with the radiance-retrieved TC B coefficient. However, several features of the along-track backscattering signature are notable. First, the backscattering is somewhat correlated with the phytoplankton particulates whose absorption is depicted in Fig. 2(a). Second, the backscattering is not highly correlated with the CDOM absorption which suggests, but does not prove, that (1) particulate detritus absorption does not dominate the CDOM absorption signature, and (2) use of a combined CDOM and detritus model is acceptable for this preliminary algorithm investigation. Finally, the total backscattering coefficients, $b_b(412) = b_{bt}(412) + b_{bw}(412)$, are nominally consistent with backscattering levels obtained by others.[3–5,35] It should be emphasized that the backscattering must be concurrently retrieved, otherwise its contribution to the original radiances will be erroneously propagated into the phytoplankton and CDOM and detritus absorption coefficients.2

In Fig. 3 the retrieval results from the 20 April 1995 outbound track are shown. The phytoplankton absorption retrieval shown in Fig. 3(a) is compared with the absorption coefficients derived from the airborne laser chlorophyll F/R measurements. No surface truthing measurements were available for comparison with the remote-sensing data acquired during the 20 April mission. Note that in this data set the phytoplankton absorption coefficient retrieval is correlated with the laser-derived phytoplankton absorption coefficient within the coastal regime at -75.0 °W longitude. The retrieved CDOM and detritus absorption coefficient, $a_d(412)$ [Fig. 3(b)], is highly correlated with the 355-nm laser-derived CDOM absorption coefficient up to -74.75 °W longitude where the retrieval then falters within the coastal waters. The retrieved b_{bt} or TCB values [Fig. 3(c)] are consistent with those given in Fig. 2(c). (Within the segment around -73.0 °W longitude of Fig. 3 there was no usable data because uncorrectable reflectance from a single large cloud severely contaminated both the laser and the water-leaving radiance data. The cloud presence was validated by a sky-viewing spectroradiometer and by direct visual observation by at least two scientific team members. Also, the data near -72.1 °W longitude was removed because of cloud contamination as determined by visual observation and a sky-viewing spectroradiometer.)

Figure 4 shows the IOP retrievals for the 20 April 1995 inbound track on the return to Wallops Island. The phytoplankton absorption coefficient retrieval [Fig. 4(a)] is compared with the absorption coefficients derived from the airborne laser F/R values. The correlation of subtle features between the retrieved phytoplankton absorption coefficient and the F/R truth data can be seen. The $a_{\phi}(412)$ absorption coefficient and the CDOM absorption coefficient laser truth data show similar agreement and correlations. Again, no backscattering truth data were available, but the TCB retrievals in Fig. 4(c) are within the expected nominal range. (Missing data segments near -73.0 °W longitude and -72.1 °W longitude in

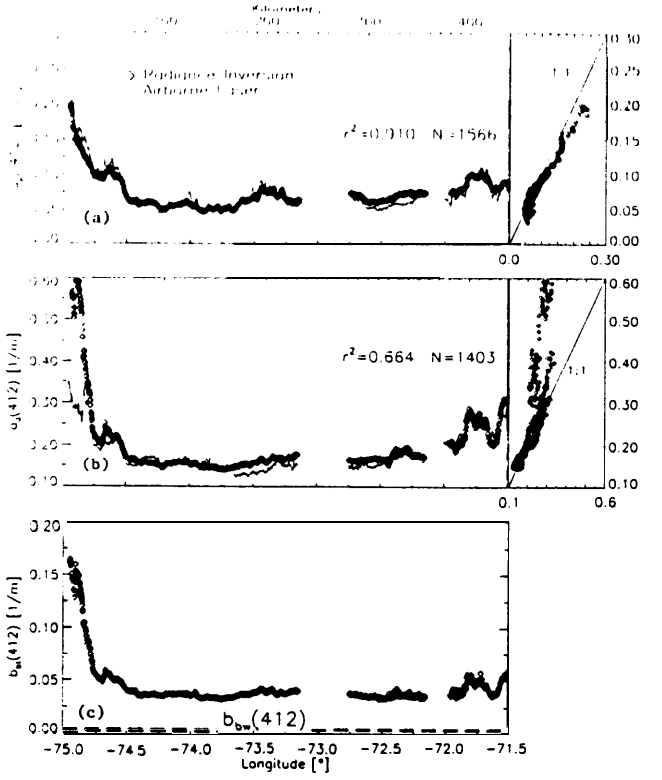

Fig. 3. (a) Along-track profile of phytoplankton absorption coefficient at 412 nm retrieved from airborne water-leaving radiances plotted with chlorophyll absorption derived from concurrent airborne laser-induced F/R measurements obtained on the outbound portion of a flight flown between Wallops Island, Virginia, and Block Island, Rhode Island, on 20 April 1995. These parameters are also graphed in the form of a scatterplot immediately to the right of the profile presentation. (b) Along-track profile of the CDOM and detritus absorption coefficient at 412 nm concurrently retrieved from the airborne water-leaving radiances is plotted along with CDOM absorption measurements derived from airborne laser-induced CDOM F/R. (c) Along-track profile of the TCB coefficient retrieved from the airborne water-leaving radiances. No truth data were available to validate the retrieved TCB. Note that the vertical scale for b_{bt} in (c) is different from (a) and (b). The blank portions of the track line at -72.3 °W longitude and -72.1 °W longitude denote lost data because of cloud contamination.

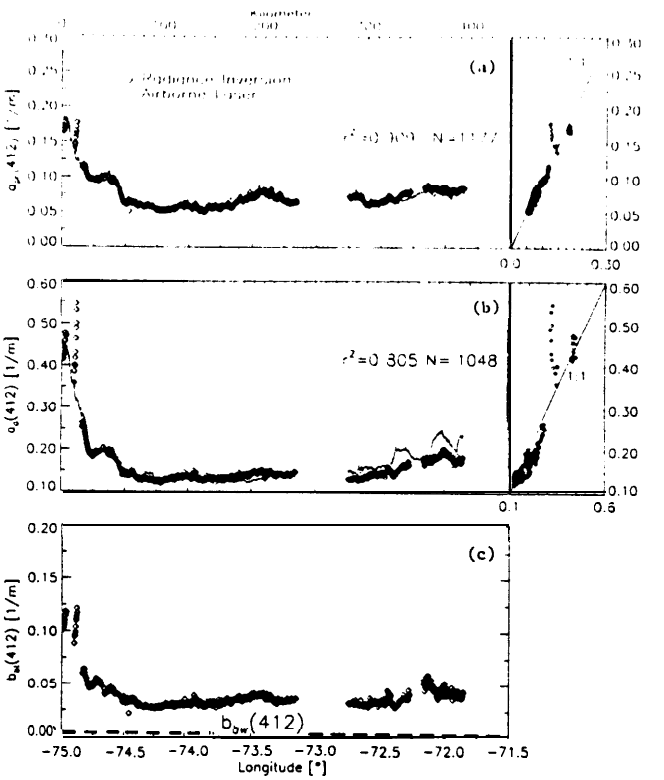

Fig. 4. (a) Along-track profile of phytoplankton absorption coefficient at 412 nm retrieved from airborne water-leaving radiances plotted with chlorophyll absorption derived from concurrent airborne laser-induced F/R measurements obtained on the inbound portion of a flight flown between Wallops Island, Virginia, and Block Island, Rhode Island, on 20 April 1995. These parameters are also graphed in the form of a scatterplot immediately to the right of the profile presentation. (b) Along-track profile of the CDOM and detritus absorption coefficient at 412 nm concurrently retrieved from the airborne water-leaving radiances plotted along with CDOM absorption measurements derived from airborne laser-induced CDOM F/R. (c) Along-track profile of the TCB coefficient retrieved from the airborne water-leaving radiances. No truth data were available to validate the retrieved TCB. Note that the vertical scale for b_{bt} in (c) is different from (a) and (b). The portions of the track line at -72.3 °W longitude and -72.1 °W longitude denote lost data because of cloud contamination.

Fig. 4 were caused by the same cloud contamination discussed in Fig. 3.)

7. Discussion

A previously published radiance model inversion theory has been successfully tested by using airborne water-leaving radiances to retrieve the CDOM and detritus absorption coefficient, the phytoplankton absorption coefficient, and the total backscattering coefficient. Linear matrix inversion of water-leaving spectral radiances was found to perform satisfactorily using airborne water-leaving radiance spectra even in the presence of instrument-induced noise. Previous investigations with the inversion methodology used simulated radiance spectra containing no noise from instrument or environmental sources.[2]

Laser-induced fluorescence from CDOM and phytoplankton chlorophyll were utilized together with concurrent ocean color radiance spectra to test the model inversion methodology for retrival of the three most dominant IOP's: phytoplankton absorption, CDOM and detritus absorption, and TCB absorption. A modest amount of supporting chlorophyll and CDOM data derived from ship samples were shown for one of the data sets used in this initial application of the model inversion methodology. The strength of the airborne laser-derived IOP truth data lies in the large volume of the concurrent active-passive paired observations coupled with the diversity of oceanographic provinces traversed during airborne experiments. Previously, airborne chlorophyll and CDOM fluorescence data had been directed primarily toward support of major field experiments,[7-9,11-15] forward

modeling of water-leaving radiances,[8] and CDOM variability mapping.[9,22]

The backscattering wavelength ratio model requires a variable exponent to provide the best IOP retrieval. The value of n affects the retrieval of the CDOM absorption coefficient more than the retrieval of the phytoplankton absorption coefficient.[2] Therefore large errors in the CDOM and detritus retrieval can be expected if n is not correct. It is recommended that data from different oceanographic regions and seasons be acquired to compile a more reliable lookup table for a general set of a_1 and a_2 parameters used to derive n. The availability of backscattering truth data would allow further improvements to the existing model. Accordingly, we recommend that more attention be paid to this important parameter.[36–38] Although shipboard backscattering instrumentation is becoming more available," the data density is still too sparse to be of any real utility for general application to different water masses. We consider knowledge of TCB to be fundamental to NASA's satellite algorithm development programs. Because there continues to be a paucity of backscattering data from ship cruises, we recommend the development of an airborne laser backscattering measurement capability. Two-channel crossed-polarization lidar systems show much promise for airborne retrieval of the total scattering coefficient, but such sensors are not yet ready for routine use.

The spatial variability of the TCB [Figs. 2(c), 3(c), and 4(c)] emphasizes the importance of including it in the retrieval computational process. Had the TCB not been solved for in the S-band retrieval, then it must by necessity be constrained by a model (or, worse yet, a fixed constant) within a 2-band matrix retrieval. For a fixed-constant backscattering model (e.g., within a 2 × 2 matrix inversion), the observed backscattering variability [Figs. 2(c), 3(c), and 4(c)] would be erroneously propagated into the phytoplankton and CDOM absorption coefficient retrievals.

The 443-nm band consistently gave poorer results than the 490-nm band when used in combination with the 412- and 565-nm bands. This suggests that it is important to avoid choosing sensor band locations within spectral regions having naturally elevated absorption and backscattering variability. In addition, we found by independent model inversion studies that the retrieval errors for all the IOP's are rather strongly dependent on the phytoplankton Gaussian spectral model. Retrieval errors are thus exacerbated by the natural spectral variability[39] of phytoplankton absorption. By choosing a single Gaussian phytoplankton spectral model[39] as done here, IOP errors are likely but can be minimized by avoiding spectral regions of high variability.

The CDOM absorption levels in the MAB are higher by ~2× than found in the Southern California Bight[22] and the western coast of Florida just outside Tampa Bay and ~3× higher than waters outside Monterey Bay, California.[19] Simulated model inversions have shown that the inversion process functions satisfactorily for $a_d(355)$ levels[2] through ~1.0 m^{-1}. Thus reasonably accurate retrievals should be expected over wide areas of the ocean. Also, chlorophyll levels during these algorithm development field experiments were no greater than ~4–5 mg/m^3. However, simulated model inversions suggest that the algorithm will continue to operate in much higher (~20-mg/m^3) phytoplankton absorption regimes.[2] Forward modeling using water-leaving radiances and ship-validated chlorophyll concentrations of 0.7-27 mg/m^3 further suggests that the inversion will perform in a satisfactory manner in high-chlorophyll regions.[8] The mathematical inversion process will operate over a wide range of IOP's with little chance of singularity, but the user must be alert because even-determined solutions may return physically unacceptable solutions (such as negative IOP's) when inaccurate data or model parameters are used.[2] Of course these conditions are easily flagged during the inversion computations.

This initial field application of the model inversion methodology worked well in shelf, slope, Gulf Stream, and Sargasso Sea water masses but not consistently in the coastal waters. The algorithm remains preliminary pending tests in other oceanic provinces and comparison with additional airborne laser-induced fluoresence data sets with supporting surface truth measurements. The application of the model inversion methodology to coastal waters will require additional refinements to the technique.

Appendix A: Nomenclature

- a_d Absorption coefficient of CDOM and detritus (m^{-1});
- a_{ph} absorption coefficient of phytoplankton particles (m^{-1});
- a_w absorption coefficient of water (m^{-1});
- b_b total backscattering coefficient (m^{-1}); $b_b = b_{bw} + b_{bt}$;
- b_{bt} TCB coefficient (m^{-1});
- b_{bw} backscattering of seawater (m^{-1});
- **D** data and model matrix;
- **F/R** chlorophyll-fluorescence/water Raman ratio for airborne laser data;
- g phytoplankton Gaussian model spectral width parameter (nm);
- **h** $-(a_w + b_{bw}v)$; vector of hydrospheric constants and water-leaving radiances;
- **N** number of samples used in regression or along-track profile;
- n total constituent backscattering spectral model exponent;
- P oceanic state vector of retrieved IOP's at their reference wavelengths;
- **S** spectral slope for the a_d model;
- v $(1 - 1/X)$ (dimensionless);
- X $b_b/(b_b + a)$ (dimensionless);
- A wavelength (nm);
- λ_b reference wavelength for TCB (nm);
- A_d reference wavelength for CDOM and detritus absorption (nm);

λ_p peak wavelength for Gaussian phytoplankton absorption model (nm);

λ_i wavelength of observational bands, $i = 1, 2, 3$.

The continued support and encouragement of the NASA Ocean Biology Program is gratefully acknowledged. We are very appreciative of the extracted chlorophyll fluorescence measurements provided by Rich Geider (University of Delaware) and the CDOM absorption measurements given by Anthony Vodacek (University of Maryland).

References

1. H. R. Gordon, D. K. Clark, J. W. Brown, 0. B. Brown, R. H. Evans. and W. W. Broenkow. "Phytoplankton pigment concentrations in the Middle Atlantic Bight: comparison between ship determinations and the coastal zone color scanner estimates," Appl. Opt. 22, 20-36 (1983).
2. F. E. Hoge and P. E. Lyon, "Satellite retrieval of inherent optical properties by linear matrix inversion of oceanic radiance models: an analysis of model and radiance measurement errors," J. Geophys. Res. **101, 16,631–16,648** (1996).
3. R. A. Maffione and D. R. Dana, "Instruments and methods for measuring the backward-scattering coefficient of ocean waters," Appl. Opt. 36, 6057-6067 (1997).
4. R. A. Maffione, D. R. Dana, and R. C. Honey, "Instrument for underwater measurement of optical backscatter," in ***Underwater Imaging, Photography, and Visibility,*** R. W. Spinrad, ed., Proc. SPIE **1537,** 173-184 (1991).
5. J. H. Smart, "Empirical relationships between optical properties in the ocean," in ***Ocean Optics XI, G.*** D. Gilbert, ed., Proc. SPIE **1750, 276–298** (1992).
6. R. A. Maffione, D. R. Dana, and J. M. Voss, "Spectral dependence of optical backscattering in the ocean," presented at OSA Annual Meeting, Portland, Ore., **10–15** September 1995, Paper MDD4, p. 57.
7. F. E. Hoge and R. N. Swift, "The influence of chlorophyll pigment upon upwelling spectral radiances from the north Atlantic Ocean: an active-passive correlation spectroscopy study," Deep Sea Res. **40, 265–277** (1993).
8. F. E. Hoge, R. N. Swift, and J. K. Yungel, "Oceanic radiance model development and validation: application of airborne active-passive ocean color spectral measurements," Appl. Opt. **34,** 3468–3476 (1995).
9. F. E. Hoge, M. E. Williams, R. N. Swift, J. K. Yungel, and A. Vodacek, "Satellite retrieval of the absorption coefficient of chromophoric dissolved organic matter in continental margins," J. Geophys. Res. 100, **24,847–24,854** (1995).
10. M. P. F. Bristow, D. Nielsen, D. Bundy, and F. Furtek, "Use of water-Raman emission to correct airborne laser fluorosensor data for effects of water optical attenuation," Appl. Opt. 20, 2889–2906 (1981).
11. R. C. Smith, 0. B. Brown, F. E. Hoge, K. S. Baker, R. H. Evans, R. N. Swift, and W. E. Esaias, "Multiplatform sampling (ship, aircraft. and satellite) of a Gulf Stream warm core ring," Appl. Opt. 26, 2068–2081(1987).
12. J. W. Campbell and W. E. Esaias, "Spatial patterns in temperature and chlorophyll on Nantucket Shoals from airborne remote sensing data. May 7-9, 1981," J. Mar. Res. 43, 139-161 (1985).
13. J. W. Campbell and W. E. Esaias, "Basis for spectral curvature algorithms in remote sensing of chlorophyll," Appl. Opt. 22, 1084–1093(1983).
14. J. J Walsh, C. D. Wirick. L. J. Pietrafesa, T. E. Whitledge, F. E. Hoge, and R. N. Swift, "High-frequency sampling of the 1984 spring bloom within the Mid-Atlantic Right: synoptic shipboard, aircraft, and in situ perspectives of the SEEP-I Experiment," Cont. Shelf Res. **8,** 529–563 (1988).
15. J. Martin, et al., "Testing the iron hypothesis in ecosystems of the equatorial Pacific Ocean," Nature (London) **371,** 123–129 (1994).
16. F. E. Hoge, A. Vodacek, and N. V. Blough, "Inherent optical properties of the ocean: retrieval of the absorption coefficient of chromophoric dissolved organic matter from fluorescence measurements," Limnol. Oceanogr. 38, 1394–1402 (1993).
17. G. M. Ferrari and S. Tassan, "On the accuracy of determining light absorption by 'yellow substance' through measurements of induced fluorescence," Limnol. Oceanogr. 36, 777-786 (1991).
18. G. M. Ferrari, M. D. Dowell, S. Grossi, and C. Targa, "Relationship between the optical properties of chromophoric dissolved organic matter and total concentration of dissolved organic carbon in the southern Baltic Sea region," Mar. Chem. 55, 299-316 (1996).
19. F.E. Hoge, A. Vodacek, R. N. Swift, J. K. Yungel, and N. V. Blough, "Inherent optical properties of the ocean: retrieval of the absorption coefficient of chromophoric dissolved organic matter from airborne laser spectral fluorescence measurements," Appl. Opt. 34, 7032-7038 (1995).
20. W. A. Hovis and J. S. Knoll, "Characteristics of an internally illuminated calibration sphere," Appl. Opt. 22, 4004-4007 (1983).
21. J. L. Mueller, "The second SeaWiFS intercalibration round-robin experiment, SIRREX-2, June 1993," NASA Tech. Memo. 104566, S. B. Hooker and E. R. Firestone, eds. (NASA Goddard Space Flight Center, Greenbelt, Md., **1994),** Vol. 16.
22. F. E. Hoge, R. N. Swift, J. K. Yungel, and A. Vodacek, 'Fluorescence of dissolved organic matter: a comparison of North Pacific and North Atlantic Oceans during April 1991," J. Geophys. Res. 98, **22,779–22,787** (1993).
23. F. E. Hoge and R. N. Swift, "Active-passive correlation spectroscopy: a new technique for identifying ocean color algorithm spectral regions," Appl. Opt. 25, 2571-2583 (1986).
24. F. E. Hoge and R. N. Swift, "Phytoplankton accessory pigments: evidence for the influence of phycoerythrin on the submarine light field," Remote Sensing Environ. 34, 19-25 (1990).
25. F. E. Hoge and R. N. Swift, 'Oil film thickness measurement using airborne laser-induced water Raman backscatter," Appl. Opt. **19,** 3269–3281 (1980).
26. F. E. Hoge and R. N. Swift, "Airborne simultaneous spectroscopic detection of laser-induced water Raman backscatter and fluorescence from chlorophyll *a* and other naturally occurring pigments," Appl. Opt. 20, 3197-3205 (1981).
27. F. E. Hoge and R. N. Swift, "Airborne dual laser excitation and mapping of phytoplankton photopigments in a Gulf Stream warm core ring," Appl. Opt. 22, 2272-2281 (1983).
28. F. E. Hoge and R. N. Swift, "Airborne detection of oceanic turbidity cell structure using depth-resolved laser-induced water Raman backscatter," Appl. Opt. 22, 3778-3786 (1983).
29. F. E. Hoge. R. E. Berry, and R. N. Swift, "Active-passive airborne ocean color measurement: 1. Instrumentation," Appl. Opt. 25, 39-47 (1986).
30. F. E. Hoge. R. N. Swift, and J. K. Yungel, "Active-passive airborne ocean color measurement: 2. Applications," Appl. Opt. 25, 48–57(1986,.
31. H. R. Gordon, 0. B. Brown, R. H. Evans, J. W. Brown, R. C. Smith, K. S. Baker, and D. K. Clark. "A semianalytic radiance model of ocean color," J. Geophys. Res. 93, 10,909–10,924 (1988).
32. W. H. Press, S. A. Teukolsky, W. T. Vetterling, and B. P. Flannery, *Numerical Recipes in Fortran*, 2nd ed. (Cambridge U. Press, Port Chester, N.Y.. 1992).

33. J. Aiken, G. F. Moore, C. C. Trees, S. B. Hooker, and D. K. Clark, "The SeaWiFS CZCS-typo pigment algorithm," NASA Tech. Memo. 104566. S. B. Hooker and E. R. Firestone, eds. (NASA Goddard Space Flight Center, Greenbelt, Md., 1995), Vol. 29.
34. S. Sathycndranath, L. Lazzara, and L. Prieur, "Variations in the spectral values of the specific absorption of phytoplankton," Limnoi. Oceanogr. 32, 403-415 (1987).
35. C. S. Roesler and M. J. Perry, 'In situ phytoplankton absorption, fluorescence emission, and particulate backscattering spectra determined from reflectance," J. Geophys. Res. 100, 13,279–13,294 (1995).
36. Z. P. Lee, K. L. Carder, S. K. Hawes, R. G. Steward, T. G. Peacock, and C. 0. Davis, "Model for the interpretation of hyperspectral remote-sensing reflectance," Appl. Opt. 33, 5721–5732 (1994).
37. A. D. Weideman, R. H. Stnvn, J. R. V. Zanefeld, and M. R. Wilcox, "Error in predicting hydrosol backscattering form remotely sensed reflectance," J. Geophys. Res. 100, 13,163–13,177 (1995).
38. C. S. Roesler and M. J. Perry, "In situ phytoplankton absorption, fluorescence emission, and particulate backscattering spectra determined from reflectance," J. Geophys. Res. 100, 13.279-13.294 (1995).
39. N. Hoepffner and S. Sathyendranath, "Determination of the major groups of phytoplankton pigments from the absorption spectra of total particulate matter," J. Geophys. Res. 98, 22,789–22,803 (1993).

APPENDIX C

Spatial variability of oceanic phycoerythrin spectral types derived from airborne laser-induced fluorescence emissions

Frank E. Hoge, C. Wayne Wright, Todd M. Kana, Robert N. Swift, and James K. Yungel

Reprinted from APPLIED OPTICS / Vol. 37, No. 21 / July 20, 1998

Spatial variability of oceanic phycoerythrin spectral types derived from airborne laser-induced fluorescence emissions

Frank E. Hoge, C. Wayne Wright, Todd M. Kana, Robert N. Swift, and James K. Yungel

We report spatial variability of oceanic phycoerythrin spectral types detected by means of a blue spectral shift in airborne laser-induced fluorescence emission. The blue shift of the phycoerythrobilin fluorescence is known from laboratory studies to be induced by phycourobilin chromophore substitution at phycoerythrobilin chromophore sites in some strains of phycoerythrin-containing marine cyanobacteria. The airborne 532-nm laser-induced phycoerythrin fluorescence of the upper oceanic volume showed distinct segregation of cyanobacterial chromophore types in a flight transect from coastal water to the Sargasso Sea in the western North Atlantic. High phycourobilin levels were restricted to the oceanic (oligotrophic) end of the flight transect, in agreement with historical ship findings. These remotely observed phycoerythrin spectral fluorescence shifts have the potential to permit rapid, wide-area studies of the spatial variability of spectrally distinct cyanobacteria, especially across interfacial regions of coastal and oceanic water masses. Airborne laser-induced phytoplankton spectral fluorescence observations also further the development of satellite algorithms for passive detection of phytoplankton pigments. Optical modifications to the NASA Airborne Oceanographic Lidar are briefly described that permitted observation of the fluorescence spectral shifts.

OCIS codes: 010.3640, 010.4450, 300.2530, 300.6450, 300.6280.

1. Introduction

Since 1979, laser-induced phycoerythrin (PE) fluorescence has been observed from airborne platforms, specifically the NASA Airborne Oceanographic Lidar (AOL).[1] Until now, phytoplankton fluorescence in the yellow band (580-nm region) was ascribed only to the general PE pigment class,[2] and it has been used as a diagnostic signal for the presence of marine cyanobacteria, cryptophytes, or both in surface waters. PE exists in a number of distinct spectral forms, however, depending on species and photoacclimative state. These spectral types tend to be segregated in the oceans across inshore-offshore gradients related to nutrient status and clarity of the water.[3,4] Remote measurement of the spatial variability of these spectral types by use of the AOL was a goal of the present research. (A long-term goal of this research is to use such spectral fluorescence emissions in the development of satellite retrieval algorithms, eventually leading to global oceanic speciation mapping in the surface layer.)

PE is a class of pigment-protein macromolecule with chromophores that absorb light in the 480–560-spectral region. In cyanobacteria the functional light-harvesting unit is a hexameric protein aggregate (sometimes associated with an additional pigment-protein monomer) that contains 34 to 38 covalently bound chromophores. These chromophores are of two types: phycoerythrobilin (PEB), which absorbs in the 550–565-nm region, and phycourobilin (PUB), which absorbs in the 495-nm region. PEB is necessary for energy transfer between units of the photosynthetic light-harvesting antenna and is therefore found in all PE-containing marine cyanobacteria. Some strains of cyanobacteria have PUB substituted at selected chromophore binding sites on the PE molecule, conferring greater light absorption in the blue-green region of the spectrum. A high degree of PUB substitution with dominant absorption peaks at 495 nm is notable in specific

F. E. Hoge and C. W. Wright are with the Wallops Flight Facility, Goddard Space Flight Center, National Aeronautics and Space Administration, Wallops Island, Virginia 23337. T. M. Kana is with Horn Point Environmental Laboratories, University of Maryland, P.O. Box 775, Cambridge, Maryland 21613. R. N. Swift and J. K. Yungel are with the Wallops Flight Facility, E. G. & G. Inc., Wallops Island, Virginia 23337.

Rcceivcd 8 October 1997; revised manuscript received 19 March 1998.

0003-6935/98/214744-06$15.00/0

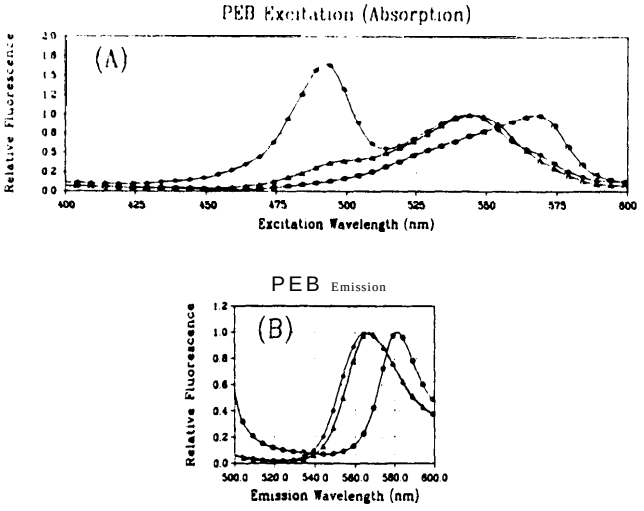

Fig. 1. PEB excitation spectra and fluorescence emission spectra of three cultures of phytoplankton that have PE: PUB rich (WH 8102; diamonds), PUB intermediate (WH 7803; triangles), and PUB deficient (WH 8018; circles). (A) The peak of the excitation spectrum shifts toward blue wavelengths when PUB chromophores are substituted within the hexameric protein aggregate. (B) As with the excitation spectra, the peak of the fluorescence emission spectrum shifts toward blue wavelengths when PUB chromophores are substituted within the hexameric protein aggregate.

strains of the ecologically important marine cyanobacterium genus *Synechococcus.5 The* PE spectral absorption band peaks near 565 nm when only PEB chromophores are present [Fig. l(A)]. The presence of PUB chromophores (with absorption-band peak at 495 nm) causes a 10–15-nm blueshift in the peak wavelength of the PEB absorption spectrum. Specifically, for PUB-containing PE the PEB absorption band occurs near 550 nm, regardless of the relative amounts of PUB and PEB [Fig. l(A)]. Notice that 532-nm laser emission can be absorbed by both PEB and PUB chromophores (though not optimally by either).

PE fluorescence, regardless of the presence or absence of PUB, is always redshifted relative to the PEB absorption peak, indicating that only PEB chromophores fluoresce5 [Fig. l(B)]. For PUB-deficient PE, the fluorescence emission band of PEB peaks at -580 nm [Fig. 1(B)]. However, the peak fluorescence emission wavelength from PUB-containing PE is blueshifted [Fig. 1(B)]. This spectral shift in fluorescence emission provides the possibility of identifying spectral strains by means of a single-wavelength excitation lidar system by measurement of the emission spectra of PE fluorescence.

Recent modifications to the original receiver optics of the AOL have resulted in significant rejection of backscattered 532-nm radiation accompanied by a substantial reduction of scattered light within the spectrometer. These improvements now permit observation of laser-induced fluorescence in the 560–570-nm band, thus facilitating observation of the shorter-wavelength emission of PUB-rich cyanobacteria. We report observations of airborne laser-induced fluorescence associated with PE containing different levels of PUB. The PUB and PEB spectral variations were observed during flights conducted over coastal, shelf, slope, Gulf Stream, and Sargasso Sea water masses of the western North Atlantic Ocean in early April 1995.

2. Materials and Methods

A. Airborne Data Acquisition

The requisite data were acquired on 3 April 1995 with the AOL flown aboard the NASA Goddard Space Flight Center P-3B aircraft. The laser-induced fluorescence measurement methods were analogous to those already published.[6,7] Briefly, a 532-nm laser pulse is transmitted vertically downward into the ocean to induce phycoerythrin and chlorophyll fluorescence emission from waterborne phytoplankton and water Raman emission from the surrounding seawater molecules.

The concurrent phycoerythrin (~540–595-nm), chlorophyll (~670–690-nm), and water Raman (~645-nm) spectral emissions are collected by a telespectroradiometer. The original AOL system[8–12] was modified to provide rejection of the 532-nm laser excitation wavelength from the instrument spectrometer and substantial reduction of scattered light. Specifically, a narrow-band holographic notch transmission filter placed into the collimated segment of the light path effectively rejects backscattered 532-nm laser radiation from the spectrometer. (The 532-nm pulse reflected from the holographic notch filter is in turn viewed by a photomultiplier and is used to temporally define the ocean surface target and initiate digitization of the fluorescence spectra.) Additional modifications include the removal of rigid light guides and all turning mirrors that constitute the original optical axis. A fiber optic face plate now occupies the focal plane of the new in-line optical path and transports the spectral radiation to mechanically reconfigured banks of original photomultiplier tubes. The resolution of each of the 84 channels of the fiber optic faceplate system is ~4 nm. However, the number of photomultiplier tubes currently available within the redesigned spectrometer is only 28; therefore we optically combined groups of three fiber optical channels at each photomultiplier tube to achieve -12-nm resolution per output band for this experiment. The signal path from the photomultiplier tubes through and including digitization remain essentially the same as reported previously.[8–12] Compared with the original light guides, the fiber optic channels have superior scattered-light rejection attributed to a considerably smaller viewing or acceptance angle.

A spectral and radiometric calibration is performed before and after each flight mission by viewing an internally illuminated 0.75m-diameter calibration sphere[13] placed beneath the aircraft telescope viewing port. Immediately following the 0.75-m sphere calibration, a lo-cm-diameter calibration sphere within the AOL system is viewed by mechanical in-

troduction (at the focal plane of the telescope) of the radiation via fiber optics. The small calibration sphere permits immediate transfer of the 0.75-m sphere calibration into the aircraft domain for periodic in-flight calibration. The LO-cm sphere calibration is followed by viewing 40-ns pulsed radiation from a bank of red LED's located behind the diffraction grating and in front of the fiber optic faceplate. The pulsed LED's provide transfer of the ground (and onboard) dc tungsten lamp calibrations to the wide-bandwidth pulsed portion of the AOL detection–amplification-digitization system.

The redesigned AOL fluorosensor is flown along with several additional sensor components and subsystems. These include two infrared Heimann KT-19 radiation thermometers to measure sea surface temperature (SST), a down-looking 256-channel spectroradiometer to gather ocean color radiance, and an uplooking 256 channel spectroradiometer equipped with a cosine collector to acquire downwelling solar n-radiance. Both of the auxiliary spectroradiometers are set to provide spectral coverage between -400 and -720 nm. The SST profile data acquired with the Heimann radiometers are presented in Section 3 below to aid in the interpretation of the phycoerythrin fluorescence profiles. The ocean color radiance and solar k-radiance data gathered with the two auxiliary spectroradiometers are not included in this paper but will be used in follow-on studies with the laser-induced phycoerythrin fluorescence data.

B. Laboratory Procedures

In vivo fluorescence excitation and emission spectra were determined on cultivated *Synechococcus* clones containing PE with high, medium, or no PUB chromophores typical of three spectral classes of marine *Synechococcus.* Clones were obtained from the Woods Hole culture collection and grown at ~50 $\mu E\ m^{-2}\ s^{-1}$ and 20 °C in F/2 (-Cu) media with a Sargasso Sea water base. Fluorescence measurements were made on an SLM/Aminco Model 500C spectrofluorometer with 4-nm excitation- emission bandpasses, corrected emission signals, and excitation ratio mode.

3. Results

A. Laboratory Observations

Fluorescence excitation and emission spectra for three *Synechococcus* strains are shown in Fig. 1. These strains represent maximum and minimum PUB/PEB ratios (and a typical intermediate form found among numerous isolates of *Synechococcus* from around the world). Laser light (532 nm) excites all spectral forms, mainly by exciting the blue absorption tail of PEB. PUB absorption is weak at 532 nm.[5] Because of the possibility of mixtures of spectral types in the water column and variations in quantum yield of PE fluorescence owing to photoacclimative and nutrient response processes,[14,15] quantitative estimates of PE based on spectral fluorescence are imprecise. However, it is possible to develop an index of the relative occurrence of PUB-containing forms by quantifying the ratio of fluorescence in the short- and long-wavelength emission bands.

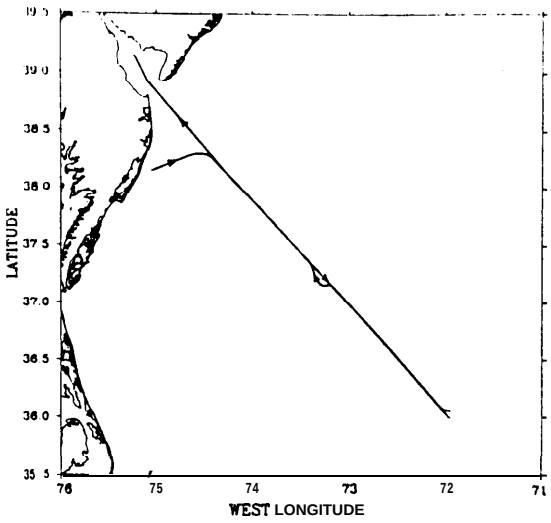

Fig. 2. Flight tracks of the NASA P3-B aircraft with the AOL system on 3 April 1995. The flight was initiated from Wallops Island toward the northeast, reoriented ~90°, and directed southeast to ~72 °W longitude and ~36 °N latitude. The flight track then traversed toward the northwest and terminated within Delaware Bay. The flight track deviation at 73.25 °W longitude and ~37.25 °N latitude was made to avoid a military field operation that was being conducted in that vicinity.

The sensitivity of this index to PE with and without PUB can be seen in the separation between the two fluorescence emission bands (Fig. 1). With the new capability of the AOL to resolve the 566-nm band, it is possible to detect the emission band of PUB-containing organisms, which yield a signifkantly higher ratio of the 566-593 optical channels than that obtained from PE lacking PUB. Thus the spectral fluorescence emission of PE-rich *Synechococcus* cultures suggests that naturally occurring species that have PUB can potentially be distinguished from PUB-lacking species by use of airborne laser spectrometry. The actual performance of a 532-nm source for defining relative PEB and PUB amounts is not easily determined from an analysis of laboratory excitation and emission spectra of cultures that contain PEB and PUB. Airborne field results are a better indicator of the potential effectiveness of the laser source and the entire methodology.

B. Airborne Observations

Figure 2 shows the flight track of the AOL on 3 April 1995. The flight was initiated from Wallops Island toward the northeast, reoriented ~90°, and directed southeast to 72 °W longitude and 36 °N latitude. There the flight track was reversed and traversed toward the northwest and terminated within Delaware Bay. The flight track deviation near 73.25 °W longitude and 37.25 °N latitude was made to avoid a

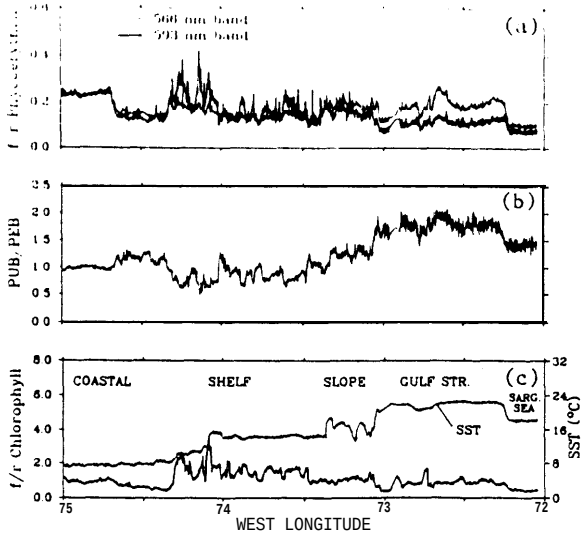

Fig. 3. (a) 532-nm laser-induced and water Raman-normalized PE fluorescence in the 566- and 593-nm AOL bands acquired during the west-to-east (outbound) flight track. (b) Ratio of the 566-nm fluorescence to 593-nm fluorescence. In the slope waters at -73.4 °W longitude the 566/593 nm ratio begins increasing in the offshore direction. (c) 532-nm laser-induced and water Raman-normalized chlorophyll fluorescence acquired during the outbound flight track. The chlorophyll fluorescence is highly correlated with the PEB fluorescence within the shelf water mass, except within the colder water flanking the coastline at the western end of the flight track. The SST data are from the airborne infrared radiometer.

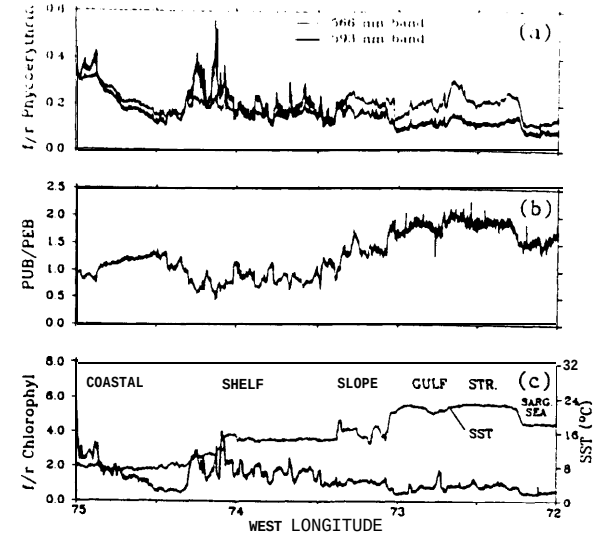

Fig. 4. (a) 532-nm laser-induced and water Raman-normalized PE fluorescence in the 566- and 593-nm bands acquired during the east-to-west (inbound) flight track. (b) Ratio of 566-nm fluorescence to 593-nm fluorescence. (c) 532-nm laser-induced and water Rarnan-normalized chlorophyll fluorescence acquired during the inbound flight track. The chlorophyll fluorescence is highly correlated with the PEB fluorescence within the shelf water mass. The SST data are from the airborne infrared radiometer.

military field operation that was being conducted in that vicinity.

Figure 3(a) shows the 532-nm laser-induced PE fluorescence in the 566- and the 593-nm bands (both bands have a width of -12 nm) acquired during the west-to-east (outbound) flight track. (The 593-nm band was used in lieu of the 580-nm band to provide wider spectral separation.) The ratio of the fluorescence signal in the 566-nm band to that in the 593-nm band is plotted in Fig. 3(b), and profiles of the SST and laser-induced chlorophyll fluorescence are shown in Fig. 3(c) to aid in the interpretation of the PE fluorescence profiles. Figure 4 contains the corresponding profiles acquired during the east-to-west (inbound) flight track. (The laser-induced PE and chlorophyll fluorescence bands have been normalized by the water Raman signal at -645 nm to remove variability in attenuation properties within the upper portion of the water column.[1,16]) One can readily see the precision or high measurement reproducibility of the AOL fluorosensor by visually comparing the fluorescence profiles from the outbound and the inbound flight tracks in Figs. 3 and 4, respectively. The locations of even relatively fine features are apparent in the contrasted profiles captured with the aircraft flying in the opposite direction. [The western portions of profiles should not be directly compared with one another west of 74.3 °W because the flight paths were not overlapping (see Fig. 2).] The locations of the coastal, shelf, slope, Gulf Stream, and Sargasso Sea water masses have been labeled in both Figs. 3 and 4.

The along-track profiles of the PE fluorescence bands [Figs. 3(a) and 4(a)] suggest the presence of both PUB and PEB pigments over the entire flight line. However, the relative strength of the laser-induced PE fluorescence in the 566- and 593-nm bands varies systematically. This systematic variability is especially apparent in Figs. 3(b) and 4(b), in which the 566-nm fluorescence has been ratioed to the 590-nm fluorescence. The intensity of fluorescence attributed to PUB-containing PE is seen to be elevated over the slope, Gulf Stream, and Sargasso Sea regions, whereas the intensity of fluorescence from PUB-lacking PE appears highest over the shelf region.

These airborne and laboratory observations are consistent with known distribution patterns for the two pigments; i.e., phytoplankton containing higher portions of the PEB pigment are generally associated with coastal waters, whereas the PUB-bearing organisms, in general, are the dominate PE pigment in offshore, oligotrophic waters.[3,4] The chlorophyll fluorescence can be seen to covary with the PEB pigment over most of the flight line, except for the easternmost portion of the outbound survey. In the inbound survey (Fig. 4) the strong correspondence between chlorophyll and PEB fluorescence continues within the eastern portion of the flight line at the entrance to Delaware Bay.

4. Discussion

Laser-induced fluorescence from the phycoerythrin PEB pigment fluorescence has been remotely ob-

served since 1979.[1] However, the presence of 532-nm laser light scattered into the fluorosensor spectrometer resulted in masking the presence of shorter-wavelength PE fluorescence. Recent modifications to the fluorosensor spectrometer (especially the implementation of a narrow-band holographic notch filter, use of fiber optics instead of light guides, and elimination of turning mirrors) have resulted in almost complete rejection of backscattered laser light and a substantial decrease in all scattered light. Laser-induced PE fluorescence spectra acquired with the AOL over coastal, shelf, slope, Gulf Stream, and Sargasso Sea waters of the Middle Atlantic Bight during early April 1995 contain an ~12-nm band centered at 566 nm, which is distinct from the band centered at 593 nm. The capability to measure remotely the spectral shift associated with PUB-containing PE suggests a potential application of airborne laser fluorescence methodology to wide-area mapping of the relative spatial variability of PE. This application may find more use in coastal–midshelf regions (and in coastal-oceanic transition zones) where the relative presence of the chromophoric types would be expected to be more variable, as can be seen from the April 1995 airborne fluorescence data set.

The excitation spectra of cultures (Fig. 1) and the excitation spectra of filtered surface samples[17] strongly suggest that the best bands for passive (solar) detection of PUB and PEB absorption are ~495 nm for PUB and ~555 nm for PEB. However, an important application of airborne wide-area fluorescence variability is the actual development of algorithms to retrieve the PUB and PEB absorption coefficients from water-leaving radiance data. Application of such algorithms to satellite ocean color imagery could lead to global PUB and PEB pigment maps similar to the chlorophyll scenes produced from Coastal Zone Color Scanner data. For example, concurrently observed water-leaving radiances can be used to identify optimum bands for retrieving PUB and PEB pigment absorption by application of methods similar to active-passive correlation spectroscopy.[18] Also, optimum PUB and PEB absorption band locations can potentially be improved by use of the airborne laser PE fluorescence data (together with concurrent chlorophyll and chromophoric dissolved organic matter laser-induced fluorescence data[6,7] within radiance models[19]) Once the optimum color band locations have been identified, the PUB and PEB absorption coefficients can, at least in principle, be retrieved from radiance or reflectance models.20 Finally, the arduous task of establishing valid specific absorption coefficients for PUB and PEB must be accomplished before the absorption coefficients of these pigments can be converted into concentrations.

The PUB and PEB identification algorithm herein uses only two bands, located on the bluest and reddest portions of the PE fluorescence emission spectrum. Future efforts will investigate the use of other algorithms, including the centroid algorithm. That algorithm calculates the centroid of the entire PE emission band. The centroid shifts to bluer wavelengths in the presence of additional PUB. Comparative analyses will be used to determine whether PUB and PEB identification is improved.

The passive observation of PE pigment by active–passive (laser-solar) correlation spectroscopy methods[18] has been reported." Now, following laser observations of the PEB variability, the potential exists to investigate the feasibility of detecting and eventually quantifying both PUB and PEB pigment absorption coefficients by use of oceanic water-leaving radiances. The presence of both PUB and PEB absorption within water-leaving radiances will be established as before, except that both the PUB and the PEB pigments will now be sought by correlation spectroscopy'8 methods. These analyses are beyond the scope of this paper, and future investigations will address the potential detection of both PUB and PEB pigments by use of oceanic upwelled radiances.

References

1. F. E. Hoge and R. N. Swift, "Airborne simultaneous spectroscopic detection of laser-induced water Raman backscatter and fluorescence from chlorophyll a and other naturally occurring pigments," Appl. Opt. 20, 31973205 (1981).
2. F. E. Hoge and R. N. Swift, "Phytoplankton accessory pigments: evidence for the influence of phycoerythrin on the submarine light field," Remote Sensing Environ. 34, 19-25 (1990).
3. R. J. Olson, S. W. Chisholm, E. R. Zettler, and E. V. Armbrust, "Analysis of Synechococcus pigment types in the sea using single and dual beam flow cytometry," Deep-Sea Res. 35, 425–440 (1988).
4. R. J. Olson, S. W. Chisholm, E. R. Zettler, and E. V. Armbrust, 'Pigments, size, and distribution of Synechococcus in the North Atlantic and Pacific Oceans," Limnol. Oceanogr. 35, 45-58 (1990).
5. L. J. Ong and A. N. Glazer, "Phycoerythrins of marine unicellular cyanobacteria. I. Bilin types and locations and energy transfer pathways in Synechococcus spp. phycoerythrins," J. Biol. Chem. 266, 9515-9527 (1991).
6. F. E. Hoge, R. N. Swift, J. Y. Yungel, and A. Vodacek, "Fluorescence of dissolved organic matter: a comparison of North Pacific and North Atlantic Oceans during April 1991," J. Geophys. Res. 98, 22,779–22,787 (1993).
7. F. E. Hoge and R. N. Swift, "The influence of chlorophyll pigment upon upwelling spectral radiances from the North Atlantic Ocean: an active-passive correlation spectroscopy study," Deep-Sea Res. 40, 265-277 (1993).
8. F. E. Hoge and R. N. Swift, "Oil film thickness measurement using airborne laser-induced water Raman backscatter," Appl. Opt. 19, 3269-3281 (1980).
9. F. E. Hoge. R. N. Swift, and E. B. Frederick, "Water depth measurement using an airborne pulsed neon laser system," Appl. Opt. 19, 871-883 (1980).
10. F. E. Hoge and R. N. Swift, "Airborne dual laser excitation and mapping of phytoplunkton photopigments in a Gulf Stream warm core ring," Appl. Opt. 22, 2272-2281 (1983,.
11. F. E. Hoge, R. E. Berry, and R. N. Swift, "Activcpassive airborne ocean color measurcmcnt. 1. Instrumentation," Appl. opt. 25, 39–47 (1986).
12. F. E. Hoge, R. N. Swift, and J. K. Yungel, "Active–passive airborne ocean color measurement. 2. Applications," Appl. opt. 25, 48–57 (1986).
13. W. A. Hovis and J. S. Knoll, "Characteristics of an internally

illuminated calibration sphere," Appl. Opt. 22, 4004–4007 (1983).
14. T. M. Kana, N. L. Feiwel, and L. C. Flynn, "Nitrogen starvation in marine *Synechococcus* strains: clonal differences in phycobiliprotein breakdown and energy coupling," Marine Ecol. Prog. Ser. 88, 75–82 (1992).
15. T. M. Kana and P. M. Glibert, "Effect of it-radiances up to 2000 $\mu E\ m^{-2}\ s^{-1}$ on marine *Synechococcus* WH7803. I. Growth, pigmentation, and cell composition," Deep-Sea Res. 34, 479-495 (1987).
16. M. Bristow, D. Nielsen, D. Bundy, and F. Furtek, "Use of water&man emission to correct airborne laser fluorosensor data for effects of water optical attenuation," Appl. Opt. 20, 2889-2906 (1981).
17. M. M. Vernet, B. G. Mitchell, and 0. Holm-Hansen, "Adaptation of *Synechococcus in situ* dctcrminod by variability in intracellular phycocrythrin-543 at a coastal station off the Southern California coast. USA," Marine Ecol. Prog. Ser. 63, 9-16 (1990).
18. F. E. Hoge and R. N. Swift. "Active-passive correlation spectroscopy: a new technique for identifying ocean color algorithm spectral regions," Appl. Opt. 25, 2571–2583 (1986).
19. F. E. Hoge, R. N. Swift, and J. K. Yungel, "Oceanic radiance model development and validation: application of airborne active-passive ocean color spectral measurements," Appl. Opt. 34, 3468–3476 (1995).
20. F. E. Hoge, M. E. Williams, R. N. Swift, J. K. Yungel, and A. Vodacek, "Satellite retrieval of the absorption coefficient of chromophoric dissolved organic matter in continental margins," J. Geophys. Res. 100, 24,847–24,854 (1995).

APPENDIX D

JOURNAL OF GEOPHYSICAL RESEARCH, VOL. 101, NO. C7, PAGES 16,631–16,648, JULY 15, 1996

Satellite retrieval of inherent optical properties by linear matrix inversion of oceanic radiance models: An analysis of model and radiance measurement errors

Frank E. Hoge
NASA Goddard Space Flight Center, Wallops Flight Facility, Wallops Island, Virginia

Paul E. Lyon
EG&G Washington Analytical Services, Inc., Wallops Flight Facility, Wallops Island, Virginia

Abstract. The linear summability of inherent optical properties (IOPs) is exploited to provide matrix equations for retrieval of phytoplankton absorption, dissolved organic matter, and constituent backscatter. Spectral models for the phytoplankton pigment absorption coefficient, chromophoric dissolved organic matter (CDOM) absorption coefficient, and total constituent backscatter (TCB) coefficient are first used to calculate 5×10^5 water-leaving spectral radiances for a wide range of normally distributed IOP values at 410, 490, and 555 nm. Then, the spectral radiances are inverted to simultaneously provide phytoplankton pigment absorption coefficient, CDOM absorption coefficient, and total constituent backscatter coefficient on a pixel-by-pixel basis to demonstrate that (1) matrix inversion is very rapid and well conditioned, (2) the IOPs are exactly determined when the water-leaving radiances and IOP spectral models are error free, (3) for equal radiance errors sequentially occurring in one of three sensor bands, phytoplankton pigment retrieval errors are generally higher than CDOM and TCB coefficient errors, (4) retrieval errors for all the IOPs are strongly dependent on phytoplankton pigment spectral model Gaussian width errors, (5) phytoplankton pigment absorption and CDOM absorption retrieval errors are more sensitive to CDOM spectral slope errors than the TCB coefficient retrievals, and (6) TCB wavelength-ratio-exponent errors produce less impact on the phytoplankton absorption coefficient retrieval than upon the CDOM absorption or the TCB coefficient retrievals.

Introduction

Study of the global biogeochemical cycles requires quantification of the amount of organic matter found in all the world's oceans [*Siegenthaler and Sarmiento*, 1993]. It is also desirable to know the concentration of chlorophyll (hereafter generically called phytoplankton pigment) because it too contributes to the net atmosphere-ocean carbon dioxide flux. Present empirical radiance ratio algorithms applied to satellite ocean color data provide only an estimate of the phytoplankton pigment and cannot account for the chromophoric dissolved organic matter (CDOM) and the absorption of numerous other constituents.

One method to retrieve CDOM and other constituents is by the inversion of oceanic radiance models (or alternately, reflectance models). Oceanic radiance models describe the generation of upwelled water-leaving spectral radiance caused by backscatter and absorption of the incident downwelling solar irradiance. In radiance models, total absorption is the sum of the absorption of the water molecules and constituents. Likewise, total backscatter is the sum of the backscatter of the water and constituents. This summability of absorption (and backscatter) is exploited to provide equations that fully describe the retrieval of inherent optical prop&ties (IOPs) from upwelled water-leaving radiances.

It is the objective of this paper to (1) describe the feasibility of the linear matrix inversion of radiance models, (2) show that the inversion is very rapid and free of singularities, (3) quantify errors in IOP retrievals as induced by errors in the upwelled water-leaving radiances, and (4) quantify errors in IOP retrievals as induced by model uncertainties. The analyses are limited to three sensor bands and IOP models. No attempt is made to apply the linear matrix inversion to actual airborne and satellite-derived water-leaving radiance data to retrieve IOPs (from which the constituent concentrations can be obtained).

Paper number 96JC01414.
0148-0227/96/96JC-01414$09.00

The Oceanic Radiance Model

The oceanic radiance model [*Gordon et al.*, 1988] chosen for the retrieval has been utilized for prediction of upwelled radiance at the sea surface as a function of phytoplankton pigment concentration [*Hoge* er al., 1995a]. It has been used to successfully calculate water leaving radiances using phytoplankton absorption derived from airborne laser-induced and water-Raman-normalized chlorophyll fluorescence [*Hoge* et *al.*, 1995a]. The model has also been inverted by sequential convergent iteration to retrieve the CDOM absorption coefficient from satellite coastal zone color scanner (CZCS) data [*Hoge et al.*, 1995b]. The inversion methods described herein are fully applicable to reflectance models with only minor modifications [*Carder and Steward*, 1985; *Carder et al.*, 1986, 1989, 1991;

Morel, 1988; *Sathyendranath et al.*, 1989; *Roesler and Perry*, 1995]. (Before applying these techniques to satellite or airborne data, the reader may wish to include bidirectional reflectance effects [*Morel and Gentili*, 1991, 1993; *Morel et al.*, 1995] that were outside the scope of the present study. Also, geometrical shape factors should be included in the model; otherwise, backscatter coefficient retrievals can contain errors of ≤40% depending on the solar angle and hydrosol constituents [*Weideman et al.*, 1995].)

The complete water-leaving radiance model [*Gordon et al.*, 1988] is

$$L_w(\lambda) = F_0 t(\theta_0) \cos(\theta_0) MR/Q, \quad (1)$$

where F_0 is the extraterrestrial solar irradiance, θ_0, is the solar zenith angle, $t(\theta_0)$ is the diffuse transmittance of the atmosphere, and R is the irradiance reflectance just beneath the sea surface. There, $R = E_u/E_d$, where E_u and E_d are the upwelling and downwelling irradiances, respectively, just beneath the surface. Q is the ratio of the upwelling radiance to the upwelling irradiance toward zenith. M is defined by

$$M = (1 - \rho)(1 - \bar{\rho})/m^2(1 - rR), \quad (2)$$

where ρ is the Fresnel reflectance of the sea surface for normal incidence, $\bar{\rho}$ is the Fresnel reflection albedo of the sea surface for irradiance from the sea and sky, m is the index of refraction of seawater, and r is the water-air reflectance for totally diffuse irradiance. For the $(1 - rR)$ term, $r \sim 0.48$ and accounts for the effect of internal reflectance of the upwelling radiance field by the sea surface. The maximum value of R for case 1 waters is 0.08-0.09 so the term rR is small in blue waters but may be much larger in coastal waters. Nearly independent of wind speed, the value of ρ is taken to be 0.021 over the visible spectrum. *Gordon et* al. [1988] further indicate that $\bar{\rho}$ depends in a complicated manner on the solar zenith angle through the dependence of the relative amounts of direct sunlight and diffuse skylight incident on the sea surface. They indicate that $\bar{\rho} < 0.1$ when $\theta_0 < 60°$ which is typical of most CZCS applications. Finally, *Gordon* et *al.* [1988] suggest that for $0 \le \theta_0 \le 60°$, the term $(1 - \bar{\rho})$ would be expected to vary between 0.934 and 0.979. For these conditions, M was chosen to be a constant -0.55. The extraterrestrial solar irradiance F_0 values were taken from *Gregg and Carder* [1990].

Gordon et *al.* [1988] have determined that for $\theta_0 \ge 20°$, R/Q can be directly related to the total absorption a and the total backscatter b_b by

$$R/Q = (l_1 X + l_2 X^2) \quad (3)$$

where $l_1 = 0.0949$, $l_2 = 0.0794$, and

$$X = b_b/(b_b + a). \quad (4)$$

Gordon et al. [1988] also concluded that the error in (3) is significantly less than 10% for a wide range of realistic scattering phase functions and that for $\theta_0 \le 20°$, R/Q depends on the details of the scattering phase function in the backward direction. Thus for the work herein one should expect errors no greater than the above amounts due to the radiance model alone. The highest possible accuracy was desired for our study findings. Accordingly, terms in X^2 were retained. The wavelength variable A is suppressed unless specifically required. Normalized water leaving radiance, $[L_w(\mathrm{A})]_N$, is that which would exit the sea surface if the Sun were at zenith and it' the atmosphere were absent; $L_w(\lambda) = [L_w(\lambda)]_N t(\theta_0) \cos(\theta_0)$. For the computations herein the solar zenith angle θ_0 was held fixed at zero degrees and the atmosphere assumed to be absent such that $t(\theta_0) \cos(\theta_0) = 1$.

The total backscatter coefficient b_b is the scalar sum of the backscatter of seawater b_{bw} and all constituents b_{bi}. That is, $b_b = b_{bw} + b_{bi}$. Herein, b_{bi} is called the total constituent backscatter (TCB) coefficient. Likewise, a is the total absorption and is the scalar sum of the absorption of seawater a, and all constituents a,. The a, and b_{bw} constants were obtained from *Smith and Baker* [1981]. Any number of absorbing (and backscattering) constituents can be accommodated, Herein, assume for the moment that the absorption is caused by three absorbing constituents: phytoplankton a_{ph}, chromophoric dissolved organic matter a,,,,, and detritus a,,,,. The sum $a_i = a_{ph} + a_{CDOM} + a_{detr}$ is called the total constituent absorption (TCA). Thus the total absorption is $a = a_w + a_{ph} + a_{CDOM} + a_{detr}$. Nevertheless, it is desirable in this initial study to reduce the complexity of the analyses without severely compromising the understanding of the final results. To do this, recall that the detritus absorption has the same spectral form as the CDOM: it declines exponentially with increasing wavelength [*Hoepffner and Suthyendranath*, 1993; *Roesler et al.*, 1989]. The spectral slope of the detritus is, however, considerably more variable. Ranging from 0.004 to 0.020 (1/nm) it encompasses the generally accepted CDOM slope of 0.014 (1/nm). The mean spectral slope of detritus is -0.011 ± 0.002 (1/nm) [*Roesler* et *al.*, 1989]. To reduce the intricacy of our analyses, we will assume that the spectral average over all detritus absorption yields a slope that is equal to the CDOM spectral slope. With this assumption we represent the combined absorption as $a_{CDOM} + a_{detr} = a_d$. (At the conclusion of the matrix methodology discussion it will be evident how one can extend the matrix inversion to separately include both the CDOM and the detritus absorption. Because of the dominant character of CDOM, and for brevity, the a_d may subsequently be referred to as CDOM absorption.)

Retrieval of Inherent Optical Properties by Linear Matrix Inversion

Equation (4) can be solved in terms of total absorption coefficient a and total backscatter coefficient b_b

$$a + b_b(1 - 1/X) = 0. \quad (5)$$

where X is given by the solution of (1) and (3). Next, define $v = (1 - 1/X)$ and separate the seawater absorption and seawater backscatter contributions from the total constituent absorption and total constituent backscatter,

$$a_i + b_{bi} v = -(a_w + b_{bw} v). \quad (6)$$

Then, for wavelengths A,, where $i = 1, 2, 3$, the equations describing the IOPs are

$$a_{ph}(\lambda_i) + a_d(\lambda_i) + b_{bi}(\lambda_i) v(\lambda_i) = h(\lambda_i), \quad (7)$$

where $h(\lambda_i)$ is defined as the right side of (6) that contains the column matrix. or vector, of hydrospheric constants (seawater absorption and backscatter) and oceanic water-leaving radiances. Equation (7) contains three unknowns for each spectral radiance measurement. Additional equations are provided by IOP spectral models for a_{ph}, a_d, and h_{bi} as follows.

Starting first with $b_{bi}(\mathrm{A},)$. the following model is used to describe the total constituent backscatter coefficient at a n y

wavelength λ_i relative to the total constituent backscatter at a reference wavelength λ_r,

$$b_{bt}(\lambda_i) = b_{bt}(\lambda_r)(\lambda_r/\lambda_i)^n, \quad (8)$$

where n is a constant. This TCB coefficient model was chosen by analogy with previous work. For example, *Morel* [1977] suggested a wavelength-ratio model for particulate backscattering and subsequently *[Morel,* 1988] provided a backscatter model for phytoplankton that also varied inversely with wavelength. ***Smith and Baker*** [1981] suggested a similar model during their study of clear natural water. For nonabsorbing backscatterers such as coccoliths, ***Gordon et al.*** [1988] used a $(550/\lambda)^n$ where $n > 1$. ***Suthyendrunuth et*** al. [1989] suggested a $(1/\lambda)^n$ model for detrital particles. ***Lee et al.*** [1994] used a similar model and showed that the exponent can vary from 0 to ***2.4. Maffione*** et ***al.***'s [1995] field measurements showed that the spectral backscatter exponent can vary from 2.0 to 4.1. ***Hoge et al.*** [1995b] used this particulate backscatter model with n = 1.5 during retrieval of the CDOM absorption coefficient from both satellite and airborne water-leaving radiances. Moreover, a diffuse attenuation coefficient model ***[Gordon,*** 1989, 1994] can be inverted to (1) provide an alternative numerical TCB coefficient model and/or (2) show that the $(\lambda_b/\lambda_i)^n$ spectral model is a reasonable choice especially in the ~410- to 580-nm range. The diffuse attenuation coefficient model is $K \cong 1.0395\ D_0(a + b_b)$ where K is the diffuse attenuation coefficient and D_0 is the downwelling distribution function. Since $b_b = b_{bw} + b_{bt}$ and $a = a_w + a_{ph} + a_d$, the desired total constituent backscatter is $b_{w} = (K/1.0395\ D_0) - a_w - a_{ph} - a_d - b_{bw}$. Field and laboratory measurements, derived models, and reasonable approximations are available to allow an estimate of b_{bt} (Appendix A). The mean of b_{bt} over the range of all absorbers, $\langle b_{bt} \rangle$, is shown to be reasonably represented by $(\lambda_b/\lambda_i)^{3.3}$ (Appendix A). The reference wavelength λ_r is arbitrary but clearly should be chosen to be within a spectral region where backscatter is expected. The reference wavelength need not coincide with the sensor observational bands. Finally, the radiance model presented in (1) or (7) can be inverted to obtain a spectral backscatter numerical model (Appendix A). Both the K model and radiance model inversions yield similar results and suggest that the inverse wavelength model is generally acceptable from ~410 to 580 nm. However, the possible use of an exponential backscattering model such as $\exp[-s(\lambda_i - \lambda_b)]$ (where s is the spectral slope of the backscatter) will be discussed after the matrix formulation is completed.

Furthermore,

$$a_d(\lambda_i) = a_d(\lambda_d) \exp[-S(\lambda_i - \lambda_d)], \quad (9)$$

(where S is the CDOM/detritus spectral slope) is a good representation of the spectral absorption coefficient of chromophoric dissolved organic matter at any wavelength λ, [*Bricaud* et *al.*, 1981; *Hoge et* al., 19933 relative to the CDOM absorption coefficient at an arbitrary reference wavelength λ_r. The reference wavelength λ_r need not coincide with the sensor observational bands. However, reference wavelengths in the red are avoided since the CDOM absorption is lower in these regions. The above model could be implemented numerically, but there seems to be no compelling reason since the CDOM spectral slope parameter S is not highly variable in the global ocean [*Blough*, 1993; *Carder et al.*, 1986, 199 *I*; *Hoge et al.*, 1993].

Finally, a single Gaussian is used to represent the phytoplankton absorption coefficient in the chosen spectral regions [*Hoepffner and Sathyendranath*, 1993]. While a single Gaussian would appear to be an ovcrsimplitication. *Lee et al.* [1996] have shown excellent results from 400 to 570 nm which encompass the spectral range of our study. For more complex analytical studies, several Gaussians can be used to more accurately represent the phytoplankton absorption including chlorophylls and carotenoids. Thus

$$a_{ph}(\lambda_i) = a_{ph}(\lambda_g) \exp[(\lambda_i - \lambda_g)^2/2g^2], \quad (10)$$

where g is a parameter that defines the spectral width of the Gaussian about the peak wavelength λ_g. The Gaussian peak need not be located precisely coincident with the phytoplankton pigment absorption peak as long as the spectral width parameter g permits accurate representation of the relative specific absorption coefficient in all three sensor observational bands. At this point the "reference" absorption $a_{ph}(\lambda_g)$ is obtained only at the Gaussian peak wavelength λ_g, but this apparent constraint can be easily removed (Appendix B). The above analytical model can be implemented numerically. A possible form for the numerical model in terms of the specific absorption is $a_{ph}(\lambda_i) = a_{ph}(\lambda_g)[a^*(\lambda_i)/a^*(\lambda_g)]$. Tabular values for the specific absorption $a^*(\lambda_i)$ have been given by ***Hoepffner and Suthyendrunuth*** [1993].

The substitution of (8), (9), and (10) into (7) yields

$$a_{ph}(\lambda_g) \exp[(\lambda_i - \lambda_g)^2/2g^2] + a_d(\lambda_d) \exp[-S(\lambda_i - \lambda_d)] + v(\lambda_i) b_{bt}(\lambda_b)(\lambda_b/\lambda_i)^n = h(\lambda_i). \quad (11a)$$

Equation (11a) contains only three unknowns, $a_{ph}(\lambda_g)$, $a_d(\lambda_d)$, and $b_{bt}(\lambda_b)$, at any wavelength λ_i. Thus a consistent solution can be obtained using only three sensor wavelengths λ_1, λ_2, and λ_3. The inversion matrices are easily obtained by sequentially writing (lla) for λ_1, λ_2, and λ_3. Essentially, the three observational sensor wavelengths at λ_1, λ_2, and λ_3 enumerate or label the rows of the matrices, while the three constituents at their reference wavelengths $a_{ph}(\lambda_g)$, $a_d(\lambda_d)$, and $b_{bt}(\lambda_b)$ label the columns Of the explicit matrix arrangement Of (lla) so that

$$\begin{bmatrix} \exp[(\lambda_1 - \lambda_g)^2/2g^2] & \exp[-S(\lambda_1 - \lambda_d)] & (\lambda_b/\lambda_1)^n v(\lambda_1) \\ \exp[(\lambda_2 - \lambda_g)^2/2g^2] & \exp[-S(\lambda_2 - \lambda_d)] & (\lambda_b/\lambda_2)^n v(\lambda_2) \\ \exp[(\lambda_3 - \lambda_g)^2/2g^2] & \exp[-S(\lambda_3 - \lambda_d)] & (\lambda_b/\lambda_3)^n v(\lambda_3) \end{bmatrix} \cdot \begin{bmatrix} a_{ph}(\lambda_g) \\ a_d(\lambda_d) \\ b_{bt}(\lambda_b) \end{bmatrix} = \begin{bmatrix} h(\lambda_1) \\ h(\lambda_2) \\ h(\lambda_3) \end{bmatrix} \quad (11b)$$

The oceanic state vector of unknown IOPs at their reference wavelengths, $\mathbf{p} = [a_{ph}(\lambda_g), a_d(\lambda_d), b_{bt}(\lambda_b)]^T$, where T denotes the transpose, is the solution of a matrix equation of the form

$$\mathbf{Dp} = \mathbf{h} \quad (12)$$

where **D** is the data and model (hereafter called data-model) matrix and **h** is the vector of seawater absorption and backscatter hydrospheric constants and radiance data. It is important to emphasize that the **D** matrix must be inverted for every pixel or oceanic radiance spectrum since it contains radiance data in addition to model parameters. It is clear that the matrix inversion can be extended to any number of constituents as long as accurate IOP models can be found to satisfactorily

represent the spectral absorption and backscatter of each (and sufficient sensor bands are available in the observational data to yield a solution). (The column vectors in the D matrix can be reformulated so that the constants that represent the spectral models can be referenced to A_1. This simplifies the matrix inversion and retrieves constituents as they exist at measured radiance wavelengths. Accordingly, an alternate form of the **D** matrix is given in Appendix B for these specific reference wavelengths. Additionally, suggestions for the derivation of constituent concentrations from the IOP vector p are given in Appendix C.) Equation (12) is comparable to the well-known linear matrix equation $\mathbf{Ax} = \mathbf{b}$ whose solutions have been extensively studied. The direct solution to (12) is represented by

$$\mathbf{p} = \mathbf{D}^{-1}\mathbf{h}. \quad (13)$$

$\mathbf{D}^{-1}$ denotes the inverse of the data and model matrix **D**. Overdetermined least squares, weighted least squares, or other solutions are not within the scope of this paper. Instead, the analyses focus on even-determined solutions wherein the number of IOPs (unknowns) is equal to the number of sensor bands (equations). In this case the solutions, if obtainable, are unique.

The matrix formulation of the radiance mode1 inversion exemplified by (llb), (12), and (13) is a powerful framework for IOP retrievals as well as analysis of errors in the retrievals. It is of fundamental importance to determine if very large changes arise in p when small changes occur in **D** and **h**. If large changes occur, then the inversion problem is unstable or ill conditioned and may need reformulation to render it more stable. If the solution is found to be stable, it is then important to further quantify the errors in p caused by errors in **D** and **h**.

Sensitivity of p to Perturbations in D: Analysis of the Singularity of D

Some limited information about potential uncertainties in **p** can be obtained by analytical (as opposed to numerical) examination of the singularity of **D** in (llb). Of course, if the columns (or rows) of **D** are linearly dependent, then column (or row) degeneracy occurs, the determinant vanishes (det **D** = 0), and **D** is singular.

It is instructive to analyze the singularity of **D** for some specific, but important, conventional oceanic conditions that may produce model-induced singularity in **D** and prevent successful inversion or IOP retrieval. Suppose that within a deep-ocean or blue-water region, a phytoplankton patch has sufficiently senesced or collapsed so that only detritus and its CDOM remain. The desired IOPs are detritus absorption coefficient, CDOM absorption coefficient, and the total constituent backscatter coefficient. (The constituent backscatter is provided principally by the detritus since CDOM is a molecular constituent.) Under these conditions the particulate absorption in column 1 of (1 lb) is detrital in spectral form and is modeled by $\exp[-q(\lambda - \lambda_{det})]$ where q is the detrital absorption spectral slope [*Hoepffner and Sathyendranath*, 1993; *Roesler et al.*, 1989]. Since the CDOM in column 2 is modeled by $\exp[-S(\lambda - \lambda_{CDOM})]$, linear dependence and singularity are assured when $q = S$. But from a physical standpoint this is exactly what is expected when $S = q$: the detritus and CDOM are not distinguishable on the basis of their absorption and one can only retrieve the combined detritus + CDOM absorption coefficient, a_{det} + CDOM, and the TCB coefficient. If $q \approx S$, then D can be nonsingular but unstable with large uncertainties expected in **p**. If q is sufficiently different from S, then a stable D may result in an acceptable inversion. (If q is "nearly equal to" S, then D may be stable but "near" an unstable matrix. It is possible to estimate how near $\mathbf{D} \cdot \mathbf{p} = \mathbf{h}$ is to singularity [*Gulob and Van Loan*, 1989] through the reciprocal of the condition number to be discussed in a later section.)

Another important oceanic condition allows an analytical expression to be derived for the singularity of **D**. Low chlorophyll circumstances occur in the Middle Atlantic Bight during winter and summer seasons. During these time periods the constituent absorption is so dominated by CDOM that the phytoplankton chlorophyll absorption can be ignored [*Hoge et al.*, 1995b]. Accordingly, the retrieval of CDOM and TCB IOPs is given by

$$\begin{bmatrix} \exp[-S(\lambda_1 - \lambda_d)] & (\lambda_b/\lambda_1)^n v(\lambda_1) \\ \exp[-S(\lambda_2 - \lambda_d)] & (\lambda_b/\lambda_2)^n v(\lambda_2) \end{bmatrix} \cdot \begin{bmatrix} a_d(\lambda_d) \\ b_{bt}(\lambda_b) \end{bmatrix} = \begin{bmatrix} h(\lambda_1) \\ h(\lambda_2) \end{bmatrix} \quad (14)$$

It can be readily shown that singularity (det **D** = 0) will occur for

$$\exp[S(\lambda_2 - \lambda_1)] - [v(\lambda_1)/v(\lambda_2)](\lambda_2/\lambda_1)^n = 0. \quad (15)$$

Or $S(\lambda_2 - \lambda_1) - \ln[v(\lambda_1)/v(\lambda_2)] - n \ln[\lambda_2/\lambda_1] = 0$. This latter expression shows the intimate relationships that exist between (1) the IOP model parameters S and n and (2) and the radiance model (through the v_i) in order to produce singularity in the **D** matrix (and eventually lead to sensitivities in **p** as near-singularity is approached). The observational wavelengths λ_1 and λ_2 can be chosen to be different fixed constants and since the CDOM spectral slope parameter S is not highly variable in the global ocean [*Blough et al.*, 1993; *Carder et al.*, 1986; *Carder et al.*, 1991; *Hoge et al.*, 1993], then $S(\lambda_2 - \lambda_1)$ is a constant. Hence (15) shows that near singularity the sensitivity in $\mathbf{p} = [a_d, b_{bt}(\lambda_b)]^T$ is influenced by radiance variations (via the ratio $v(\lambda_1)/v(\lambda_2)$) and the known spatial variations in n [*Lee et al.*, 1994; *Maffione et al.*, 1995]. Since the spectral locations, λ_1 and λ_2, can be adjusted, (15) further suggests that sensor wavelengths play a role in defining the singularity of **D** and sensitivity of **p**. (Obviously, if $\lambda_1 = \lambda_2$, then det **D** is identically zero and singularity is assured.)

Furthermore, for a low chlorophyll condition in the Middle Atlantic Bight, it can be shown that the TCB coefficient can be modeled by an expression that is similar to the CDOM and detritus models: $\exp[-s(\lambda_1 - \lambda_2)]$ where s is the spectral slope of the backscatter. With this model, and for ignorable phytoplankton absorption, the IOP retrieval equations are

$$\begin{bmatrix} \exp[-S(\lambda_1 - \lambda_d)] \exp[-s(\lambda_1 - \lambda_b)]v(\lambda_1) \\ \exp[-S(\lambda_2 - \lambda_d)] \exp[-s(\lambda_1 - \lambda_b)]v(\lambda_2) \end{bmatrix} \cdot \begin{bmatrix} a_d(\lambda_d) \\ b_{bt}(\lambda_b) \end{bmatrix} = \begin{bmatrix} h(\lambda_1) \\ h(\lambda_2) \end{bmatrix} \quad (16)$$

The analytical expression for singularity (det D = 0) is

$$\exp[(S - s)(\lambda_1 - \lambda_2)] - [v(\lambda_2)/v(\lambda_1)] = 0. \quad (17)$$

Or $(S - s)(\lambda_1 - \lambda_2) - \ln[v(\lambda_2)/v(\lambda_1)] = 0$. Since $\lambda_1 \neq \lambda_2$ by choice, then $S = s$ does not guarantee singularity since $\ln[v(\lambda_1)/v(\lambda_2)]$ will still be nonzero so long as the wavelength choice produces $v(\lambda_1) \neq v(\lambda_2)$. Thus (17) suggests that an

exponential model can be used for CDOM and concurrently used for the TCB model.

Returning to the 3 × 3 phytoplankton. CDOM, and backscatter retrieval given by (1 lb). the singularity condition det **D** = 0 gives an expression that contains three cofactors that are very similar to the singularity condition for (14). When expanded using the elements of the phytoplankton column, det **D** = 0 yields

$$\begin{aligned}&\exp[(\lambda_1-\lambda_g)^2/2g^2]\{\exp[-S(\lambda_2-\lambda_d)](\lambda_b/\lambda_3)^n v(\lambda_3)\\&\quad-\exp[-S(\lambda_3-\lambda_d)(\lambda_b/\lambda_2)^n v(\lambda_2)]\}\\&\quad+\exp[(A,-\lambda_g)^2/2g^2]\{\exp[-S(\lambda_1-\lambda_d)](\lambda_b/\lambda_3)^n v(\lambda_3)\\&\quad-\exp[-S(\lambda_3-\lambda_d)(\lambda_b/\lambda_1)^n v(\lambda_1)]\}\\&\quad+\exp[(\lambda_3-\lambda_g)^2/2g^2]\{\exp[-S(\lambda_1-\lambda_d)](\lambda_b/\lambda_2)^n v(\lambda_2)\\&\quad-\exp[-S(\lambda_2-\lambda_d)(\lambda_b/\lambda_1)^n v(\lambda_1)]\}=0.\end{aligned}\tag{18}$$

The complexity of this equation suggests that singularity will be infrequent. The numerical studies herein verified the infrequency. This equation prominently illustrates the attractiveness of numerical methods, since laborious analysis of this latter relationship will, in the end, yield only the circumstances for singularity.

If singularity, or near singularity, is encountered using standard inversion methods, there are ways of dealing with the equations. The singular value decomposition (SVD) methodology will allow a diagnosis and a solution [*Press* et *al.*, 1994].

Sensitivity of p to Perturbations in D and h: Numerical Considerations

The above analysis of the singularity of **D,** while providing some useful insight, is of very limited quantitative use. Additional analyses are needed to more fully quantify and understand possible sensitivities in **p** resulting from uncertainties in **D** and **h.**

Relative to **h,** the data-model matrix **D** plays the major role in the propagation of errors into **p.** For example, for **Dp = h,** consider the system of equations **(D + Δ)p' = (h + S),** where A and δ represent uncertainty or perturbation of **D** and **h,** respectively, and **p'** is the perturbed solution of **p.** (Perturbations within **D** arise from the radiance model, water-leaving radiances through the $v(\lambda_i)$ and from the IOP models. Similarly, uncertainties in **h** arise from the radiance model, water-leaving radiances through $v(\lambda_i)$, and the hydrospheric constants (or IOP constants a, and b_{bw}) for seawater). It can be shown that to first order [Ortega 1990],

$$\|\mathbf{p}-\mathbf{p}'\|/\|\mathbf{p}\| \le \kappa(\mathbf{D})(\|\Delta\|/\|\mathbf{D}\| + \|\delta\|/\|\mathbf{h}\|) \tag{19}$$

where

$$\kappa(\mathbf{D}) = \|\mathbf{D}\|\,\|\mathbf{D}^{-1}\| \tag{20}$$

is the condition number of **D.** The ‖ symbols denote the norm of a vector or a matrix. Equation (19) simply states that to first order, the relative error in **p** can be $\kappa(\mathbf{D})$ times the relative error in **D** and **h.** Thus the propagation into **p** of the relative errors of both **D** and **h** is governed by the condition number of **D.** For any norm, $1 \le \kappa(\mathbf{D}) \le \infty$. For the limiting cases, $\kappa(\mathbf{D}) = I$; **D** is said to be perfectly conditioned, while for $\kappa(\mathbf{D}) = \infty$, **D** is singular. For intermediate values of $\kappa(\mathbf{D})$ the interpretation of the condition number is very subjective and must be evaluated separately. For "large" $\kappa(\mathbf{D})$ the **D** matrix is said to be ill conditioned and large errors may be found in p. For "small" $\kappa(\mathbf{D})$ the **D** matrix is said to be well conditioned and smaller errors may be found in **p.** The condition number $\kappa(\mathbf{D})$ has an important relationship to the eigenvalues of D

$$\kappa(\mathbf{D}) = |\Lambda|_{max}/|\Lambda|_{min} \tag{21}$$

where $|\Lambda|_{max}/|\Lambda|_{min}$ are the maximum and minimum absolute values of the eigenvalues of **D.** This relationship is important for two reasons. First, it provides an alternate method of computing the condition number, and second, it shows that the errors propagated into the inherent optical properties **p** are strongly influenced by the ratio of the largest eigenvalue and the smallest eigenvalue. But the ratio of eigenvalues is not necessarily a good condition number for nonsymmetric matrices [Ortega, 1990]. Accordingly, (21) is not recommended for analysis of nonsymmetric ocean color **D** matrices.

Considering the (1) subjectivity of the condition number, (2) desire for high accuracy, (3) need to analyze a large number of oceanic situations or watermasses, and (4) significant computing power available, it was decided to address the error analyses by direct propagation of specific error sources in the model parameters and radiances via a very large statistically derived database.

Generation of the Water-Leaving Radiance Data

The synthetic water-leaving radiance data are not restricted to particular water types. Instead, a very wide range of random IOPs (encompassing virtually any water mass type encountered in the world's oceans) has been chosen. This very general approach produces combinations of IOPs that occur infrequently, for example, a very large a_{ph} and a very small b_{bt}. *The* inclusion of such worst-case IOP combinations leads to a more complete and stringent test of the inversion methodology. A wide range of IOP values also gives confidence that the results of this study can be applied to actual observed radiances without concern for global location or water type.

To produce the IOPs, a Gaussian random number generator based on the Box/Muller method was used to independently generate a_{ph}, then a_d, and finally b_{bp}. Equations (8), (9), and (10) are used first within (1) to generate the required radiances (e.g., at observational wavelengths A,, A,, and λ_3) [Press et *al.*, 1994]. In order to insure that a representative collection of IOPs was available, at least 5×10^5 values of each IOP were generated. Little change in the final results was found if more values were used. The wavelengths chosen for the study correspond to bands that are near those bands available on future satellite sensors: 410, 490, and 555 nm. These bands were also chosen since they have, in our experience, frequently proven to provide good retrieval of IOPs when actual field data are being tested. The 443-nm band was specifically avoided since it has not performed well in our field/data-model retrievals and in empirical [*Aiken et* al., 1995] pigment retrievals. The reference wavelength was chosen to be 410 nm.

Phytoplankton Pigment Absorption

The range of phytoplankton pigment absorption coefficient at the reference wavelength, $a_{ph}(A_{,,}) = a_{ph}(4$ IO). was chosen to be **-0** to **0.74** m^{-1}. The upper range corresponds to a nominal pigment concentration of about 20 mg m^{-3} for a phytoplankton species having a specific absorption coefficient of 0.04 m^2 (mg m^{-3})$^{-1}$ at 443 nm [*Morel*, 1988]. (Unless stated otherwise, the 0.04 m^2 (mg m^{-3})$^{-1}$ value is used

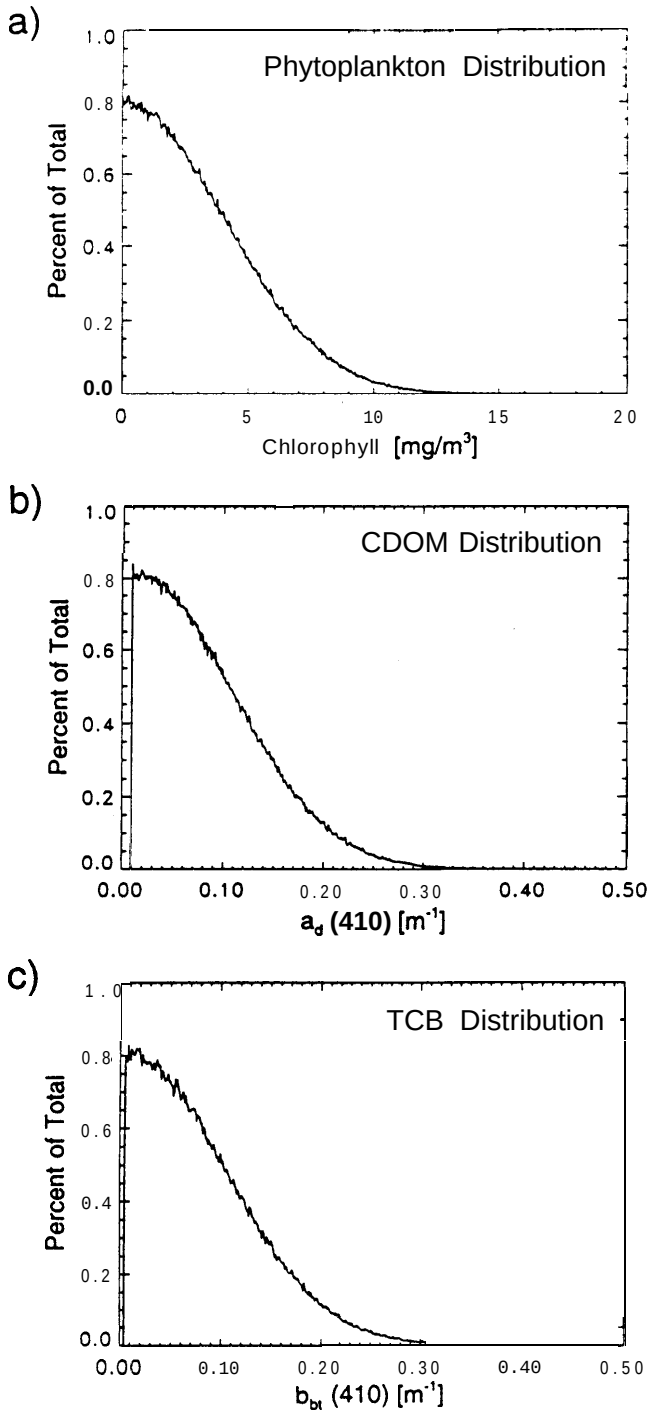

Figure 1. Distribution of the randomly generated sets of 5 x IO- inherent optical properties (IOPs). (a) The phytoplankton pigment concentration corresponds to an a_{ph}(4 10) absorption range of ~0–0.74 m^{-1}. (b) Chromophoric dissolved organic matter (CDOM) absorption coefficient a,,(4 10). (c) Total constituent backscatter (TCB) coefficient b_{bt}(4 10).

throughout this paper). A normally distributed random number generator was used to first select an arbitrary value of a_{ph}(4 IO). Then, the phytoplankton absorption coefficient at other wavelengths was obtained by using the spectral model in (IO).

Chromophoric Dissolved Organic Matter Absorption

The range of chromophoric dissolved organic matter absorption at the reference wavelength, 410 nm. was chosen to range from 0.01 to 0.5 m^{-1}. The upper range was chosen to exceed typical CDOM absorption coefficients found at the mouth of the Delaware Bay [*Hoge et al.*, 1993]. As before a normally distributed random number generator was used to select a value of a_d(4 IO) to generate the radiance at the reference wavelength. The absorption coefficient of chromophoric dissolved organic matter at other wavelengths was then obtained by using the spectral model in (9).

Total Constituent Backscatter

The range of total constituent backscatter coefficient at the 410-nm reference wavelength was chosen to be 0.0005 to 0.05 m^{-1}. The upper range was chosen to exceed backscatter coefficients that result from coccolithophore blooms [*Balch* et al., 1991]. Again, a normally distributed random number generator was used to select an arbitrary value of b_{bt}(4 10) to generate radiances. The total constituent backscatter coefficient at other wavelengths was then obtained by using the spectral model in (8). Figures la, lb, and lc shows the frequency distribution of the 5×10^5 randomly generated sets of IOPs corresponding to phytoplankton absorption, CDOM absorption, and total constituent backscatter coefficients at 410 nm, respectively, the $a_{ph}(410)$, $a_d(410)$, and $b_{bt}(410)$.

IOP Retrieval Results

The inversion of the D matrix was performed in several ways: Cramer's method, Gauss-Jordon elimination, lower-upper (LU) triangular decomposition, and SVD [*Press* et al., 1994]. The SVD method is an excellent analytical tool and allows a quantitative evaluation of singularities. The SVD revealed no singularities for the wide range of IOPs retrieved. The LU decomposition exhibited less round-off error than the Gauss-Jordan elimination. Cramer's method was used most often in this study because of its computational simplicity when solving only three simultaneous equations.

The results are discussed sequentially according to the following error conditions: (1) no errors exist in the radiances and no errors exist in the IOP spectral models, (2) errors exist sequentially in the 555 or 490 or 410 radiances (but not in the IOP spectral models), (3) the same magnitude error occurs simultaneously in the 555, 490, and 410 nm radiances, (4) errors exist only in the IOP spectral models (but not in the radiances), and (5) along-track profiles of retrieved IOPs are shown for a fixed 5% error in the 555-nm radiances and then for a phytoplankton absorption model Gaussian thickness error of 5%.

For radiance and model parameter uncertainties, error surfaces are used to illustrate the probability that 5×10^5 retrieved IOPs fall within displayed error bins (Figures 2 through 8). The shape of the error surface is an important factor for each radiance and model error and the reader is encouraged to carefully examine these surfaces to appreciate the behavior of the expected errors. Applied errors are shown on one horizontal axis. IOP retrieval error bins on the other horizontal axis. and the probability of any one retrieved IOP having a particular error displayed on the vertical axis. Error surfaces with a wide. flat shape show that errors will have a broad range of values with almost equal probabilities of occurrence. Conversely, error surfaces that are tightly grouped depict errors

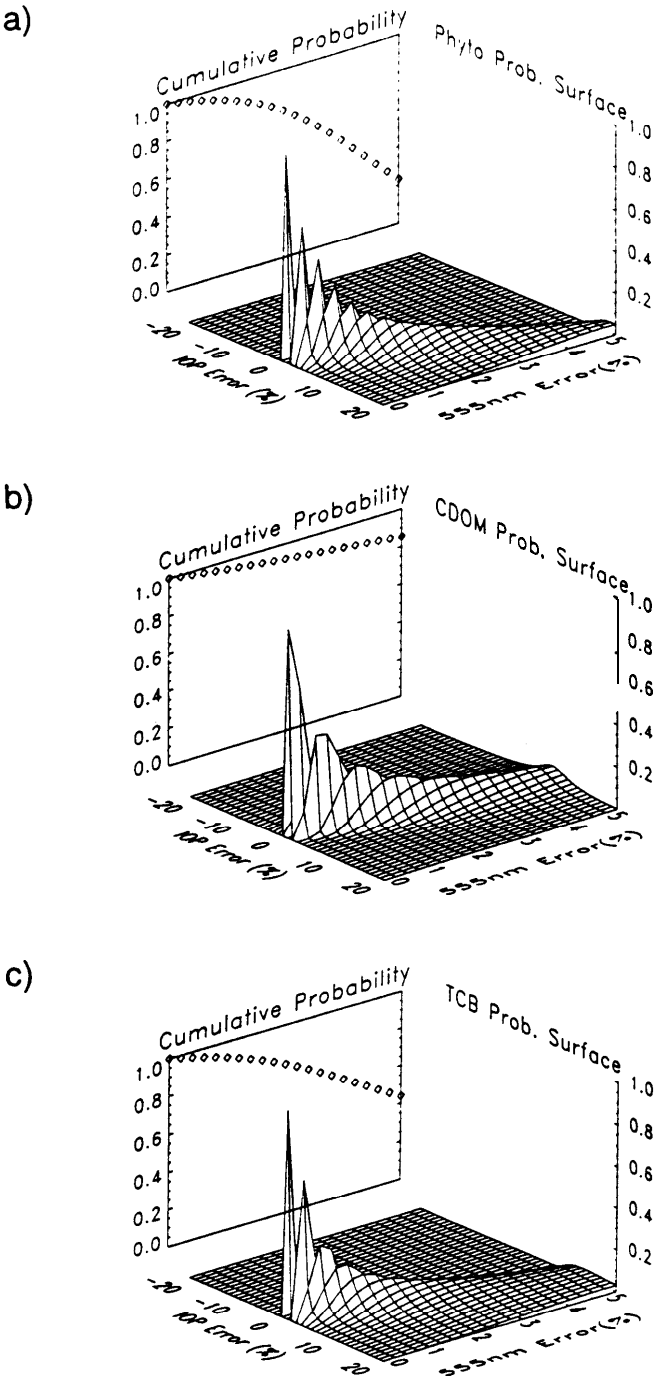

Figure 2. Uncertainty induced in retrieved IOPs by errors of ≤5% in the 555-nm radiances. The probability of 5 x 10^5 retrieved IOPs falling within error bins is shown along the vertical axis. Error in (a) phytoplankton chlorophyll absorption coefficient, (b) CDOM absorption coefficient, and (c) total constituent backscatter coefficient is shown. The CDOM absorption coefficient retrieval probability surface exhibits a more narrow range of errors than the phytoplankton chlorophyll absorption or the total constituent backscatter coefficient. The cumulative probability shows that pigment errors are less likely to be within ±20% than those for CDOM absorption or total constituent backscatter.

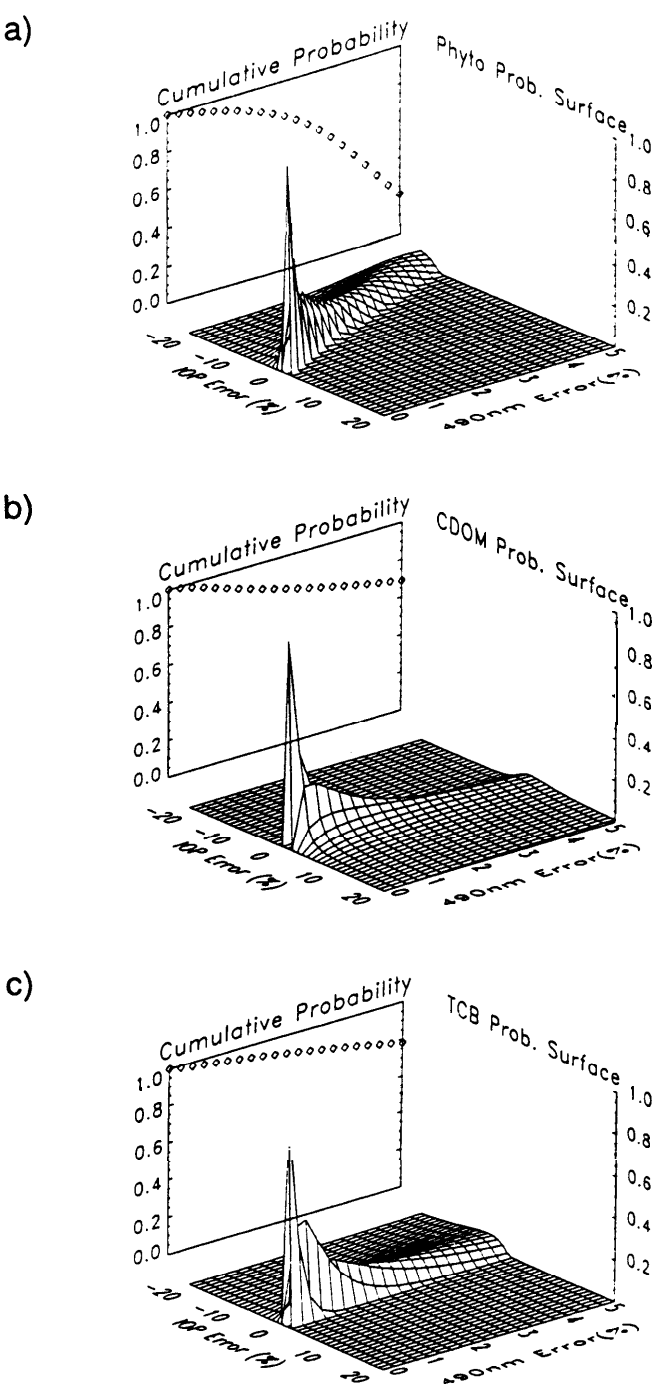

Figure 3. Uncertainty induced in IOPs by errors of ≤5% in the 490-nm radiances. The probability of 5 x 10^5 retrieved IOPs falling within error bins is shown along the vertical axis. Error in (a) phytoplankton absorption coefficient, (b) CDOM absorption coefficient, and (c) total constituent backscatter coefficient is shown. Phytoplankton absorption coefficient is very sensitive to 490-nm radiance errors. For only a 5% error in the 490-nm radiance, 80% of phytoplankton absorption coefficient will have errors that exceed ±20%. The total constituent backscatter is the least impacted by 490-nm radiance errors.

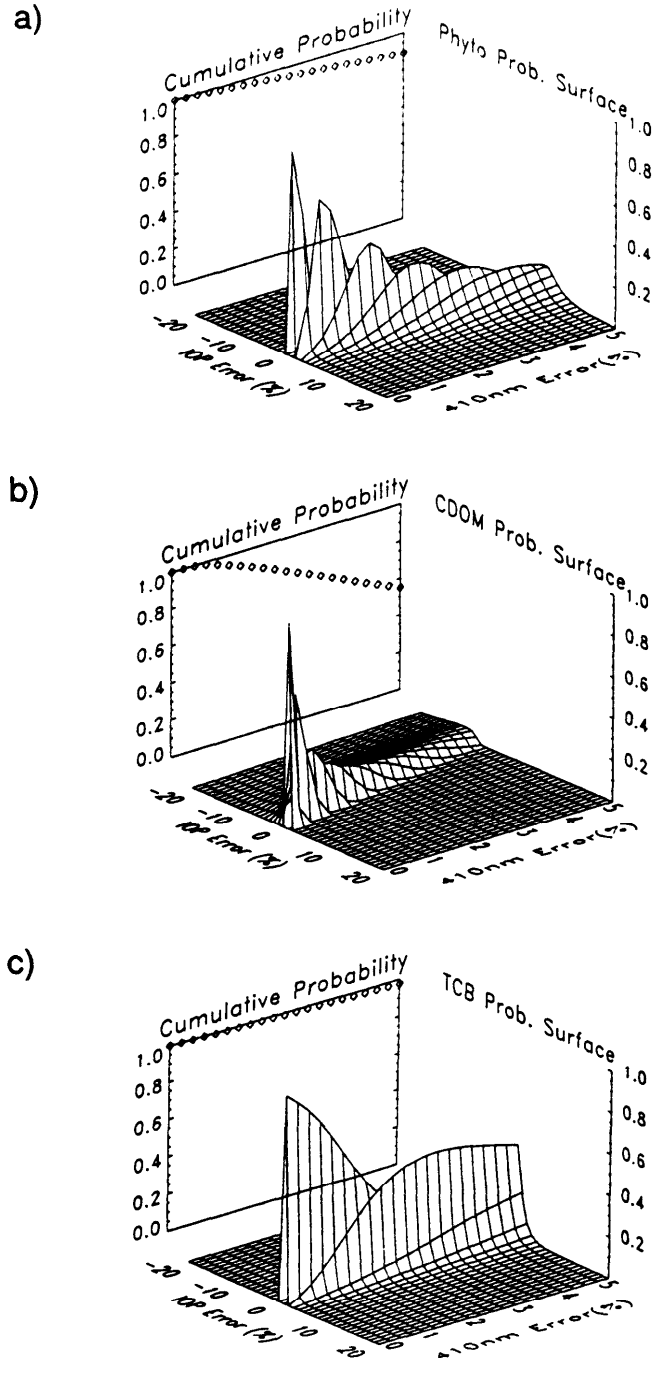

Figure 4. Uncertainty induced in the **IOPs** by errors of ≤5% in the **410-nm** radiances. The probability of 5×10^5 retrieved **IOPs** falling within error bins is shown along the vertical axis. Error in (a) phytoplankton absorption coefficient, (b) CDOM absorption coefficient, and (c) total constituent backscatter coefficient is shown. The phytoplankton absorption and total constituent backscatter are more likely to be retrieved with less error than the CDOM absorption when 410-nm radiance errors are present.

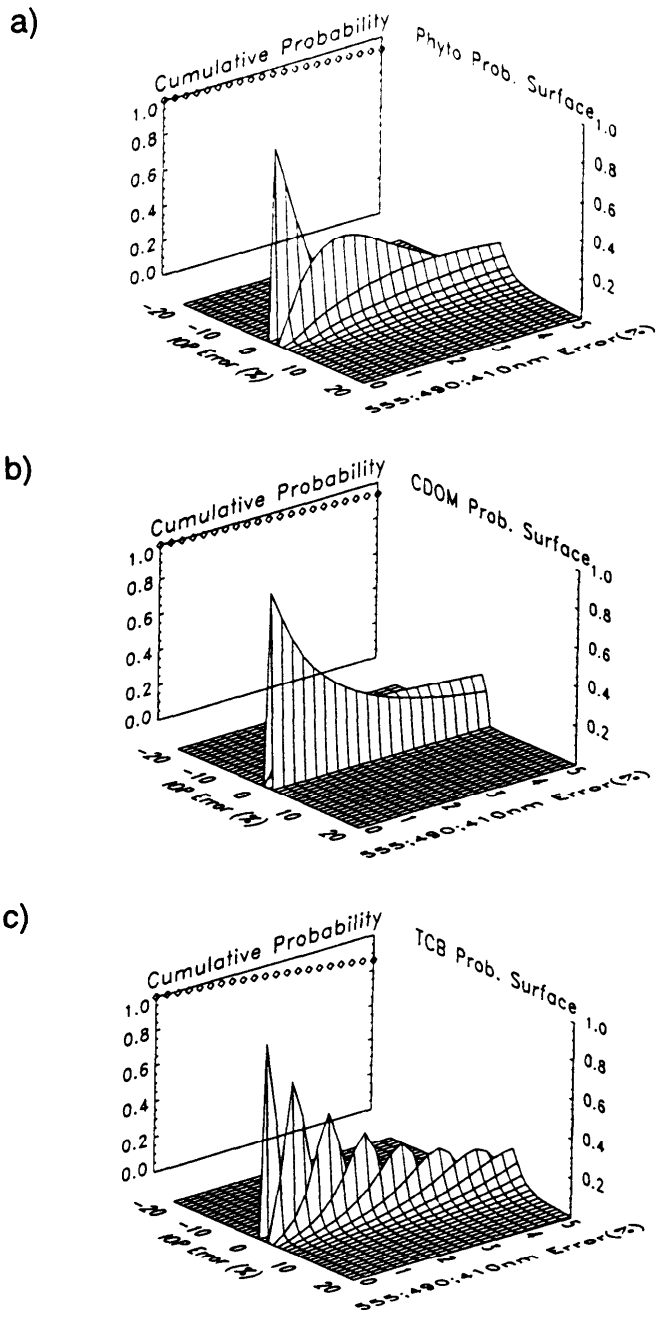

Figure 5. IOP retrieval errors induced by equal errors occurring simultaneously in the 555, 490, and 410-nm bands. The probability of 5×10^5 retrieved **IOPs** falling within error bins is shown along the vertical axis. Error in (a) phytoplankton absorption coefficient, (b) CDOM absorption coefficient, and (c) total constituent backscatter coefficient is shown. The TCB coefficient retrieval errors are higher than those of **phytoplankton** and CDOM. Fortunately, the cumulative probability for all the retrieved **IOPs** is ≥86%, suggesting only a ~14% chance that the IOP errors will exceed ±20%.

that will fall in a smaller range of values. On the facing panel of each plot is the cumulative probability of a retrieved IOP showing the portion of 5×10^5 values falling inside the chosen (and displayed) ±20% error range. For textual brevity, only the most **likely** errors are discussed.

IOP Retrieval Using Error-Free Radiances and Error-Free IOP Spectral Models

The 5×10^5 radiances calculated from the randomly generated **IOPs** were inverted according to (13). The residuals of the **IOPs** ("observed" minus computed; not graphically shown)

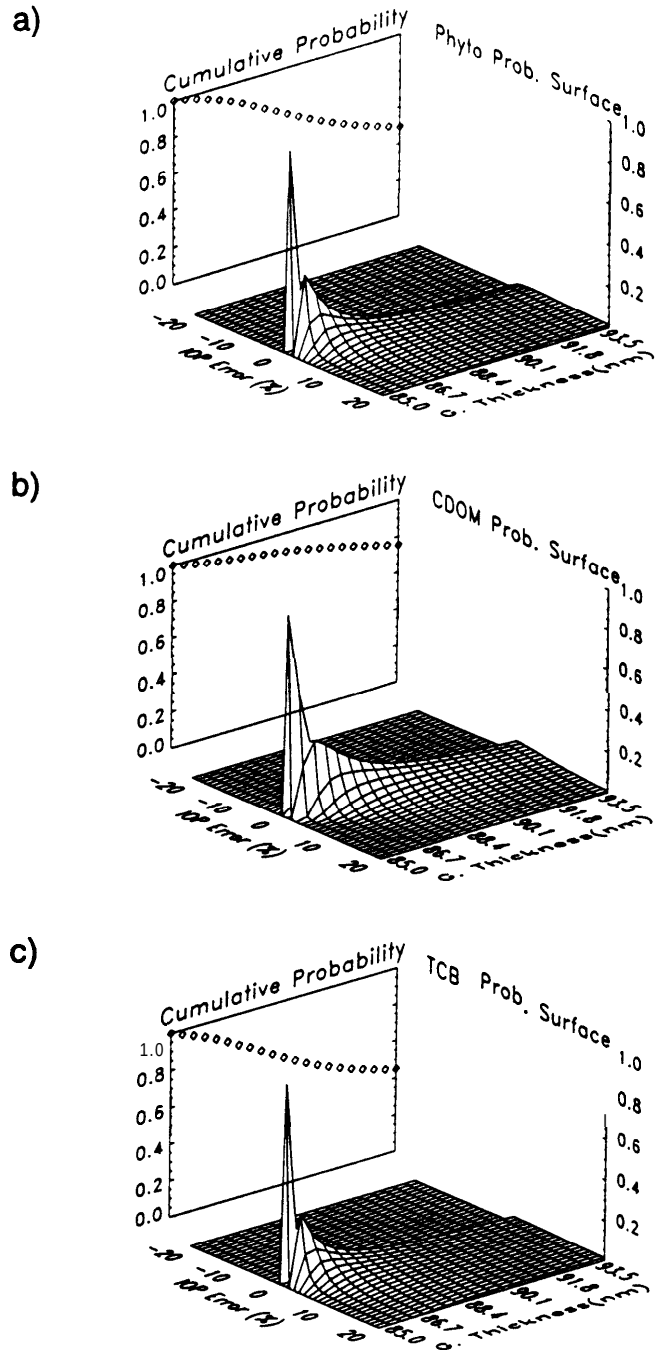

Figure 6. Uncertainties induced in the IOPs by errors of up to 10% in the width or thickness g of the Gaussian model used to represent the phytoplankton absorption. The probability of 5×10^5 retrieved IOPs falling within error bins is shown along the vertical axis. Error in (a) chlorophyll absorption coefficient, (b) CDOM absorption coefficient, and (c) total constituent backscatter coefficient is shown. The CDOM absorption will probably be retrieved with less error than the chlorophyll absorption or the total constituent backscatter. The chlorophyll and total constituent backscatter are retrieved with almost equal success when errors occur in the phytoplankton absorption model thickness g.

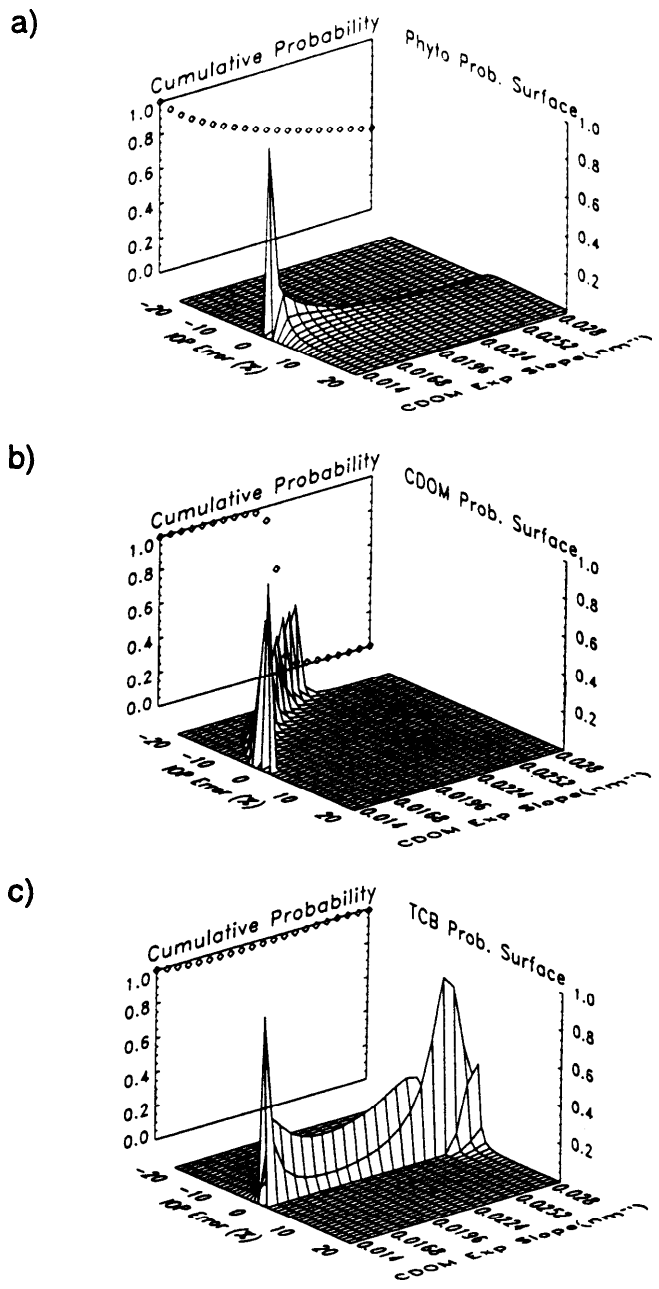

Figure 7. Uncertainty induced in IOPs by errors of ≤100% in the CDOM absorption model spectral slope S. The probability of 5×10^5 retrieved IOPs falling within error bins is shown along the vertical axis. Error in (a) chlorophyll absorption coefficient, (b) CDOM absorption coefficient, and (c) total constituent backscatter coefficient is shown. Almost all values of the total constituent backscatter are retrieved with errors within ±20%. The cumulative error for chlorophyll steadily declines as the CDOM spectral slope error increases. When the CDOM spectral slope errors exceed ~55%, the CDOM retrieval error always exceeds ±20%.

were zero to the precision of the computer. All computations were performed in double precision (15 digits). The inversions were quite rapid and no singular matrices were encountered. Thus IOPs obtained by matrix inversion are rapidly and exactly determined when water-leaving radiances and the IOP spectral models are both error free. Of course, speed of computation is very important when the inversions are applied to satellite images.

IOP Retrieval Errors Induced by Water-Leaving Radiance Uncertainties

Water-leaving radiances contain uncertainties due to scale, bias, and noise. Additional water-leaving radiance uncertain-

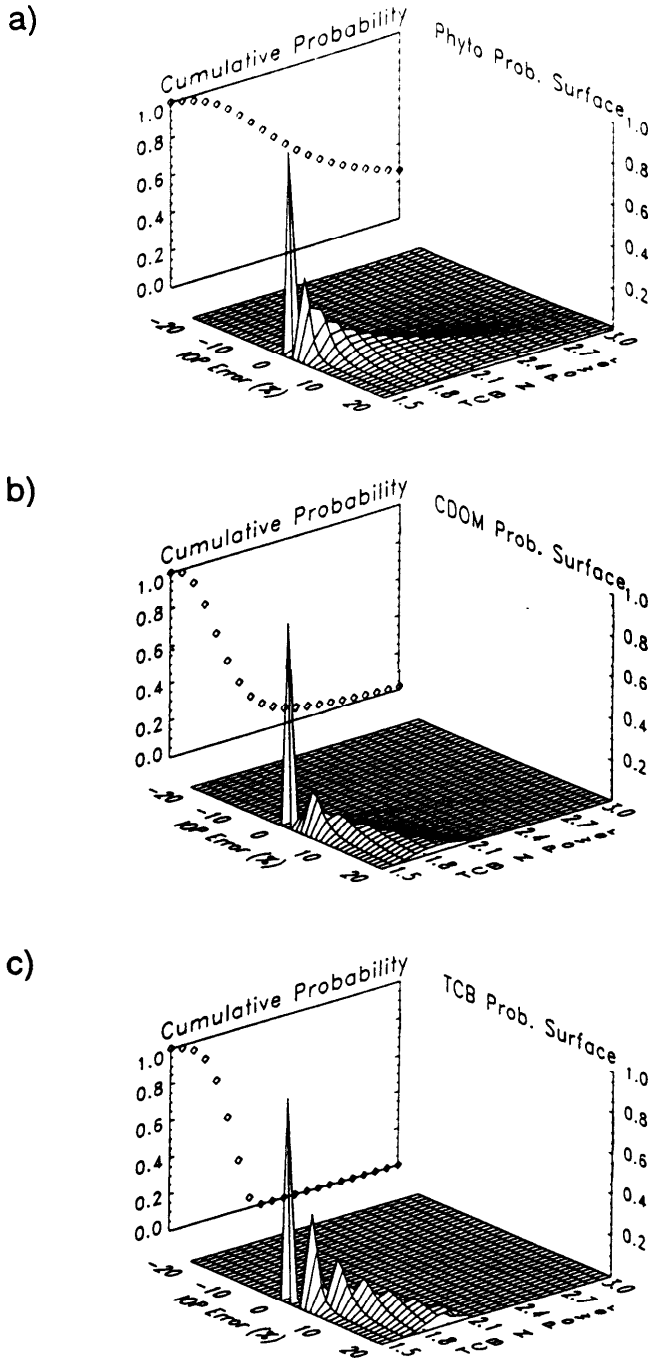

Figure 8. Uncertainty induced in IOPs by errors of up to 100% in the total constituent backscatter wavelength ratio exponent n. The probability of 5×10^5 retrieved IOPs falling within error bins is shown along the vertical axis. Error in (a) phytoplankton absorption coefficient, (b) CDOM absorption coefficient, and (c) total constituent backscatter coefficient is shown. The phytoplankton absorption coefficient is impacted the least of the three constituents by errors in ***n.*** CDOM and total constituent backscatter are impacted severely by small errors in ***n.*** When the exponent error exceeds ~35%, the total constituent backscatter retrieval error will always be $>\pm 20\%$.

ties occur during the normalization of the at-satellite radiances to remove the atmospheric radiance (by Rayleigh, aerosol, ozone corrections) and reduce the solar zenith angle to zero. To determine how these water-lcaving radiance measurement uncertainties propagate into the IOPs, error analyses were performed using the previously generated radiance data. The approach was to increase the water-leaving radiance by up to 5% just prior to inversion. (Reducing the radiance yielded essentially the same results.) The inversion equations used the same IOP models as originally used to generate the radiances; thus no model errors were present in this portion of the study. To simplify the study, errors were (I) introduced into only one sensor band at a time or (2) introduced into all three bands concurrently. These are discussed in the following three sections.

IOP errors induced by 555-nm radiance uncertainty. The 555-nm radiances were increased by ≤5% just prior to inversion. The error induced in a retrieved IOP is shown in the IOP error probability plots of Figures 2a, 2b, and 2c corresponding to phytoplankton absorption, CDOM absorption, and total constituent backscatter. The probability of 5×10^5 retrieved IOPs falling within error bins is shown along the vertical axis. (For consistency the same numerical scales and layout are subsequently used for Figures 3 and 4 corresponding to discussions of radiance errors introduced into the 490-nm and 410-nm bands, respectively).

Phytoplankton absorption retrieval: From Figure 2a it is seen that a 0.5% error in the 555-nm radiances will yield an error of -2% in the phytoplankton absorption. (The jagged or irregular character of the error surfaces for small errors should be ignored since it is an artifact resulting from the use of a 1% error bin to generate the voluminous error surface data.) However, since the cumulative probability is -0.97, then the results show that for -0.5% error, the phytoplankton absorption error will seldom exceed $\sim\pm 20\%$ for any of the wide range of oceanic conditions. When the error in the 555-nm radiance reaches 5.0%, the most probable error in the a_{ph} retrieval is -20%. The cumulative probability is now only ~23%, indicating that there is a 77% chance that the a_{ph} retrieval error will exceed $\pm 20\%$. The results suggest that the retrieved a_{ph} are highly sensitive to errors in the 555-nm radiances.

CDOM absorption retrieval: In Figure 2b the CDOM/detritus absorption retrieval a_d is seen to be less impacted than the a_{ph}. When the error in the 555-nm band is 1.5%, the a_d retrieval error will probably be -2%. The cumulative probability is now ~97%, and there is only a -3% chance that the error will be $>\pm 20\%$. When the error in the 555-nm band reaches 5%, the a_d retrieval error will probably be -7% with a wide range of errors. But since the cumulative probability is now ~85%, then there is only a 15% chance that the error will be $>\pm 20\%$.

Total constituent backscatter retrieval: For an error in the 555-nm radiances, Figure 2c shows that the errors in the total constituent backscatter b_{bt} are very similar to those for phytoplankton absorption (compare Figures 2a and 2c). The cumulative error of being within $\pm 20\%$ is less impacted than phytoplankton pigment although the error surfaces are similar. When the error in the 555-nm band reaches 5%, the b_{bp} retrieval error is likely to be -13%. But since the cumulative probability is now ~43%, there is a -57% chance that the error will be $>\pm 20\%$.

Comparing Figures 2a, 2b, and 2c, it is seen that the cumulative probability for a_{ph} is declining more rapidly than that of the b_{bp} and u,,. Thus far fewer a_{ph} are within the $\pm 20\%$ error range as the 555-nm radiance errors continue to increase to and beyond 5%. Accordingly, the a_d and h,,, retrievals are more likely to have less error (than the a_{ph}) as the errors in the

555-nm band increase with CDOM being the least impacted of the three IOPs.

IOP errors induced by 490-nm radiance uncertainty. The following errors are induced by 490-nm radiance uncertainty.

Phytoplankton absorption retrieval: The phytoplankton pigment absorption coefficient IOP errors caused by 490-nm radiance errors (Figure 3a) are similar in mngnitudc (but opposite in sign) to those induced by errors in the 555-nm radiances (Figure 2a). The phytoplankton pigment IOP error surfaces for 490-nm radiance errors are thus almost mirror images of those for 555-nm errors (compare Figure 2a with Figure 3a). When the error in the 490-nm radiance reaches 5.0%, the most probable error in the a_{ph} retrieval is ~20%. The cumulative probability is only ~20%, indicating that there is an 80% chance that the a_{ph} retrieval error will exceed ±20%. The results suggest that the retrieved a_{ph} are slightly more sensitive to errors in the 490-nm radiances than to errors in the 555-nm radiances (compare Figure 2a and 3a, especially the cumulative probability).

CDOM absorption retrieval: In Figure 3b the CDOM absorption retrieval a_d is again seen to be less impacted than the a_{ph}. When the error in the 490-nm band reaches 5.0%, the a_d retrieval error will probably be only -3%. The cumulative probability is now ~68%, and there is a 32% chance that the error will be >±20%. There is a higher probability that the a_d retrieval will be more strongly affected by a 490-nm error than by a 555-nm error (compare Figures 2b and 3b, especially the overall shape of the surface).

Total constituent backscatter retrieval: For an error in the 490-nm radiances, Figure 3c shows that the errors in the total constituent backscatter b_{bt} are opposite in sign to those with 555-nm errors (compare Figures 2c and 3c). When the error in the 490-nm band reaches 5%, the b_{bt} retrieval error is likely to be -7% with a wide range of values. But since the cumulative probability is now ~78%, there is an 22% chance that the error will be >±20%.

In summary, by comparing the cumulative probability plots for Figures 2a, 2b, and 2c with those of Figures 3a, 3b, and 3c, it is seen that 490-nm errors induce (1) slightly more a_{ph} and a_d retrieval error than 555-nm radiance errors and (2) less b_{bt} retrieval error than 555-nm radiance errors.

IOP errors induced by 410-nm radiance uncertainty. The following errors are induced by 410-nm radiance uncertainty.

Phytoplankton absorption retrieval: From Figure 4a the a_{ph} errors are more tightly clustered than the 555-nm and 490-nm a_{ph} error. As the error in the 410-nm radiance errors reaches 5%, the most probable error in the a_{ph} retrieval is now only -5%. The cumulative probability is ~88%, indicating that there is an 12% chance that the a_{ph} retrieval error will exceed ±20%. Comparing the cumulative probability in Figures 2a. 3a, and 4a the retrieved a_{ph} are more sensitive to errors in the 490- and 555-nm radiances than to errors in the 410-nm radiances.

CDOM absorption retrieval. From Figure 4b, as the error in the 410-nm radiance reaches 5%, the most probable error in the a_d retrieval is now ~9–10%. For 5% errors the cumulative probability is ~55%, indicating that there is an -45% chance that the a_d retrieval error will exceed ±20%. Comparing Figures 2b, 3b, and 4b, the retrieved a_d are increasingly more sensitive to the same magnitude error as one proceeds from 555 nm through 490 nm to the 410-nm band.

Total constituent backscatter retrieval: In Figure 4c, for an error in the 410-nm radiances, the errors in the total constituent backscatter b_{bt} are also very tightly clustered. When the 410-nm radiance error reaches 5%, the cumulative probability is ~98%, indicating that there is only a -2% chance that the b_{bt} retrieval error will exceed ±20%. Furthermore, the most probable error is only -O-l%.

When the cumulative probability for the errors in each of the three bands is compared, the b_{bt} retrieval is seen to be increasingly less sensitive to the same magnitude error as one progresses from 555 nm through 490 nm to the 410 nm band. This is the opposite effect as seen for the a_d retrievals.

Table 1. Effect of Phytoplankton, Chromophoric Dissolved Organic Matter (CDOM), and Total Constituent Backscatter (TCB) Spectral Model Parameter (g, S, n) Errors Upon the Corresponding Inherent Optical Property (IOP) Spectral Model Values at 490 nm and 555 nm

	Change in 490-nm Spectral Model Value	Change in 555-nm Spectral Model Value
Phytoplankton model (10% error in Gaussian thickness)	1.4%	14.8%
CDOM model (100% error in S exponent)	67.4%	86.9%
TCB model (100% error in n factor)	30.6%	57.5%

IOP Retrieval Errors Induced by Equal Uncertainty in 555-, 490-, and 410-nm Bands

The most obvious effect of equivalent errors in all three bands is the impact on the TCB coefficient retrieval. (Compare the error surface of Figure 5c with the surfaces in Figures 5a and 5b.) When the 555-, 490-, and 410-nm radiance errors reach 5%, the most probable error in the TCB coefficient retrieval reaches ~7%, while the phytoplankton pigment and CDOM are both <4%. Fortunately, the cumulative probability for each of the retrieved IOPs is ≥86%, suggesting only a -14% chance that the errors will exceed ±20%.

IOP Retrieval Errors Induced by IOP Spectral Model Uncertainties

Errors in the a_{ph}, a_d, and b_{bt} IOPs were studied by incrementally adding a positive bias to certain important model parameters. These parameters were (1) the "thickness'* of the Gaussian describing the phytoplankton pigment absorption, g, in equation (IO) and (2) the spectral slope S of the CDOM spectra! absorption in equation (9) and the total constituent backscatter power law exponent n in equation (8). It was found that IOP retrievals were very sensitive to errors introduced into the Gaussian thickness g. For this reason an error range of only 10% was used for the thickness g. For the CDOM spectra! slope the IOPs are relatively insensitive to the CDOM spectra! slope so an error range of 100% was used. The value of the total constituent backscatter power law exponent n is not very well known. Thus. in order to include more latitude. an error range of 100% was also used. Table I shows how these applied errors affect the spectral models normalized at the reference wavelength A, within the D matrix.

IOP retrieval errors induced by phytoplankton spectral absorption model uncertainty. The Gaussian thickness g in (IO) was varied by up to 10% just prior to inversion. Thus the range of g was $85.0 \le g \le 93.5$. For a 1% error in the thickness an

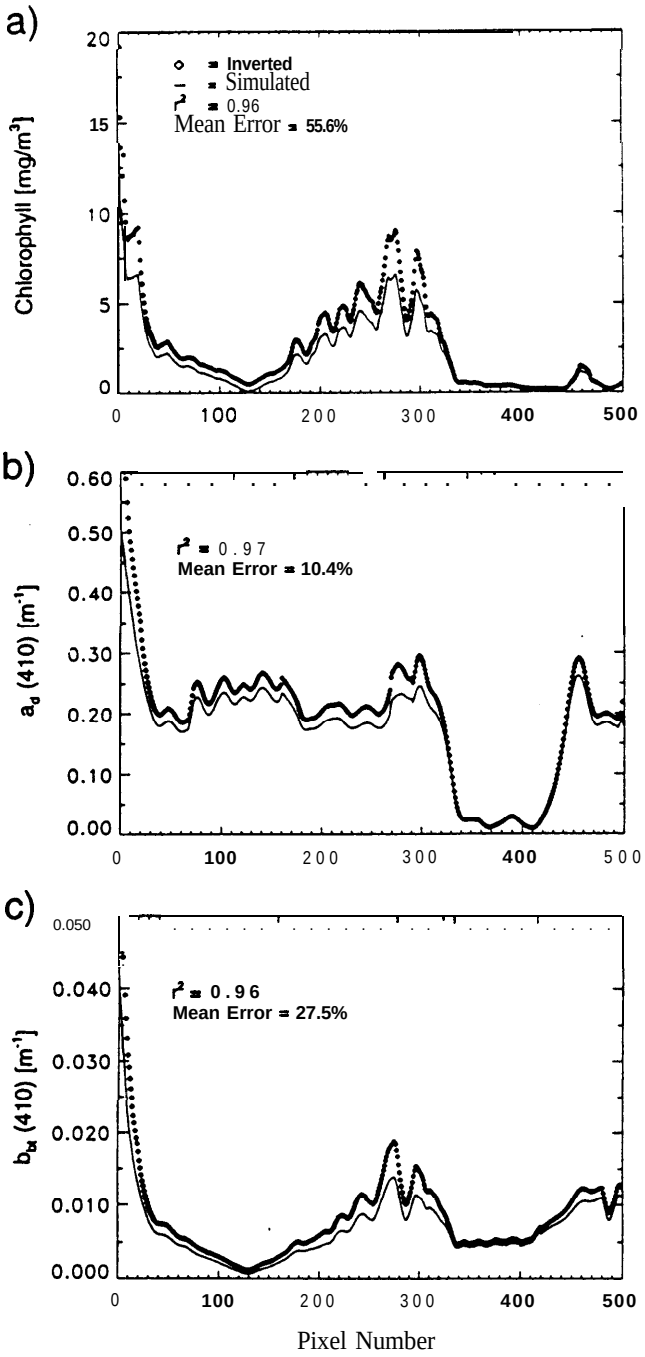

Figure 9. A simulated along-track profile showing the effect of a constant 5% radiance measurement uncertainty in the 555-nm band. (a) The general shape of the along-track phytoplankton absorption coefficient profile is rather faithfully reproduced. However, peak errors of -570% in the retrieved pigment are present. Mean phytoplankton absorption coefficient errors were -56%. (b) The CDOM absorption coefficient retrieval is affected very little by the 555-nm radiance error. (c) The total constituent backscatter coefficient retrieval errors ranged from -10 to 40% with a single pixel having an error of -108%.

a_{ph} retrieval will probably have an error of 1–10% (Figure 6a). The cumulative probability shows that the a_{ph} error has **only** -2.5% probability of falling outside the ±20% range. If the thickness error reaches 5%, there is a -25% probability that the a_{ph} retrieval error will exceed ±20%. For a 10% error in the thickness. there is a ~52% chance that the a_{ph} retrieval will exceed ±20%. This high sensitivity to thickness errors is a genuine concern since the natural variability of phytoplankton spectral absorption [*Sathyendranath et* al., 1987; *Bricaud et al.,* 1995; Cleveland, 1995] is rather high and can inherently lead to large a_{ph} retrieval errors.

For retrieval of a,, and b_{bt} the effect of the thickness error is very similar to that of the a_{ph} retrieval (see Figures 6b and 6c) and the conclusions are likewise similar. However, a, is the least impacted IOP.

IOP Retrieval errors induced by CDOM absorption spectral-slope model uncertainty. The CDOM spectral slope S in (9) was varied by up to 100% just prior to inversion. Accordingly, the range of S was $-0.014 \leq S \leq -0.028$. Comparing the error probability surfaces of Figures 7a, 7b, and 7c, a_{ph} is rather strongly impacted by CDOM spectral slope errors. The cumulative probability shows that the a_{ph} errors begin to exceed ±20% even for small CDOM spectral slope errors. In Figure 7b the CDOM retrieval is severely impacted when the slope error exceeds -50%. Figure 7c suggests that most b_{bt} errors will fall within ~±20% over the entire 100% slope **error** range. For a 100% error in the CDOM slope the cumulative probability remains high for b_{bt}. The most probable errors for b_{bt} are between − 1 and 1% for the whole range of errors applied to the CDOM absorption spectral slope.

IOP retrieval errors induced by total constituent backscatter wavelength ratio exponent uncertainty. The total constituent backscatter wavelength ratio exponent n in (8) was then varied by up to 100% just prior to inversion. The range of n was $1.5 \leq n \leq 3$ .O. Figures 8a, 8b, and 8c show that phytoplankton absorption is the least influenced by the errors applied to n. In Figure 8a, about half of the phytoplankton retrievals will have an error >±20% as the error in n reaches 60%. Figures 8b and 8c show that CDOM absorption and TCB retrievals are severely impacted by errors in n. As the error in n exceeds ~35%, most CDOM absorption and TCB errors will exceed ±20%. Examples of the effects of radiance and model errors on retrieved IOPs are given below.

The 555-nm radiance error: For a simulated along-track observational profile consisting of 500 points, Figures 9a, 9b, and 9c show the effect of a constant 5% 555-nm radiance band measurement uncertainty upon the retrieval of all the IOPs. In Figure 9a the general shape of a simulated along-track phytoplankton absorption coefficient profile is rather faithfully reproduced and yields a deceptively high correlation coefficient of $r^2 = 0.960$. Phytoplankton absorption is retrieved with errors ranging from 22% to 570% and a mean error of -56%. Note that the phytoplankton absorption is overestimated with the positive error in the 555-nm radiance. If the error applied to 555-nm radiance was negative, the phytoplankton absorption would be underestimated. This would cause negative absorption coefficient values to be retrieved near observation 130 and near observation 440. These negative values would be physically unacceptable and serve as a vivid prompt of the deleterious effects of errors in the radiances (and especially 555-nm radiances). The reader is reminded that based on the chosen spectral IOP and radiance models, linear inversion produces those IOPs that uniquely satisfy the input radiances, regardless of the physical feasibility of the retrieval. Thus the occasional retrieval of negative IOPs should be considered a beneficial feature of the method: it is abrupt notification that additional improvements must be made to the models and

radiances in order to secure a physically acceptable solution. If negative absorption coefficient values persist, then during satellite image processing the retrieved absorptions must be flagged and removed.

In Figure 9b the CDOM IOP retrieval is affected much less by the 555-nm radiance error than phytoplankton IOP retrieval, and a correlation coefficient $r^2 = 0.965$ is found. More importantly, the minimum retrieval error along the entire simulated trackline was 0.01% with a maximum error of ~90%. The mean retrieval error was 10.4%.

Figure 9c illustrates that the total constituent backscatter IOP retrieval is also reproduced reasonably well as a result of the 5% error in the 555-nm radiances and a correlation of $r^2 = 0.957$ is found. The retrieval errors ranged from 10 to 108% with the mean error equal to 28%. The above results are seen to be consistent with the findings presented in Figure 2 that phytoplankton absorption and TCB retrievals are impacted more severely than CDOM absorption by errors in the 555-nm radiance band.

Phytoplankton model errors: For the same simulated along-track observational profile, Figures 10a, 10b, and 10c show the effect of a constant 5% uncertainty in the phytoplankton Gaussian model thickness upon the retrieval of all the IOPs.

In Figure 10a the general shape of the along-track phytoplankton pigment profile is still rather faithfully reproduced and yields a correlation coefficient of $r^2 = 0.933$. The minimum retrieval error was 0.2%, while peak errors reached ~117%. The mean retrieval error was ~8.8%.

In Figure 10b the CDOM IOP retrieval is affected very little by the phytoplankton Gaussian model thickness error and a correlation coefficient of $r^2 = 0.944$ is found. The minimum retrieval error was 0.01% and a single peak error of ~103% was obtained. A mean retrieval error of 4.8% was determined for the entire trackline. Only six out of 500 data points had errors that exceeded 20%.

In Figure 10c the total constituent backscatter IOP is also retrieved reasonably well as a result of the 5% error in the model thickness error. A correlation of $r^2 = 0.934$ is found. The minimum retrieval error was 0.21% and a peak error of ~120% was seen. The mean retrieval error was 8.8%. Although the data are limited to 500 points, the results are consistent with those presented in Figure 6.

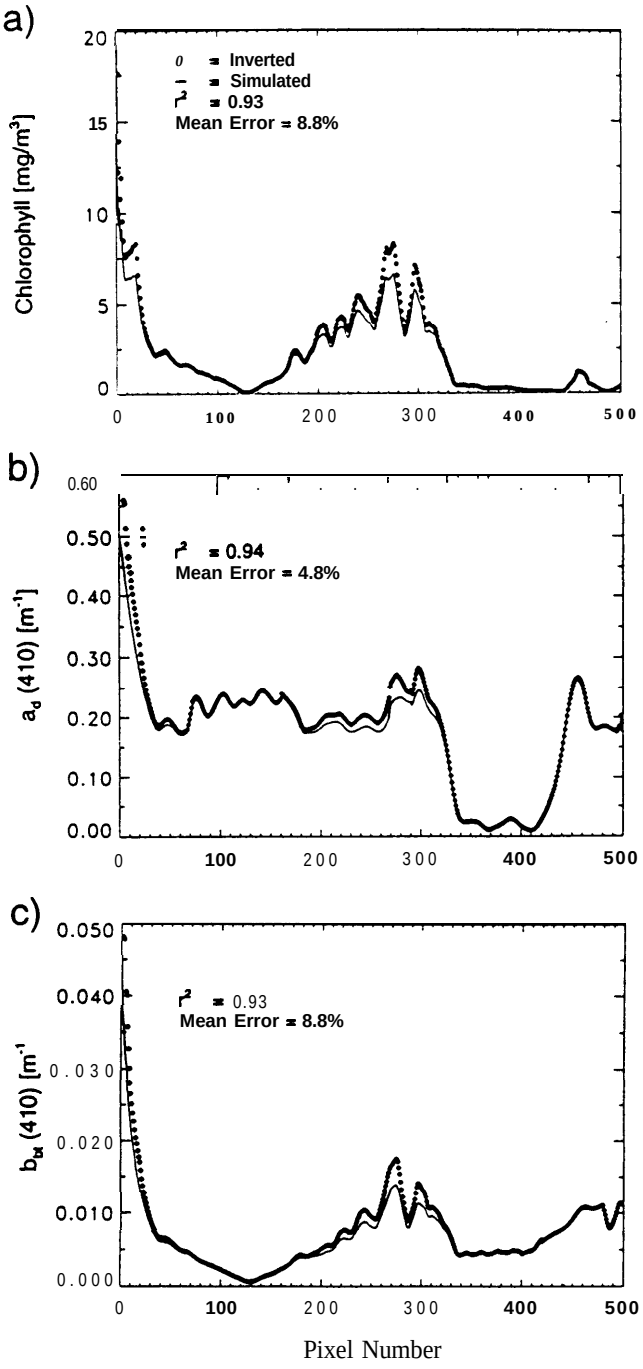

Figure 10. A simulated along-track profile showing the effect of a 5% error in the phytoplankton Gaussian absorption model thickness g. (a) The chlorophyll absorption is retrieved rather well, but peak errors reached ~ 117%. (b) The CDOM absorption coefficient retrieval is affected very little by the phytoplankton Gaussian absorption model thickness error. The CDOM mean retrieval error was ~5%. (c) Total constituent backscatter coefficient mean retrieval error was ~9%.

Discussion

It is generally agreed that IOPs of multiple oceanic constituents cannot be retrieved by empirical radiance ratios. To mitigate the deficiencies of simple band ratios, a radiance model was recast in matrix form by exploiting the linear summability of the IOPs. It was then shown that IOPs can be concurrently and rapidly retrieved by standard matrix inversion methods without incurring singularities. The results strongly suggest that model-based retrievals should be used to replace radiance ratios that are presently limited to phytoplankton pigment and diffuse attenuation recoveries.

In this study we were also interested in quantifying errors in the retrieved IOPs as caused by radiance measurement errors and IOP model errors. This was necessary in order to establish that the methodology was practical and possessed no obvious undesirable properties. Remarkably, no singularities were found during inversion of the 5×10^5 spectral radiances produced from a wide range of oceanic constituent absorption and backscatter combinations. Only three bands were used in this study. More bands and different wavelengths are recommended for study before declaring that the linear inversion procedure is totally without complications. In the interest of brevity and simplicity, analyses of four or more bands were not described herein.

Unfortunately, the retrieval errors for all the IOPs are rather strongly dependent on the phytoplankton spectral model. Retrieval errors will thus be exacerbated by the natural spectral variability of phytoplankton absorption. By choosing a single phytoplankton spectral model for all inversions, IOP errors are very likely. Instead of choosing a single phytoplankton spectral model. wc may eventually be compelled to use an increasing number of color bands to retrieve spectral segments of the phytoplankton model in order to further improve the CDOM and backscatter retrievals. But this procedure has rapidly diminishing returns because the CDOM and backscatter models must themselves be accurately known at the new color band positions in order that the phytoplankton retrieval not be further degraded. It is important to note that for a three-band inversion, the single Gaussian phytoplankton spectral model need only fit the phytoplankton absorption curves through the three wavelength regions used in the inversion. The errors caused by the phytoplankton spectral model uncertainties would be minimized by choosing wavelengths which have the lowest variability relative to each other. See Appendix B for additional discussion of the Gaussian spectral model and Appendix A for more information about the backscatter spectral model. Additional field experiment data are needed to determine the viability of using a single phytoplankton absorption model for IOP retrievals with specific band sets in various oceanographic regions. Perhaps more importantly, copious amounts of field data are needed to further study the linear matrix inversion procedure. These field data are now being actively sought by our laboratory [*Hoge* et al., 1995a].

The errors induced in the retrievals by the wavelength-ratio exponent n are another concern. Since this exponent exhibits natural variability within oceanic provinces, its uncertainty leads to considerable errors in the a_d and b_{bt} retrievals.

The algorithm described herein is presently undergoing tests using airborne field data validated by laser-induced fluorescence of chlorophyll and CDOM. Preliminary findings to be published suggest that (1) the proposed single Gaussian phytoplankton model and the CDOM mode1 both function rather well but (2) the wavelength-ratio particulate backscatter model may require additional formulation to achieve the desired results.

Appendix A: Oceanic Particulate Backscatter Spectral Models

Oceanic particulate backscatter spectral models, or TCB models. can be derived from (1) a recently available diffuse attenuation coefficient model [Gordon, 1989, 1994] and (2) direct inversion of the radiance model given by equation (1) in the main body of this paper. This appendix describes both inversions and how the $(\lambda_{ref}/\lambda)^n$ model used in the main body of this paper approximates the derived spectral backscatter over specific wavelength regions in the blue green.

TCB Model by Inversion of a Diffuse Attenuation Coefficient Model

The diffuse attenuation coefficient model [*Gordon*, 1989, 1994] is

$$K \cong 1.0395 D_0 (a + b_b), \qquad (A1)$$

where D_0 is the downwelling distribution function [*Gordon*, 1989, 1994], a is the total absorption. and b_b is the total backscatter The total backscatter b_b is the rigorous linear sum of the backscatter of seawater, b_{bw}, and all constituents b_{bi}, such that $b_b = b_{bw} + b_{bi}$. Thus from (A1) the total constituent backscatter (TCB), b_{bi}, is

$$b_{bi} = (K/1.0395 D_0) - a - b_{bw}. \qquad (A2)$$

The numerical values and models for K, D_0, a, and b_{bw} required for the inversion will now be identified. First, the b_{bw} spectral values can be obtained from published tables [*Smith and Baker*, 1981]. The D_0 is a function of the solar zenith angle and wavelength [*Gordon*, 1994]. Between 440 and 550 nm and for zenith angles between 0° and 80°, the D_0 varies between 1.019 and 1.346 [*Gordon*, 1994]. For convenience of the development herein a nominal value of 1.1 is chosen for all wavelengths and solar zenith angles. (This chosen value for D_0 actually corresponds to a wavelength of 480 nm and a zenith angle of 30". When more precision is required, other tabular values [*Gordon*, 1994] can be used.)

The total absorption a is the sum of the absorption of seawater, a_w, phytoplankton pigment (mainly chlorophyll) a_{ph}, chromophoric dissolved organic matter (CDOM) a_{CDOM}, and detritus a_{detr}. Or

$$a = a_w + a_{ph} + a_{CDOM} + a_{detr}. \qquad (A3)$$

The a_w are tabulated constants [*Smith and Baker*, 1981]. The a_{ph} is computed from

$$a_{ph} = a^*(\lambda_{ref}) \bar{a}_{ph}(\lambda) C, \qquad (A4)$$

where $a^*(\lambda_{ref})$ is the specific absorption coefficient of phytoplankton at a chosen normalization wavelength λ_{ref} and $\bar{a}_{ph}(\lambda)$ is the spectral absorption of phytoplankton whose value is unity at the normalization wavelength. The phytoplankton absorption coefficients tabulated by *Hoepffner and Sathyendranath* [1993] were used for $\bar{a}_{ph}(\lambda)$ after renormalization to the reference wavelength chosen for the calculations herein. The CDOM (yellow substance) absorption a_{CDOM} is modeled by [*Bricaud et al.*, 1981]

$$a_{CDOM} = a_{CDOM}(\lambda_{ref}) \exp[-0.014(\lambda - \lambda_{ref})], \qquad (A5)$$

where λ_{ref} is some reference wavelength. The detritus absorption a_{detr} is similarly modeled by [*Hoepffner and Sathyendranath*, 1993; *Roesler et al.*, 1989]

$$a_{detr} = a_{detr}(\lambda_{ref}) \exp[-q(\lambda - \lambda_{ref})], \qquad (A6)$$

where λ_{ref} is some reference wavelength. The detritus slope q is taken to be 0.011 although the value is considerably more variable than the CDOM slope [*Hoepffner and Sathyendranath*, 1993; *Roesler et al.*, 1989].

Finally, to complete the inversion, a suitable model for the. diffuse attenuation K must be identified. Two potential models are available [*Baker and Smirh*, 1983: *Morel*, 1988]. The model of *Morel* [1988] is chosen since it provides a better fit to available ship data [*Morel*, 1988] and to airborne active-passive data [*Hoge* et *al.*, 1995a]. The model is expressed as [*Morel*, 1988]

$$K(\lambda) = K_w(\lambda) + \chi_c(\lambda) C^{e(\lambda)} \qquad (A7)$$

where the $K_w(\lambda)$, $\chi_c(\lambda)$, and $e(\lambda)$ are tabulated [*Morel*, 1988]. This model was developed from 176 spectra. but those stations identified as turbid or dominated by CDOM were excluded by *Morel* [1988]. Also. the number of spectra available for $\lambda > 600$ nm was <100. This completes the designation of all the models required to compute the TCB, b_{bi}, from (A2).

Other than the chlorophyllous pigment concentration, only three model parameter selections need be made at the reference wavelength: (I) the phytoplankton specific absorption coefficient $a^*(\lambda_{ref})$, (2) the CDOM absorption coefficient $a_{CDOM}(\lambda_{ref})$, and (3) the detritus absorption coefficient $a_{detr}(\lambda_{ref})$. The reference wavelength is chosen to be 410 nm.

The primary constraints in the selection of the three parameter values are to maintain the retrieved backscatter b_{bt} positive (i.e., nonnegative) for the lowest chlorophyllous pigment values and to select values that are consistent with case 1 waters. Thus, since the backscatter of water is fixed and the K is determined only by the K_w and C, then appropriate values (and a physically reasonable balance between the three remaining absorption parameters) are required; otherwise the retrieved backscatter can become negative. The specific absorption coefficient for phytoplankton is highly variable especially in the 350- to 500-nm region. A value of $a^*(4\ 10) = 0.015\ m^{-1}mg^{-1}m^{-3}$ was chosen. This is probably the lowest value that could be assumed for the oceanic regions used to develop the K model [*Morel*, 1988]. The $a_{CDOM}(\lambda_{ref})$ level was selected by starting with the background yellow substance absorption given by ***Gordon et al.*** [1988]. They chose $a_{CDOM}(375)$ to be $0.06\ m^{-1}$ in order to account for the CDOM absorption in the diffuse attenuation model being used in their radiance model. This corresponds to $a_{CDOM}(410) \sim 0.045\ m^{-1}$. Recent work ***[Hoge et al.,*** 19933 suggests that a lower value could be used in deep-ocean waters. A value of $0.04\ m^{-1}$ at 410 nm is used in the computations herein. Some guidance in the choice of the detritus absorption $a_{detr}(\lambda_{ref})$ can be obtained from recent work [***Bricaud and Stramski***, 1990; ***Roesler et al.,*** 1989; ***Iturriaga and Siegel,*** 1989). However, the demand for nonnegative backscatter in the retrieval eventually constrains the detritus to rather small values. A value of $a_{detr}(410) = 0.01\ m^{-1}$ was used in all the calculations.

The $b_{bt}(\lambda)$ were computed for C = 0.3 to 30 mg m^{-3} using (A2) and the model parameters described above. The spectral backscatter was found to be relatively unchanged as the chlorophyllous pigment concentration C increased from ~1 to 30 mg m^{-3}. This suggested that the mean particulate backscatter could potentially be used to model the spectral backscatter over all wavelengths (and over all chlorophyllous pigment concentrations of C = 1-30 mg m^{-3}). Accordingly, these latter spectra were averaged to yield a mean particulate backscatter spectrum, $\{b_{bp}(h)\}$. Figure Ala shows the mean particulate backscatter spectrum, $\langle b_{bt}(\lambda)\rangle$, where the brackets specifically denote the mean of the K model inversion over C = 1-30 mg m^{-3}. The spectrum has been normalized to unity at 410 nm. The most distinctive features of the numerous TCB spectra and their resulting mean spectrum are the discernible maximum at ~420 nm, a readily distinguishable minimum at ~580 nm, followed by an undulating rise toward 660 nm reminiscent of sea water absorption effects. When used for C < 1 mg m^{-3}, this backscatter mode1 will probably be less accurate for C < 1 mg m^{-3} since the K mode1 inversion is very sensitive to the choice of the remaining absorption parameters. The mathematical model, $b_{bt}(\lambda) = b_{bt}(\lambda_{ref})(\lambda_{ref}/\lambda)^n$ for n = 3.3, is shown by the diamonds for λ = 410, 490, and 555 nm. This latter comparison suggests that the $(\lambda_{ref}/\lambda)^n$ model is a reasonably good fit over the region from ~420 to ~580 nm. If one desires a model for the entire 400–580 nm segment, then an error function or, alternatively. a skewed Gaussian can potentially be used.

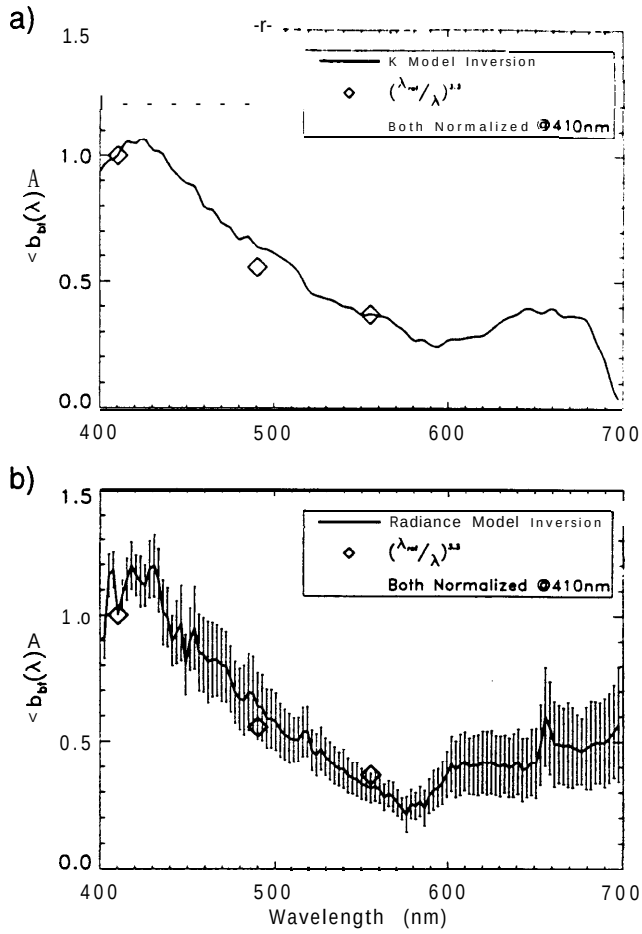

Figure Al. (a) Total constituent backscatter (TCB) spectrum obtained by inverting the K model of ***Gordon*** [1989, 1994]. The mean TCB spectrum, $\langle b_{bt}(\lambda)\rangle$, was obtained by averaging the spectra1 backscatter over all chlorophyllous pigment concentrations from C = 1 to 30 mg m^{-3}. The $(\lambda_{ref}/\lambda)^n$ backscatter mode1 for n = 3.3 is provided for comparison. (b) TCB spectrum obtained by inverting the radiance model [Gor***don*** et ***al.,*** 1988] using 14 ship surface-layer filter pad and CDOM absorption pairs together with 14 airborne water-leaving radiance spectra. The mean TCB spectrum, $\langle b_{bt}(\lambda)\rangle$, was obtained by averaging the 14 backscatter spectra. The vertical bars indicate the standard error of the mean. The $(\lambda_{ref}/\lambda)^n$ backscatter model for n = 3.3 is provided for comparison. For both inversions, the best agreement is for the ~420- to ~580-nm region. Outside this region, larger errors are encountered.

TCB Model by Direct Inversion of the Radiance Model

The radiance model ((1) in the main body of this paper) can be inverted to provide a backscatter spectrum. To do this, a contemporaneous data set consisting of airborne water-leaving spectral radiances and constituent absorbers (from ship surface water samples) obtained within the Middle Atlantic Bight was used to solve for the total constituent backscatter at 116 wavelengths between 400 and 700 nm. The water-leaving radiance model shown in (1) was arranged to solve for backscatter as shown in (AS).

$$b_{bp}(\lambda) = [h(\lambda) - a_{CDOM}(\lambda) - a_{filter}(\lambda)]/v(\lambda). \quad (A8)$$

Here $a_{filter}(\lambda)$ is the absorption measured from the filter pads and $a_{CDOM}(\lambda)$ is the measured absorption of the remaining filtrate. Fourteen ship stations from the Gulf Stream to mid-shelf were used in the calculations. An equal number of airborne spectral radiances were selected in close proximity to the ship stations. The resulting TCB spectral curve is shown in Figure A I b. The spectrum is normalized at 410 nm with error bars representing the standard deviation about the mean for the 14 stations. Also shown in the plot is the inverse wavelength model with an exponent of 3.3 plotted at the wavelengths used in this study, 410, 490, and 555 nm. Figure Alb shows that the inverse wavelength model is a close approximation for TCB in the Middle Atlantic Bight for the wavelengths 410, 490, and 555 nm. If the reference wavelength for the inverse wavelength model were moved to -440 nm and the 440-nm band used in the inversion instead of the 410-nm band, the inverse wavelength model would have a closer fit to the measured TCB spectral curve. This would improve the fit of the inverse wavelength TCB model but would cause the phytoplankton model to be compromised because of the high variability of phytoplankton absorption at 443 nm. Since the study within the main body of this paper has shown errors in the phytoplankton absorption model to be the most detrimental to the inverted IOPs, the 410-nm reference was used instead of the 440-nm band.

Appendix B: Alternative Form for the Data-Model Matrix D

The matrix formulation in (llb) can be further simplified by prudent choice of reference wavelengths. First, establish a more general reference wavelength A, for the phytoplankton pigment absorption by evaluating (10) at wavelength λ_p and forming the quotient with $a_{ph}(\lambda_i)$,

$$a_{ph}(\lambda_i) = a_{ph}(\lambda_p) \exp[(\lambda_i - \lambda_g)^2/2g^2]/\exp[(\lambda_p - \lambda_g)^2/2g^2]. \quad \text{(B1)}$$

Now, without significant loss of generality, chose the phytoplankton pigment, CDOM, and TCB reference wavelengths to coincide with the first observational band, A, = $\lambda_p = \lambda_d$ = A,. Then,

$$\begin{bmatrix} 1 & 1 & v(\lambda_1) \\ D_{21} & \exp[-S(\lambda_2 - \lambda_1)] & (\lambda_1/\lambda_2)^n v(\lambda_2) \\ D_{31} & \exp[-S(\lambda_3 - \lambda_1)] & (\lambda_1/\lambda_3)^n v(\lambda_3) \end{bmatrix} \cdot \begin{bmatrix} a_{ph}(\lambda_1) \\ a_d(\lambda_1) \\ b_{bt}(\lambda_1) \end{bmatrix} = \begin{bmatrix} h(\lambda_1) \\ h(\lambda_2) \\ h(\lambda_3) \end{bmatrix} \quad \text{(B2)}$$

where, from equation (10), $D_{21} = \exp[(A, - \lambda_g)^2/2g^2]/\exp[(A, - \lambda_g)^2/2g^2] = a_{ph}(\lambda_2)/a_{ph}(\lambda_1)$ and $D_{31} = \exp[(\lambda_3 - \lambda_g)^2/2g^2]/\exp[(A, - \lambda_g)^2/2g^2] = a_{ph}(\lambda_3)/a_{ph}(\lambda_1)$. Of course, matrix elements D_{21} and D_{31} as well as D_{22} and D_{32} need to be computed only once (and need recomputation only if the spectral model parameters g and S, respectively, are changed). Matrix elements D_{13}, D_{23}, and D,, (and $h(\lambda_1), h(\lambda_2)$, and $h(\lambda_3)$) must be computed before every inversion since they contain radiance data within the v. Inversion of (B2) provides the IOPs at wavelength A $_1$: $a_{ph}(A,), a_d(A,), b_{bt}(A,)$. The values of the IOPs at other wavelengths are given by (8), (9), and (B1).

Appendix C: Concentrations Derived From IOP Retrievals

Upon retrieval of the IOPs the constituent concentrations may be obtained from their specific absorptions. For example, the phytopiankton pigment concentration is readily obtained from C = $a_{ph}(\lambda_1)/a^*_{ph}(\lambda_1)$, where $a^*_{ph}(\lambda_1)$ is the chlorophyll-specific absorption [*Hoepffner and Sathyendranath*, 1993; *Morel*, 1988; *Sathyendranath et* al., 1987] at A,. (For application to inversion of airborne or satellite data the nonlinear variation of the specific absorption coefficient with chlorophyll concentration [*Carder et al.*, 1991; *Cleveland*, 1995; *Bricaud et al.*, 1995] may provide higher accuracy.) A rough estimate of the surface layer dissolved organic carbon can potentially be obtained from the CDOM absorption coefficient using recent absorption and fluorescence data [*Hoge et al.*, 1993; *Voducek et* al., 1995]. While considerable progress has been recently reported relative to the retrieval of hydrosol backscatter from remotely sensed reflectances [*Weideman* et al., 1995], robust relationships need to be developed for obtaining total constituent matter concentration from the TCB coefficient.

Notation

a	total absorption coefficient (m^{-1}).
a_{CDOM}	absorption coefficient of chromophoric dissolved organic matter (CDOM) (m^{-1}).
a_d	absorption coefficient of CDOM and detritus (m^{-1}).
a_{detr}	absorption coefficient of detritus (m^{-1}).
a_{filter}	absorption measured from filter pads, $a_{ph} + a_{detr}$.
a_{ph}	absorption coefficient of phytoplankton particles (m^{-1}).
a^*_{ph}	specific absorption coefficient of phytoplankton particles (m^{-1}).
a_t	$a_{ph} + a_d$, total constituent absorption (TCA) (m^{-1}).
a_w	absorption coefficient of water (m^{-1}).
b_b	total backscatter coefficient (m^{-1}).
b_{bt}	total constituent backscatter (TCB) coefficient (m^{-1}).
$\langle b_{bt} \rangle$	mean TCB coefficient (m^{-1})
b_{bw}	backscatter coefficient of seawater (m^{-1}).
CDOM	chromophoric dissolved organic matter.
czcs	coastal zone color scanner.
D	data and model matrix.
D_0	downwelling distribution function.
D_{ij}	elements of D with i, j = 1, 2, 3.
E_u	upwelling irradiance just beneath the sea surface.
Ed	downwelling irradiance just beneath the sea surface.
e	exponent from *Morel's* [1988] K model.
F_0	extraterrestrial solar irradiance (W m^{-2} nm^{-1}).
g	phytoplankton Gaussian model spectral width parameter (nm).
h	$-(a_w + b_{bw}v)$; vector of hydrospheric constants and water-leaving radiances.
IOP	inherent optical property.
K	diffuse attenuation coefficient.
l_1	0.0949.
l_2	0.0794.
L_w	water-leaving radiance (W m^{-2} nm^{-1} sr^{-1}).

m index of refraction of seawater.
M $(1-\rho)(1-\bar{\rho})/m^2(1-rR) \sim 0.55$ for nominal sea conditions [*Gordon et al.*, 1988].
n total constituent backscatter spectral model exponent.
P oceanic state vector of retrieved IOPs at their reference wavelengths.
Q ratio of the upwelling radiance to upwelling irradiance toward zenith.
r water-air reflectance for totally diffuse irradiance.
R irradiance reflectance just beneath sea surface.
S spectral slope for the a_d model (nm^{-1}).
s spectral slope for exponential constituent backscattering model.
SVD singular value decomposition.
t diffuse transmittance of the atmosphere.
TCA total constituent absorption.
TCB total constituent backscatter b_{bp}.
v $(1 - 1/X)$ (dimensionless).
X $b_b/(b_b + a)$ (dimensionless).
X_c parameter from Morel's (1988) K model.
A wavelength (nm).
λ_b reference wavelength for TCB (nm).
λ_d reference wavelength for CDOM absorption (nm).
λ_g peak wavelength for Gaussian phytoplankton absorption model (nm).
λ_i wavelength of observational bands, i = 1, 2, 3.
A_{ref} reference wavelength (nm).
ρ Fresnel reflectance of the sea surface for normal incidence.
$\bar{\rho}$ Fresnel reflection albedo of the sea surface for irradiance from the Sun and sky.
θ_0 solar zenith angle (deg).

Acknowledgments. The continued support and encouragement of NASA Headquarters are gratefully acknowledged. We thank Neil Blough, Tony Vodacek, and Mike DeGrandpre for the ship data and the NASA Airborne Oceanographic Lidar team for the water-leaving radiances, used to calculate the TCB spectra in Figure Alb of Appendix A.

References

Aiken, J., G. F. Moore, C. C. Trees, S. B. Hooker, and D. K. Clark, The SeaWiFS CZCS-Type Pigment Algorithm, edited by S. B. Hooker and E. R. Firestone, *NASA Tech. Memo. 104566,* vol. 29, 34 pp., NASA Goddard Space Flight Cent., Greenbelt, Md., 1995.

Baker, K. S., and R. C. Smith, Bio-optical classification and model of natural waters, *2, Limnof. Oceanogr., 27,* 500–509, 1982.

Balch, W. M.. P. M. Holligan, S. G. Ackleson, and K. J. Voss, Biological and optical properties of mesoscale coccolithophore blooms in the Gulf of Maine, *Limnol. Oceanogr., 36, 629-643,* 1991.

Blough, N. V.. 0. C. Zafiriou, and J. Bonilla. Optical absorption spectra of waters from the Orinoco River outflow: Terrestrial input of colored organic matter to the Caribbean, *J. Geophys. Res., 98,* 2271-2278. 1993.

Bricaud. A., and D. Stramski, Spectral absorption coefficients of living phytoplankton and nonalgal biogenous matter: A comparison between the Peru upwelling area and the Sargasso Sea, *Limnof. Oceanogr.*, 35. 562–582, 1990.

Bricaud. A.. A. Morel. and L. Prieur, Absorption by dissolved organic matter of the sea (yellow substance) in the UV and visible domains, *Limnol. Oceanogr.. 26,* 43–53, 1981.

Bricaud. A., M. Babin. A. Morel. and H. Claustrc, Variability in the chlorophyll-specific absorption coefficients of natural phytoplankton: Analysis and parameterization, *J. Geophys. Res., 100,* 13,321-13.33,. 1995.

Carder, K. L., and R. G. Steward, A remote-sensing reflectance model of a red-tide dinoflagellate off west Florida, *Limnol. Oceanogr., 30,* 286–298, 1985.

Carder, K. L., R. G. Steward, J. H. Paul. and G. A. Vargo, Relationships between chlorophyll and ocean color constituents as they affect remote-sensing reflectance models. *Limnol. Oceanogr., 31,* 403–413, 1986.

Carder, K. L.. R. G. Steward. G. R. Harvey, and P. B. Ortner, Marine humic and fulvic acids: Their effects on remote sensing of ocean chlorophyll, *Limnol. Oceanogr., 34,* 68-81, 1989.

Carder, K. L., S. K. Hawes, K. A. Baker, R. C. Smith. R. G. Steward, and B. G. Mitchell, Reflectance model for quantifying chlorophyll a in the presence of productivity degradation products, *J. Geophys. Res., 96,* 20,599–20,611, 1991.

Cleveland, J., Regional models for phytoplankton absorption as a function of chlorophyll a concentration, *J. Geophys. Res., ZOO,* 13,333–13,344, 1995.

Gordon, H. R., Can the Lambert-Beer law be applied to the diffuse attenuation coefficient of ocean water?, *Limnol. Oceanogr., 34,* 1389–1409, 1989.

Gordon, H. R., Modeling and simulating radiative transfer in the ocean, in *Ocean Optics,* edited by R. W. Spinrad, K. L Carder, and M. J. Perry, pp. 3-39, Oxford Univ. Press, New York, 1994.

Gordon, H. R., 0. B. Brown, R. H. Evans, J. W. Brown, R. C. Smith, K. S. Baker, and D. K. Clark, A semianalytic radiance model of ocean color, *J. Geophys. Res., 93,* 10,909–10,924, 1988.

Gregg, W. W., and K. L. Carder, A simple spectral solar h-radiance model for cloudless maritime atmospheres, *Limnol. Oceanogr., 35,* 1657-1675, 1990.

Gulob, G. E., and C. F. Van Loan, *Matrix Computations,* 2nd ed., Johns Hopkins Univ. Press, Baltimore, Md., 1989.

Hoepffner, N., and S. Sathyendranath, Determination of the major groups of phytoplankton pigments from the absorption spectra of total particulate matter, *J. Geophys. Res., 98,* 22,789–22,803, 1993.

Hoge, F. E., A. Vodacek, and N. V. Blough, Inherent optical properties of the ocean: Retrieval of the absorption coefficient of chromophoric dissolved organic matter from fluorescence measurements, *Limnol. Oceanogr., 38,* 1394-1402, 1993.

Hoge, F. E., R. N. Swift, and J. K. Yungel, Oceanic radiance model development and validation: Application of airborne active-passive ocean color spectral measurements, *Appf. Opt., 34, 3468-3476,* 1995a.

Hoge, F. E., M. E. Williams, R. N. Swift, J. K. Yungel, and A. Vodacek, Satellite retrieval of the absorption coefficient of chromophoric dissolved organic matter in continental margins, J. *Geophys. Res., 100,* 24,847–24,854, 1995b.

Iturriaga, R., and D. A. Siegel, Microphotometric characterization of phytoplankton and detrital absorption properties in the Sargasso Sea, *Limnol. Oceanogr., 34,* 1706-1726, 1989.

Lee, Z. P., K. L. Carder, S. K. Hawes, R. G. Steward, T. G. Peacock, and C. 0. Davis, Model for the interpretation of hyperspectral remote-sensing reflectance, *Appl. Opt., 33,* 5721-5732, 1994.

Lee, Z. P., K. L. Carder, T. G. Peacock, C. 0. Davis, and J. L. Mueller, Method to derive ocean absorption coefficients from remote-sensing reflectance. *Appl. Opt., 35,* 453–462, 1996.

Maffione, R. A., D. R. Dana, and J. M. Voss, Spectral dependence of optical backscattering in the ocean, paper presented at the Optical Society of America Annual Meeting, Opt. Soc. of Am., Portland, Oreg.. Sept. 10–15, 1995.

Morel, A., Analysis of variations in ocean color, *Limnof. Oceanogr.. 22,* 709-722, 1977.

Morel. A.. Optical modeling of the upper ocean in relation to its biogenous matter content (case I waters), *J. Ceophys. Res.. 93,* 10.749–10,768, 1988.

Morel, A., and B. Gentili, Diffuse reflectance of oceanic waters: Its dependence on Sun angle as influenced by the molecular scattering contribution, *Appl. Opt., 30,* 4427–4438, 1991.

Morel. A.. and B. Gentili, Diffuse reflectance of oceanic waters. II, Bidirectional aspects. *Appl. Opt.. 33, 6864-6879,* 1993.

Morel. A.. K. J. Voss, and B. Gentili, Bidirectional reflectance of oceanic waters: A comparison of modeled and measured upward radiance fields, *J. Geophys. Res., 100,* 13,143–13,150, 1995.

Ortega, J. M., *Numerical Analysis,* A Second Course. Soc. for Indust. and Xppl. Math., Philadelphia, Pa., 1990.

Press, W. H., S. A. Teukolsky, W. T. Vetterling, and B. P. Flannery, *Numerical Recipes in C,* 2nd ed., Cambridge Univ. Press, New York, 1994.

Roesler, C. S., and M. J. Perry, In situ phytoplankton absorption, tluorcsccncc emission. and particulate backscattering spectra determined from reflectance. *J. Geophys. Res.*. *100*,13,279–13,294,1995.

Roesler, C. S., M. J. Perry, and K. L. Carder, Modciing in situ phytoplankton from total absorption spectra in productive inland marine waters, *Limnol. Oceanogr.*, *34*,15 10-1523, 1989.

Sathyendranath. S.. L. Lazzara, and L. Prieur. Variations in the spectral values of the specific absorption of phytoplankton, *Limnol. Oceanogr.*, *32*. 403–415, 1987.

Sathyendranath, S., L. Prieur, and A. Morel, A three-component model of ocean colour and its application to remote sensing of phytoplankton pigment in coastal waters, *Int. J. Remote Sens.*, *10*, 1373-1394, 1989.

Siegenthaler, U., and S. L. Sarmiento, Atmospheric carbon dioxide and the ocean, *Nature*, 365, 119-125, 1993.

Smith, R. C., and K. S. Baker, Optical properties of the clearest natural waters (200–800 nm), *Appf. Opt., 20,* 177-183, 1981.

Vodacek, A., F. E. Hoge, R. N. Swift, J. K. Yungel, E. T. Peltzer. and N. V. Blough, The use of in situ and airborne tluorcsccncc measurements to determine UV absorption coefficients and DOC concentration in surface waters. *Limnol. Oceanogr.*, *40*, 411-415. 1995.

Weidman, A. D., R. H. Stavn, J. R. V. Zanefeld, and M. R. Wilcox. Error in predicting hydrosol backscattering from remotely sensed reflectance, *J. Geophys. Res.*. *100*,13,163–13,177, 1995.

F. E. Hoge, NASA Goddard Space Flight Center, Wallops Flight Facility. Building N-159. Wallops Island, VA 23337. (e-mail: hoge@osb1.wff.nasa.gov)

P. E. Lyon, EG&G Washington Analytical Services, Inc., Wallops Flight Facility, Wallops Island, VA 23337.

(Received September 29, 1995; revised May 2. 1996; accepted May 3, 1996.)